UNIVERSITA' DEGLI STUDI DI CAGLIARI

FACOLTA' DI INGEGNERIA

DIPARTIMENTO DI INGEGNERIA ELETTRICA ED ELETTRONICA

Organic Field-Effect Devices for detecting chemical and physical parameters

Ing. Ileana Manunza

Tesi per il conseguimento del Dottorato di Ricerca
In Ingegneria Elettronica ed Informatica

Relatore: Prof. Annalisa Bonfiglio

Corso di Dottorato di Ricerca in Ingegneria Elettronica ed Informatica
XIX Ciclo

Introduction

Organic electronics has received a lot of attention in recent years since the performance of organic thin-film transistors as well as OLED (Organic Light Emitting Diode), solar cells etc., is considerably improved. Organic field-effect transistors can be assembled on plastic films at room temperatures; they are potentially inexpensive to manufacture and mechanically flexible. The features mentioned above make them promising for low-cost and large area electronics applications. Due to these feature, so far, applications such as radio-frequency identification tags (RFID tags) and displays have been proposed. Nevertheless, the low mobility of organic semiconductors does not allow them to be employed in electronic applications where response speed and low size are fundamental. In this field, silicon technology is still having and will continue to have (unless dramatic improvement of organic semiconductor properties will be obtained) a prominent role in electronics. Therefore the “killer application” for organic field effect transistors has still to be found. This thesis is aiming at contributing to individuate an applicative field where the unique properties of organic field effect transistors would be adequately enhanced.

In fact, there is a broad range of sensing applications that increasingly demand for small, portable and low-cost sensors. Organic field-effect transistor based sensors could in fact fulfil these requirements by means of devices that exploit the advantage of an active detection of physical and chemical parameters with the mechanical properties of organic materials. Together with the increasing development in the field of smart interfaces (in particular with the impressive progresses obtained in microfluidics), this strategy could give rise to the visionary concept of “Lab on a strip”, indicating the possibility of employing a low cost, “smart” substrate (as paper, plastic, or fabric) for realizing a full (bio)chemo analysis of liquids, vapours, etc.

The main objective of this thesis is to develop totally flexible substrate-free organic field-effect based devices for detecting chemical and physical parameters. Chemical devices for the detection of pH variations in an electrolyte solution, and physical sensors for the detection of mechanical stimulus (i.e a pressure or a substrate deformation) applied on the device have been described and possible applications have been proposed. Our proposed devices are substrate-free, completely flexible and are entirely processed at room temperature with low-cost techniques (compared to conventional Silicon device fabrication techniques). These are very interesting hallmarks since only a few examples of mechanical and ion-sensitive organic sensors have been reported in literature and none of them exploits all the potential advantages of organic devices.

In the case of chemical sensors our motivation for the development of the device has been to build a cheap and disposable device for realizing pH detection in a solution. Future developments will concern the realization of device able to detect different chemical groups. For biomedical and health applications, due to the safety requirements, single-use devices are highly desirable and therefore Plastic Electronics is for sure a potentially valuable answer to these requirements.

In the case of mechanical sensors, the main peculiarity with respect to the devices reported in the literature is that the device performs at the same time both switching and sensing functions without the need of any additional element. Moreover by exploiting the properties of the structure the device can be employed as free-standing devices or it can be combined with any kind of substrate (e.g. 3D surfaces). Future developments of this kind of sensors will concern electronic skin, sensorized clothes, smart textiles, etc.

Thesis outline.

Chapter 1 of this thesis gives an overview of organic electronics with particular attention to organic semiconductor properties and organic field-effect transistors operation. In Chapter 2 the application of organic field-effect transistors to chemical, biological and mechanical sensor is reviewed. In Chapter 3 the employed materials and the device structure are described in some detail. Ion-sensitive field-effect devices are described in Chapter 4. After a description of the ISFET theory that is the basis of the working mechanism of the device, the device processing and the results are presented and discussed. Mechanical field effect device processing and results are described in Chapter 5.

Introduzione

Negli ultimi anni l'elettronica organica è diventata un argomento di grande interesse accademico e industriale. Le prestazioni dei dispositivi organici, soprattutto degli OLED (Organic Light Emitting Diode), delle celle solari e dei transistors, sono negli anni notevolmente migliorate. I vantaggi dei transistors organici sono individuabili nel fatto che essi possono essere fabbricati tramite processi che avvengono a temperatura ambiente, sono quindi potenzialmente economici da produrre e visto che possono essere assemblati su substrati non convenzionali, ad esempio su plastica, risultano essere anche in qualche modo flessibili. Queste caratteristiche li rendono promettenti in tutte quelle applicazioni che richiedano bassi costi di produzione. Alcune applicazioni come lo sviluppo di badge identificativi a radio-frequenza (RFID tags) o di display flessibili sono già state proposte. Tuttavia la bassa mobilità che caratterizza il trasporto di carica nei semiconduttori organici non ne consente l'impiego in tutte quelle applicazioni in cui siano necessarie ottime prestazioni dinamiche. In queste applicazioni la tecnologia dei dispositivi in Silicio è e rimarrà predominante almeno fino a quando non ci saranno eccezionali miglioramenti nelle prestazioni dei dispositivi organici. Questa tesi ha lo scopo di dare un contributo nell'individuare un campo di applicazione dei dispositivi organici in cui le proprietà uniche dei materiali possano essere sfruttate al meglio. In particolare per una vasta gamma di applicazioni sensoristiche c'è una crescente richiesta di sensori a basso costo che siano facilmente portabili. I sensori basati sui semiconduttori organici possono in effetti soddisfare questi requisisti attraverso dispositivi che siano in grado di rilevare parametri fisici o chimici sfruttando le proprietà dei materiali organici. Tutto ciò unito al crescente sviluppo nel settore delle cosiddette “smart interfaces”, in particolare grazie agli impressionanti progressi nel campo della microfluidica, può portare avanti lo sviluppo dell’idea del “Lab on a strip” attraverso l’uso di substrati a basso costo come plastica, carta o tessuti che però vengono resi “smart” per realizzare per esempio analisi biochimiche.

L’obiettivo di questa tesi è stato sviluppare dispositivi basati su transistor organici a effetto di campo che avessero la capacità di fungere da sensori per la rilevazione di parametri chimici e meccanici. Sono stati progettati e realizzati sensori chimici per la rilevazione della variazione del pH di una soluzione elettrolitica e sensori fisici per la rivelazione di una pressione o di una deformazione meccanica. I dispositivi realizzati sono completamente flessibili e interamente processati a temperatura ambiente con tecniche a basso costo. Questi aspetti distintivi dei dispositivi sono molto interessanti sia dal punto di vista applicativo che dal punto di vista accademico poiché pochissimi esempi di sensori meccanici e di sensori di ioni in soluzione basati su transistor a semiconduttore organico sono stati riportati in letteratura e nessuno di essi sfrutta appieno tutti i vantaggi dei dispositivi organici.

Nel caso dei sensori chimici la nostra motivazione è stata quella di provare a costruire un dispositivo usa e getta per la rilevazione della variazione del pH. Gli sviluppi futuri riguarderanno sicuramente lo sviluppo di sensori in grado di identificare diverse specie chimiche. Per applicazioni di tipo biomedico per esempio c’è una larga richiesta di dispositivi monouso e sicuramente la cosiddetta Plastic Electronics è potenzialmente in grado di soddisfare questa richiesta.

Per quanto riguarda i sensori meccanici le loro caratteristiche peculiari rispetto ai dispositivi riportati in letteratura sono dovute al fatto che il dispositivo funziona al tempo stesso da switch e da sensore senza bisogno di nessun ulteriore elemento sensibile al parametro da rilevare e a differenza di quanto accade per gli altri dispositivi riportati in letteratura. Inoltre sfruttando le caratteristiche della struttura, in particolare l'assenza del substrato, il dispositivo può essere facilmente integrato su qualunque tipo di substrato (per esempio una superficie 3D) per rilevare le deformazioni che esso subisce oppure essere usato senza nessun substrato per rilevare per esempio una pressione ad esso applicata. Gli sviluppi futuri di questo tipo di dispositivi possono essere individuati nella realizzazione di tessuti intelligenti, indumenti sensorizzati fino addirittura alla pelle elettronica per applicazioni di robotica.

La tesi è organizzata in questo modo: nel Capitolo 1 sono presentate le principali proprietà e caratteristiche dei semiconduttori organici e dei dispostivi organici ad effetto di campo; nel Capitolo 2 è illustrato lo stato dell'arte dei sensori chimici e fisici basati sui transistor organici; nel Capitolo 3 è presentata la struttura del dispositivo e i materiali utilizzati per la sua fabbricazione. I risultati ottenuti e la teoria relativa ai sensori chimici per la rilevazione di ioni in soluzione sono presentati nel Capitolo 4, mentre il Capitolo 5 è invece dedicato ai sensori meccanici.

Published Papers

I. Manunza, and A. Bonfiglio, **Pressure sensing using a completely flexible, organic transistors**, Biosensors and Bioelectronics (in press)

I. Manunza, and A. Bonfiglio, **Organic Field-Effect based devices for pressure detection**, Mater. Res. Soc. Symp. Proc., 965 (2007)

I. Manunza, A. Sulis and A. Bonfiglio, **Pressure sensing by flexible, organic, field effect transistors**, Applied Physics Letters, 89, 143502 (2006)

I. Manunza, A. Sulis and A. Bonfiglio, **Organic semiconductor field effect transistors for unconventional applications: flexible sensors and wearable devices,** Proc. Int. Workshop on Wearable and Implantable Body Sensor Networks (BSN'06),IEEE 2006

A. Loi, I. Manunza, and A Bonfiglio; **Flexible, organic, ion-sensitive field effect transistor**, APL **86**, 103512 (2005)

C. Santato, I. Manunza, A. Bonfiglio, F. Cicoria, P. Cosseddu, R. Zamboni and M. Muccini; **Tetracene Light-Emitting Transistor on flexible plastic substrates**, APL **86**, 141106 (2005)

P. Cosseddu, F. Mameli, I. Manunza, O.Sanna, and A. Bonfiglio; **An Organic Thin Film Transistor structure for optoelectronic applications**, Proc. SPIE Int. Soc. Opt. Eng. **5464**, 356 (2004)

A mamma e papà
perché hanno sempre voluto il meglio per me

A Emilio
per essere stato sempre il mio rifugio sicuro

Ad Alice e Fabio
perché da grandi useranno i miei sensori

CHAPTER 1

Organic Electronics

1.1 Introduction

Virtually all of today's microelectronic devices are made from inorganic materials, silicon and gallium arsenide, for instance. But in the past few years there has been an explosion of interest in flexible devices made from organic molecules [1-8]. Depending on their structure, they can freely carry a current like metals or switch on and off like semiconductors. In particular, flexible electronics based on organic semiconductors has become an exciting research area drawing active participation of scientists and engineers from both academia and industry. The primary research emphasis at major laboratories was confined to materials and device technologies, but now it is beginning to expand into process and device integration that enable commercial applications. The technology has become even more attractive after the demonstration of solution-processable materials, which enables the use of low-cost deposition techniques such as spin coating, screen printing, and conventional graphic arts printing technologies.

These manufacturing methods plus the use of a continuous, flexible substrate are key ingredients for manufacturing low-cost, simple organic-based products utilizing infrastructures with costs in the range of US$1 million to $10 million. This is very inexpensive when compared to the cost of a new silicon semiconductor fabrication facility, which has steadily risen and now exceeds US$3 billion. The high cost is partially due to the clean-room environment, costly chemical distribution and disposal facilities, wafer processing and handling equipment, high-resolution lithographies, and wafer testing equipment.

More recently, as organic semiconductor materials have demonstrated reliability and enhanced performance, engineers have suggested that an organic semiconductor fabrication facility could be built for $40 million [9]

Because of the relatively low mobility of the organic semiconductor layers, organic thin-film transistors (OTFTs) cannot rival the performance of field-effect transistors based on single-crystalline inorganic semiconductors, such as Silicon and Germanium, which have charge carrier mobilities (μ) about three orders of magnitude higher. Consequently, OTFTs are not suitable for use in applications requiring very high switching speeds. However, the processing characteristics and demonstrated performance of OTFTs suggest that a new market is open for organic devices, where the excellent performance of silicon technology is not required. They can be competitive for existing or novel applications requiring large-area coverage, structural flexibility, low-temperature processing, and, especially, low cost, for instance: organic RFID tags, electronic papers, organic LED drivers, sensors, etc.

An often mentioned application for flexible electronics is in electronic textiles and wearable electronics. These are fabrics that have electronics and interconnections woven into them. The large areas and the physical flexibility of the fabric do not allow for electronic integration using traditional methods, and new integration concepts are starting to emerge.

Three functional materials are required for organic transistor fabrication: conductors (electrodes), dielectrics (gate insulator), and semiconductors (active material). The material sets can vary considerably when organic devices and circuits are fabricated using different manufacturing technologies, as usable material sets depend heavily on the process used. Traditional vacuum deposited conductors, gold (Au) and platinum (Pt), and dielectrics, silicon dioxide (SiO_2) and silicon nitride (Si_3N_4), are selected when silicon-like wafer processes and infrastructure are used to fabricate organic electronics. Solution-processable conductive and dielectric inks are used when spin coating, graphic arts printing, or other similar solution-processing techniques are implemented. In addition, the selection of conductive and dielectric materials is also dependent on the compatibility with organic semiconductors, which are developed and optimized based on electrical performances, processability, and environmental sensitivity

In this chapter we will present at first an overview on organic materials with particular attention to organic semiconductors and their electrical and mechanical properties. In the last part of the chapter we will describe in detail organic semiconductor based field effect transistors.

1.2 Materials

Popularly known as ‘‘plastics’’, polymers are large molecules constructed from smaller structural units (monomers) covalently bonded together in any conceivable pattern [10]. By modifying the monomer building blocks and the bonding scheme, the mechanical and thermal properties of the polymers can be controlled. Polymers can be made ‘rubbery’ or brittle, soft or hard, soluble or non-soluble, and in practically any colour by blending with suitable chromophores. The special properties of polymers allow for a variety of convenient processing, such as injection moulding, spin coating and ‘spray’ painting. This is in striking contrast to the processing of metals and even more so, of inorganic semiconductors like silicon. Hence, polymers can be found in almost all products in our present day society: clothes, furniture, home appliances, cars, airplanes, electronics etc.

The idea of utilizing the electrically conducting properties of polymers was not proposed until the 1960’s but since then polymers have been used as active components in a variety of electronic applications. In 1977, it was discovered that an alternating bond conjugated polymer, trans-polyacetylene, could be doped and thereby transformed into a good electrical conductor [11]. This discovery led to the Nobel Prize in Chemistry 2000 being awarded to Profs. A.J. Heeger, A.G. MacDiarmid and H. Shirakawa. Early on, most of the research effort was concentrated to the conducting properties of the doped alternating-bond conjugated polymers, and alternating-bond conjugated polymers were often referred to as ‘‘conducting polymers’’.

Since then, organic conjugated polymers and oligomers have been the subject of numerous studies concerning their semiconducting properties. Figure 1.1 shows the chemical structure of some common organic materials [12] used as active layers in thin film transistors (TFTs) technology. As a matter of fact, small molecules (e.g. perylene and C_{60}), oligomers (e.g. tetracene and pentacene), as well as polymers (e.g. polythiophenes) can be used. All these materials are characterised by an extended system of delocalised π orbitals along which charge defects, called polarons and bipolarons, can move. The thin films, obtained from their deposition, are usually van der Waals type solids that have the mechanical flexibility typical of many plastic materials.

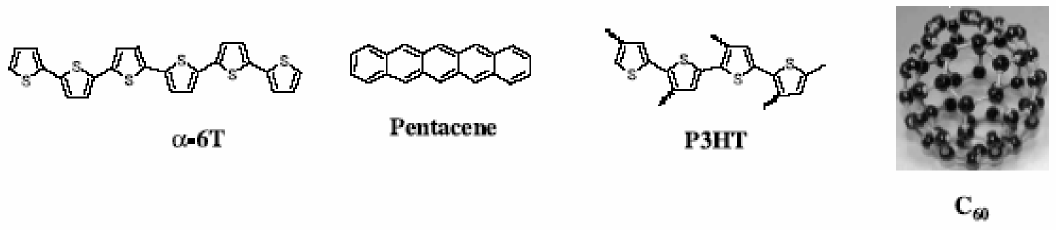

Fig.1.1 Chemical structure of some common organic materials used as transistors active layers

One of the most appealing aspects of the active materials employed in TFTs is the fact that they can be deposited using very low-cost procedures such as spin casting or spin coating. This is the case of soluble polymers such as regioregular polythiophenes. These deposition procedures are also thermally compatible with plastic substrates, because they are carried out at room temperature. One important problem remains for practical applications: organic semiconductor based transistors are so far only efficient at carrying electronic current via positive charge carriers (holes). To realize a complete electronic circuit based on organic polymers, analogous to conventional silicon chips, devices must also be able to carry negative charge (electrons).

The past decade has seen many efforts to develop so-called ‘n-channel’ organic transistors, in which electrons rather than holes, are the charge carriers [13,14].

Ultimately, materials are needed that are ‘ambipolar’ i.e. that can be used to create both n-channel and p-channel field-effect transistors (FETs) [15-17]. Until now, materials for making organic and polymer transistors have generally been lumped into one of the two categories, either n-channel or p-channel: traditional organic FET materials, such as pentacene and polythiophenes, for instance are known as p-channel materials. However, experimental results suggest that the difficulty in observing efficient transport of electrons in an organic FETs is an extrinsic effect caused by factors other than the organic semiconductor material itself. For example, a traditional p-channel FET based on pentacene can be converted into an n-channel device by inserting calcium at the interface between pentacene and the thin insulating layer used in transistors[18]. Chua et al. [19] make a convincing case that the trapping of electrons at the insulator–semiconductor interface is indeed the culprit, and they relate this trapping to electronegative hydroxyl (OH) groups in the insulator material. When they use materials that are free of hydroxyl groups, uninhibited electron transport is indeed observed Chua et al. conclude that if the trapping of electrons by electronegative groups in the insulating layer could be avoided, then n-channel behaviour would be seen in a broad range of semiconductors.

Despite the considerable progress made in recent years, achieving high carrier mobilities with organic semiconductors remains inherently difficult: the highest mobilities are in the range 1-3 $cm^2\ V^{-1}s^{-1}$ [20-22]. Efforts to increase the mobility limits have been focused on the development of better semiconductor materials and understanding their morphology and mechanism of charge transport. Nevertheless it has been noticed that the interaction between the insulator and the semiconducting materials plays an important role in the carrier transport because the morphology of the thin interfacial region is likely to be different from the bulk and the interface has been found to affect the ordering [23]. Most of the studies on organic FETs are still made with SiO_2 as the gate dielectric. However, in order to fully benefit the principal advantages of organic FETs, namely mechanical flexibility and low cost for large area electronics, it is highly desirable that SiO_2 may be substituted with polymeric gate dielectric materials. The performance of organic field-effect devices depends on the use of high-performance dielectrics that form active interfaces with low defects densities [24-32]. High capacitance is normally desirable, as it allows the reduction of the threshold voltage and operating voltage. Threshold voltages may be due to built-in charge but may also be the indication of interface states (undesirable chemical groups/sites on the insulator itself or foreign impurities) that result directly in carrier trapping. Finally, the polarity of the dielectric interface may also play a role, as it can affect local morphology or the distribution of electronic states in the organic semiconductor. [33]

In comparison to inorganic heterointerfaces, many aspects of the physics of charge transport along solution-processed heterointerfaces are still poorly understood. For a solution-processed active interface, in which either the gate dielectric material is deposited from solution onto a solution-processable semiconducting material or vice versa, it is critical to avoid dissolution or swelling effects during the deposition of the upper layer, which can lead to interfacial mixing and increased interface roughness. This can be avoided by cross-linking the lower layer. This restricts the choice of materials and requires special care to avoid introducing unwanted impurities and trapping groups. An inherent problem in the fabrication of these polymer TFTs is that a polymer semiconductor layer on an insulating layer can get damaged when the other layer is spin-coated onto the existing, underlying layer for the fabrication of the transistor. The chemical purity and composition of the gate dielectric can have dramatic effects on interfacial charge transport. For instance as previously stated, using appropriate gate dielectrics that are free of electron-trapping groups, such as hydroxyl, silanol, or carbonyl groups, n-channel FET conduction can be obtained. In contact with trapping-free dielectrics, such as benzocyclobutene (BCB), electron and hole mobilities were found to be of comparable magnitude in a broad range of polymers. Poly-vinylalcohol (PVA), poly- methylmethacrylate (PMMA), poly-vinylphenol (PVP), are some of the most promising materials used as solution-processable gate dielectrics (see Fig. 1.2).

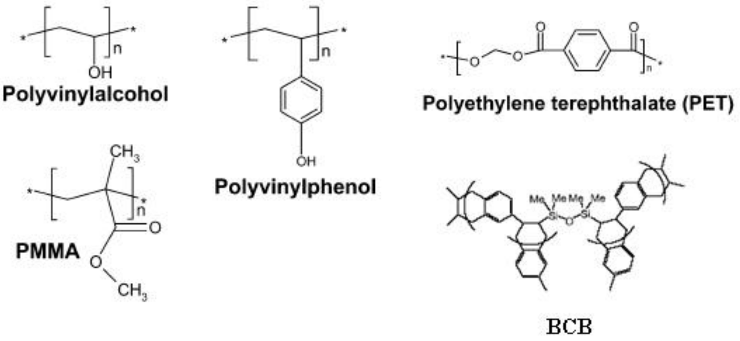

Fig.1.2: Chemical structure of some of the organic materials used as transistors gate dielectric layers

Another fundamental issue in device fabrication concerns the availability of suitable materials for contacts that so far, have been mainly fabricated with metals. Metals show several problems: first, though deposited in very thin layers, they are not mechanically flexible, and this could compromise the overall robustness of devices; secondly, employing very simple and low cost techniques for device assembly cannot be applied to metals. Therefore, in an industrial perspective, it would be desirable to employ a unique, easy technique to obtain each layer of the device [34-36]. Printing contacts with conductive polymers is one possibility, but it has several limits, as the spatial resolution of the printed pattern, and the compatibility between the employed “ink” and the printing hardware. Soft lithography [37,38] represents a step forward to obtain low dimension structures through a reliable, low cost, easy, and reproducible method. It has been successfully applied to organic materials and devices, with very interesting results and opens a possibility to fabricate flexible and efficient devices with very low dimensions.

A soft lithographic technique can be used to obtain all-organic field effect devices in a very simple and efficient way realizing contacts with a conducting polymer. Among the numerous electrically conductive polymers that have been studied and developed over the past decades, poly (3,4-ethylene dioxythiophene)/polystyrene sulfonic acid (PEDT/PSS, Fig. 1.3) has appeared to be one of the most successful materials [39,40]. It possess several advantageous properties: it is soluble and combines a low oxidation potential and a moderate bandgap with good stability in the oxidized state.

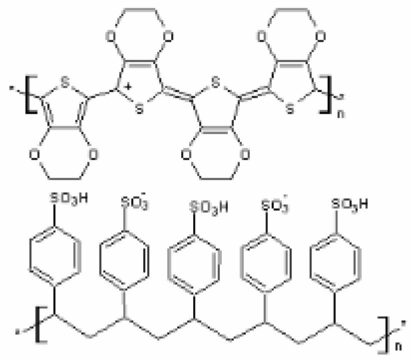

Fig. 1.3: Chemical structure of PEDOT/PSS

The viability of organic electronics, in conclusion, does not lie in the displacement of existing applications niches currently filled by conventional semiconductors, but rather lies in capturing the low cost and enormous variability inherent in organic systems that are otherwise not accessible. Success in achieving very low-cost electronics hinges almost entirely on the ability to deposit and fabricate organic electronic devices using methods that represent a revolutionary departure from those commonly used by the current high-performance electronics industry. However, much work must be done before such an ambitious goal can be realized. Although many innovative technologies have been developed relating to the fabrication of thin-film organic devices with high performance and long operational lifetime, very few of these technologies have left the laboratory. As the most sophisticated and versatile methods currently being developed in the laboratory make their way into the manufacturing environment, we can expect that organic electronic circuits whose functions are only now being envisioned will one day revolutionize the technological world in which we live.

1.3 Electrical Properties of Organic Semiconductors

Polymers are macromolecules consisting of a great number of repeating units, which are coupled to each other forming a chain [6,41]. Such linear chains can also cross-link and form more complex, three-dimensional structures, which is the case in many commercial polymers, since this improves the mechanical properties of the materials. The repeating units can of course include any group of atoms, but for the vast majority of polymers, including conducting polymers, the repeat units primarily consist of carbons. Since carbon has the electronic structure, $1s^2 2s^2 2p^2$, carbon atoms form four nearest-neighbour bonds. In σ-bonded polymers, the carbon atoms are sp^3 hybridized, and each carbon atom has four σ-bonds. In such non-conjugated polymers, the electronic structure of the chain of atoms (or chemical groups) which comprises the backbone of the macromolecule consists of only σ-bands. The large electron energy band gaps in σ-bonded polymers, $E_g(\sigma)$, renders these polymer materials electrically insulating, and generally non-absorbing for visible light.

In *conjugated polymers*, however, there exists a continuous network, often a simple chain, of adjacent unsaturated carbon atoms, i.e., carbon atoms in the sp^2 (or sp) hybridized state. Each of these sp^2 carbon atoms has a strongly bonding σ orbital lobes residing in a plane at a 120° angle to each other with the fourth remaining valence electron residing an orbital that has its lobes orthogonal to the plane defined by the other three (Fig. 1.4). Two such orbitals adjacent to each other can overlap, forming a so-called π-bond. This bonding scheme induces states that are delocalized over large segments of the polymer and decrease the gap between occupied and unoccupied states.

In a system with one-dimensional periodicity, these π-states form the electronic bands, with a π-band gap, $E_g(\pi)<E_g(\sigma)$, accounting for optical absorption at lower photon energies.

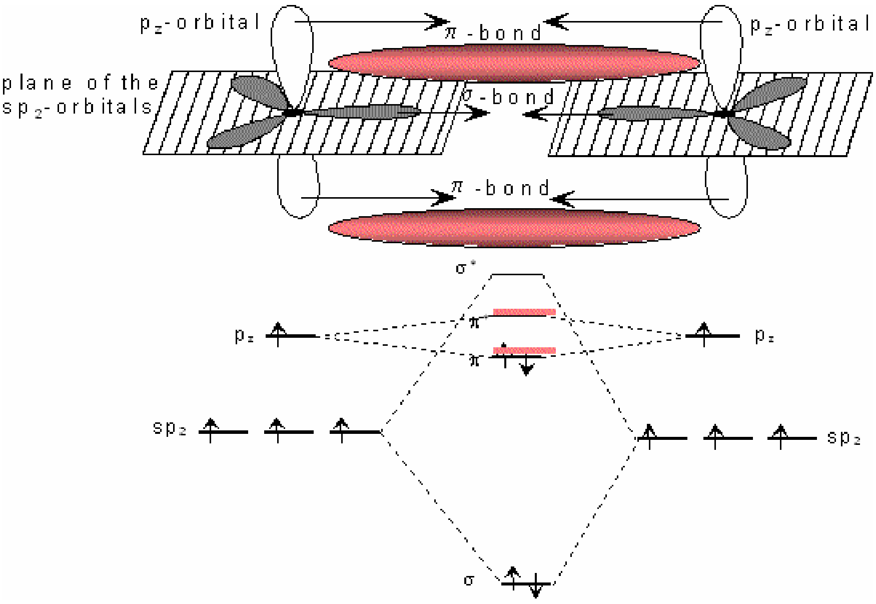

Fig. 1.4: Scheme of the orbitals and bonds for two sp^2-hybridised carbon atoms.

The essential properties of the delocalized π-electron system [42], which differentiate a typical conjugated polymer from a conventional polymer with σ-bands, are the following:

(i) the electronic band gap, E_g, is relatively small (~1-4 eV), leading to low-energy electronic excitations and semiconductor behaviour;
(ii) the polymer chains can be rather easily oxidized or reduced, usually through charge transfer with molecular dopant species;
(iii) carrier mobilities are large enough that high electrical conductivities are realized in the doped (chemically oxidized or reduced) state;
(iv) charge carrying species are not free electrons or holes, but quasi-particles, which may move relatively freely through the material, or at least along uninterrupted polymer chains.

Conjugated polymers are essentially quasi-one dimensional, i.e. there occurs covalent bonding within the chains while interactions between chains are of van der Waals type. The intrinsic low-dimensional geometrical nature of polymer chains, and the general property of conjugated organic molecules that the geometric structure is dependent upon the ionic state of the molecule, leads to the existence of the unusual charge carrying species. The charge bearing species are not free electrons or holes, but may be any one of several different types of essentially well defined quasi-particles, each consisting of a coupled charge-lattice deformation entity. The charge bearing species are "self-localized", i.e. the presence of electronic charge leads to local changes in the atomic geometry (the lattice), which, in turn, leads to localized variations in the electronic structure. These species are generated, for example, by optical absorption in the neutral system, or by charge transfer doping. Associated with these species are localized electronic states with energy levels within the otherwise forbidden electron energy gap, E_g, the so-called "gap states".

In fact, charge transfer doping and optical excitations induce large local modifications of both the electronic and the geometric structure of the polymer. This local modification introduces new energy states in the band gap that facilitate the conduction of charge. Charge transport in conducting polymers differs from that of crystalline semiconductors where electrons move in a periodic potential from the crystal lattice. For a perfect crystal, the electronic states become delocalized over the whole sample and the electron (and hole) transport occurs in energy bands. As a matter of fact, the lattice always has defects, but if the defect density is low, they can be treated as scattering centres that increase the resistivity. In contrast, conducting polymer films are usually highly amorphous, and the conducting polymers themselves tend to include a number of defects as well. Hence, the concept of three dimensional delocalized electrons and band transport no longer holds since the potential from the lattice is now random, not periodic, which results in localized electronic states. Instead electrons (and holes) are transported through so-called variable range hopping (at least for moderate doping levels), i.e., tunneling between localized states Charge carrier transport can occur via hopping between molecular sites, or from chain to chain. In this case, carrier mobilities are quite low compared with inorganic semiconductors whose room temperature values typically range from 100 to 10^4 cm^2 V^{-1} s^{-1}. In contrast, in highly ordered molecular materials where charges hop between closely spaced molecules forming a crystalline stack, mobilities of $\mu \approx 1$ cm^2 V^{-1} s^{-1}. have been observed at room temperature.

This apparently is an approximate upper bound, with the mobility ultimately limited by thermal motion between neighbouring molecules. In more disordered molecular systems and polymers, the mobilities are only 10^{-3} to 10^{-5} times this upper limit. However, deposition methods or other 'direction-inducing' processes can lead to alignment of the chains, thus increasing charge mobility over that of completely randomly disordered films. A further strategy for reducing disorder in molecular systems as well as in polymers is by shaping ordered epitaxy-like growth using crystalline substrates that impose their lattice order to the adsorbed organic films. However, this latter approach may also result in a prohibitive increase of device fabrication complexity.

The low mobility leads to low electrical conductivity σ, given by $\sigma = ne\mu$, where n is the charge carrier density and e is the electronic charge. Thus, typical conductivities of organic materials are $\sigma \approx 10^{-6}$ S cm^{-1}. In addition to low conductivity, low mobility also results in a very low charge carrier velocity, $v = \mu F \approx 10$ cm s^{-1}, where F is the electric field of $\sim 10^5$Vcm^{-1}, typical of many devices.

Traps strongly affect charge transport properties since trapped charge carriers do no longer take part in charge transport [43]. However, their columbic charge will influence the electric field distribution in a device and therewith the transport. Further, if the release rate for trapped carriers is sufficiently low, there will be a significant time necessary to reach quasi-thermal equilibrium conditions. This causes delay and hysteresis effects in alternately devices operated with alternate voltages.

For all those reasons, it is very important for basic understanding and technical applications to know the origin of such trap states and to control them. Since trap states are favourite energy sites, they are situated in the energy gap of the semiconductor. In terms of classical semiconductor physics each localized state below the conduction band edge, which is able to capture an electron, is an electron trap and each localized state above the valance band edge, which is able to capture a hole, is a hole trap. But in organic semiconductors the width of the bands can be very narrow and extended states are rarely observed. The conduction band and the valance band are usually replaced by the lowest unoccupied molecular orbital (LUMO) and the highest occupied molecular orbital (HOMO), respectively.

Especially in amorphous layers of organic thin films the density of states (DOS) is quite well represented by a Gaussian-like distribution of localized molecular orbitals of individual molecules as presented in Fig. 1.5.

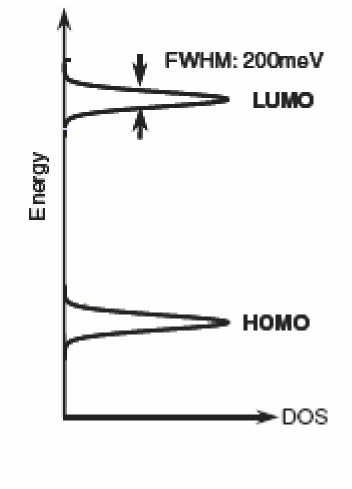

Fig. 1.5: Distribution of HOMO and LUMO levels in amorphous organic semiconductors.

.There are several sources for trap states:

(i) *Impurities*: Since the interaction between molecules in an organic solid is only weak, a specific molecule keeps its HOMO/LUMO position independent of the surrounding matrix. If the HOMO or LUMO of an incorporated molecule is positioned in the gap of the host molecules, it will form a trap state.

(ii) *Structural Defects*: Even if there are only molecules of the same species, the HOMO/LUMO levels may vary from molecule to molecule. The exact energy position of the HOMO/LUMO level is not only determined by the chemical structure of the molecule itself but also by the electronic polarisation of its surrounding. In case of polymers the effective conjugation length also affects the position of the HOMO/LUMO level. Structural imperfections will lead to a fluctuating surrounding and in case of polymers to a fluctuating conjugation length. In consequence a distribution of HOMO/LUMO levels has to be expected as presented in Fig. 5. The few states in the tail of this distribution below the transport energy will form the trap states. But structural defects are not necessarily restricted to the formation of tail states alone. If a specific kind of structural defect occurs with enhanced probability, for example, on grain boundaries in polycrystalline layers, structural defects may result in more or less discrete trap states deep in the gap.

(iii) *Geminate pairs*: Coulomb interactions are strong in organic solids. A hole and an electron will underlie a Coulomb interaction, even if several molecules separate them. Such a pair of Coulomb bond charge carriers is called geminate pair. If the recombination probability between the hole and the electron is suppressed by selection rules, a geminate pair forms a Coulomb trap. However, such traps can only occur if both types of charge carriers are present.

(iv) *Self-trapping*: An excess charge carrier residing on an organic molecule leads usually to a molecular deformation, which causes a lowering in energy for the excess charge carrier. Such a carrier together with its produced molecular deformation is a polaron. If two charge carriers share the same molecular deformation, a bipolaron is formed. Polarons or bipolarons are not really traps in the original meaning, since they are mobile. However, the mobility of a polaron or bipolaron is at least one or two orders of magnitude lower than the mobility of a “free” carrier. As long as the lowering in energy is only several tenth of meV, the effect can be neglected compared to other trap states. But in some polymers like polythiophene or polyacetylene the polaron or bipolaron formation causes a lowering in energy of several hundreds of meV. In such cases the charge carrier forms its own trap state on the polymer chain. Such a trapping mechanism is called self-trapping.

Due to the low conductivity and carrier velocities that are intrinsic to organic thin-film semiconductors, one would expect that very low bandwidth operation of common optoelectronic devices such as transistors, organic light emitting diodes (OLEDs) and photodetectors would provide a significant, if not fatal, limitation to their application in modern electronic systems. Although in many cases this is indeed true, the applications open to organic electronics are not targeted at simply replacing conventional electronics niches served by materials such as crystalline silicon.

1.4 Organic Field-Effect Transistors

1.4.1 Introduction

The concept of field-effect controlled current dates back to 1930. More than thirty years elapsed before the first device that really matched that early concept was realized, namely, the silicon-based metal-oxide- semiconductor field-effect transistor (MOSFET). Nowadays MOSFETs are omnipresent in our environment. Millions of them are located in the processors that equip personal computers and other microelectronic devices.

Besides its technological interest, the field-effect transistor can also be viewed as a tool for studying charge transport in solid materials. In particular, it gives direct access to charge mobility. For this reason, the electric field induced effect has been used in low mobility materials such as hydrogenated amorphous silicon (a-Si:H). In this case, an alternative geometry was used, the thin-film transistor (TFT), which differs from the conventional MOSFET in that the conducting channel is constituted by an accumulation layer rather than an inversion layer. It was only later that the technological interest of a-Si:H TFTs emerged, when applications where large area is needed appeared. Today, a-Si:H TFTs are largely used in the active matrix of liquid crystal display (AM-LCD). Organic semiconductors have been known since the late 1940s. However, apart from a very small number of preliminary works on conjugated small molecules and polymers, the first transistor based on an organic semiconductor was only reported in 1986 with a device made on an electrochemically grown polythiophene film. The possibility of fabricating organic TFT (OTFT) with small conjugated molecules was shown in 1989 with sexithiophene.

In spite of considerable improvements during the last years, the performance of OTFTs remains far beyond that of their inorganic counterpart, except for a-Si:H. For this reason, applications are envisioned where low fabrication costs and large area are of primary importance. These include electronic bar codes and identification tags, and, to a lesser extent, active matrix elements for organic flat panel displays. With this in mind, more and more industrial groups have recently initiated research programs in the field of organic transistors.

1.4.2 Operating Mode

An OTFT is analogous to its inorganic counterpart in basic design and function [44]. It is a three-terminal device, in which a voltage applied to a gate electrode controls current flow between a source and drain electrode under an imposed bias. Within the basic TFT design, there are two types of device configuration: top contact and bottom contact. The former involves building source and drain electrodes onto a preformed semiconductor layer, whereas the latter is constructed by depositing the organic over the contacts. A basic schematic of both structures is shown in Fig. 1.6. Top contact devices have been reported to have superior performance compared with their bottom contact counterparts [20]. Each of these devices has particular advantages and disadvantages in the fabrication process, which will be discussed below.

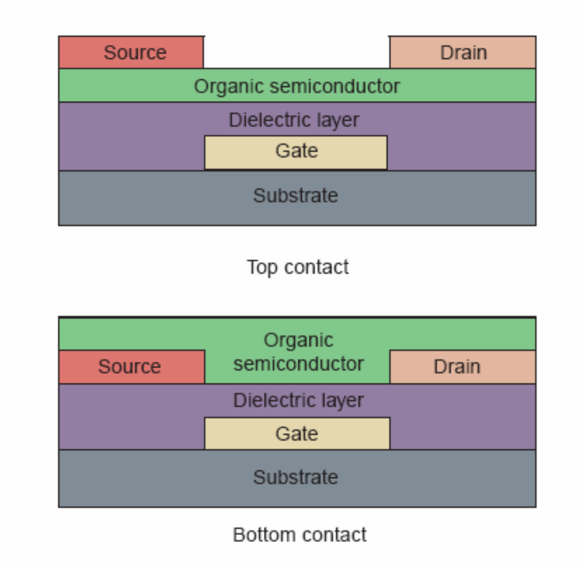

Fig. 1.6: Top and bottom contact OTFT architectures.

To demonstrate the operating mode of the thin-film transistor, typical current–voltage characteristic is shown in Fig. 1.7.

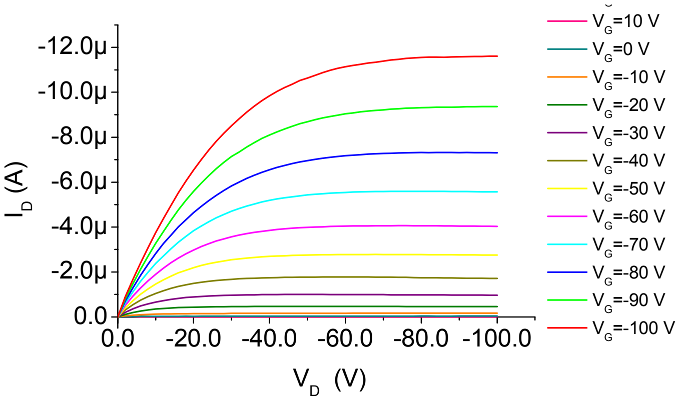

Fig. 1.7: Output characteristic of a typical Organic Thin Film Transistor

These curves were measured on a device made of pentacene as the semiconductor and gold as source and drain electrodes. The Fermi level of gold and HOMO-LUMO levels of pentacene are shown in Fig. 1.8. When a positive voltage is applied to the gate, negative charges are induced in the device channel.

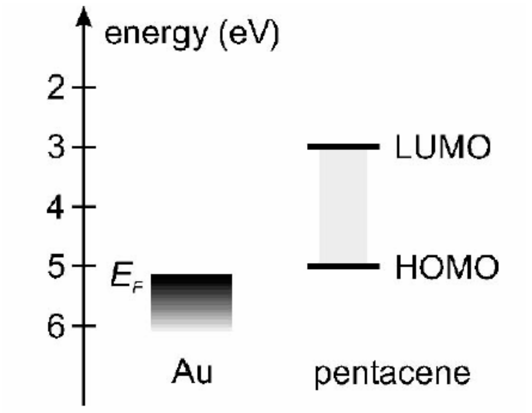

Fig. 1.8: Work function of gold compared to the energy of the frontier orbitals of pentacene.

As it can be seen in Fig. 1.8, the Fermi level of gold is far away from the LUMO level, so that electron injection is very unlikely.

Accordingly, no current passes through the pentacene layer, and the small measured current essentially comes from leaks through the insulating layer. When the gate voltage is reversed, holes can be injected from the source to the semiconductor, because the Fermi level of gold is close to the HOMO level of pentacene. Accordingly, a conducting channel forms at the insulator-semiconductor interface, and charge can be driven from source to drain by applying a second voltage to the drain. For this reason, pentacene is said to be a *p*-type semiconductor.

When a voltage is applied between source and gate, a charge is induced at the insulator-semiconductor interface. This charge forms a conducting channel the conductance of which is proportional to the gate voltage.

At low drain voltages, the current increases linearly with drain voltage (Fig. 6), following Ohm’s law. When the drain voltage is compared to gate voltage, the voltage drop at the drain contact falls to zero and the conducting channel is pinched off. This corresponds to the so-called saturation regime where the current becomes independent of the drain voltage.

1.4.3 Analytical model

The usual way [45] to calculate the current-voltage characteristic of a Field-Effect Transistor consists of estimating the elemental resistance *dR* of an elemental segment *dx* of the conducting channel, given by Equation 1.1, where *Z* is the channel width, μ the carrier mobility, and *Q(x)* the surface charge at *x* (Fig.1.9)

$$dR = \frac{dx}{Z\mu|Q(x)|} \tag{1.1}$$

In a thin-film device, we have to account for both the bulk charge, Q_0, and that in the accumulation layer $Q_s(x)$. If the latter extends all over the channel (i.e., there is no depletion region), Q_0 is a constant while the charge induced in the accumulation layer is given by Equation 1.2

$$Q_s(x) = -C_i\left[V_g - V_{fb} - V_s(x) - V(x)\right] \tag{1.2}$$

where C_i is the capacitance of the insulating layer and V_g the gate voltage. V_{fb} is the so-called flat-band potential, which accounts for any work-function difference between the semiconductor and the gate, and $V_s(x)$ is the ohmic drop through the semiconductor.

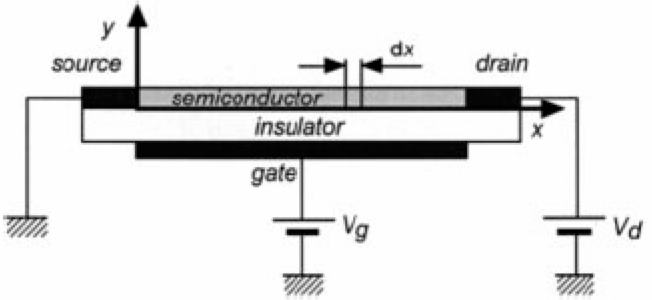

Fig. 1.9:. Schematic view of an organic field-effect transistor (OFET).

It can be shown that for gate voltages in excess of a few volts, most of the ohmic drop occurs through the insulator, so that this contribution can be neglected in the most general case. The last term accounts for the drain bias V_d. In the gradual channel (long channel) approximation, which is used here, one assumes that the electric field along y (perpendicular to the channel) largely exceeds that along *x* (parallel to the channel). This is the case when the channel length L is substantially larger than the insulator thickness. Then, *V(x)* only depends on the drain voltage, and gradually increases from 0 to V_d as one moves from the source to the drain. The drain current Id is now obtained by integrating Equation 1.4.

$$dV = I_d dR = \frac{I_d dx}{Z\mu\left|Q_s(x) + Q_0\right|} \tag{1.3}$$

Note that, because we are dealing with an accumulation layer, *Q(x)* and Q_0 have identical sign. For a constant mobility and integrating from source ($x = 0$, $V = 0$) to drain ($x = L$, $V = V_d$) we obtain Equation 1.4.

$$I_d = \frac{Z}{L}\mu C_i\left[\left(V_g - V_0\right)V_d - \frac{V_d^2}{2}\right] \tag{1.4}$$

We define here a zero voltage, V_0, given by Equation 1.5, where the sign of the right-hand side corresponds to that of the majority carriers.

$$V_0 = \pm\frac{qn_0 d_s}{C_i} + V_{fb} \tag{1.5}$$

The zero voltage accounts for the fact that a non-zero drain current flows in the device at zero gate bias; its sign is inverse to that of the gate bias. The field-effect mobility in the linear regime can be estimated from the so-called transconductance, Equation 1.6, obtained by deriving Equation 1.4 with respect to the gate voltage.

$$g_m = \left|\frac{\partial I_d}{\partial V_g}\right|_{V_d = const} = \frac{Z}{L}\mu C_i V_d \tag{1.6}$$

Equations 1.4 and 1.6 correspond to the linear regime, where $V_d < V_g$. When $V_d > V_g$, the accumulation layer near the drain changes to a depletion layer. In the depletion regime, there is no free charge at the insulator-semiconductor interface; instead, an insulating layer grows there, which reduces the effective thickness of the bulk semiconductor film, so that the drain current is now given by Equation 1.7, where W is the depletion layer width

$$I_d dx = Zqn_0\mu\left(d_s - W(V)\right)dV \tag{1.7}$$

We assume that the accumulation layer extends from the source up to a point where *V(x)* = V_g, beyond which it is replaced by a depletion layer. The drain current is hence given by the sum of two integrals (Eq. 1.8).

$$I_{dsat} = \frac{Z}{L}\mu\left[Ci\int_{0}^{V_g}\left(V_g - V_0 - V\right)dV + qn_0\int_{Vg}^{Vdsat}\left(d_s - W\right)dV \right] \qquad (1.8)$$

The result, after some simplifications is given by Equation 1.9,

$$I_{dsat} = \frac{Z}{2L}\mu C_i\left(V_g - V_p\right)^2 \qquad (1.9)$$

Equation 1.9 is frequently used to estimate the mobility of OFETs through a plot of the square root of I_{dsat} as a function of the gate voltage. However, its validity rests on several underlying assumptions, namely a constant mobility, and the equality between the density of free carriers and that of dopants.

Most efforts to improve OFETs have been aimed at the enhancement of the field-effect mobility, which governs most of the electrical characteristics of the device. Best results to date have been obtained with well defined molecules, the most prominent of which are the thiophene oligomers and pentacene. Differences can often be observed in mobility values calculated in the linear region and the saturation region. The linear region mobility can be affected by contact problems, and in such cases there are departures from the linearity of the I_D versus V_D curve which can lead to underestimation of mobility.

Another important parameter for practical uses is the on-off current ratio, that is, the ratio between the drain current at given drain and gate voltages (on state), and the drain current at the same drain voltage and at zero (or positive) gate voltage (off state).

Extracting key parameters such as mobility and threshold voltage from the current-voltage characteristics of OFETs has become a controversial issue. In most cases, basic equations are easy to use, and at first glance, they satisfactorily describe the actual curves. However, their derivation rests on several approximations that are not always fulfilled, particularly in organic semiconductors. There are now well documented experimental facts that cast doubts on the validity of an overly simplified mobility estimation. Among these, are the bias dependence of the mobility and problems with contact resistance.

To date, a comprehensive, widely accepted method for interpreting current-voltage curves does not yet exist.

1.4.4 Parameter Extraction Methods

Charge mobility μ in OFETs is gate voltage dependent [46]. The dependence comes form the fact that charge transport is limited by traps localized near the transport band edge. When a gate voltage V_g is applied, the Fermi level at the insulator-semiconductor interface moves towards the band edge, leading to the filling of the traps; consequently, trapping becomes less efficient and mobility increases. The gate bias dependence poses serious problems for the determination of the charge mobility. The voltage distribution in transistors is controlled by two independent biases. Therefore, the voltage drop through the insulator is not the same at the source and at the drain; as soon as a drain voltage V_d is applied, the voltage drop is V_g at the source and V_g-V_d at the drain. This means that being the mobility gate-bias dependent, it will vary all along the conducting channel.

The gate-bias dependence of the mobility can be expressed using Eq. 1.10 where V_t is the threshold voltage and K and γ empirical parameters.

$$\mu = \left(V_g - V_t\right)^{\gamma} \tag{1.10}$$

An approach to estimate the mobility consist of using numerical simulations. An alternative, more straightforward approach consist of carrying out the measurements under the lowest possible value of V_d, so that the mobility remains practically constant all along the conducting channel. In practice, the most useful curve is the transfer characteristic (Id vs. Vg) in the linear regime.

It has been demonstrated that the field-effect mobility in polycrystalline organic films is improved when the grain size is increased. It seems, therefore, reasonable to assume that charge transport is limited by grain boundaries [47]l. A model where transport is controlled by grain boundaries has been used to describe the charge transport in the polycrystalline organic materials [48-50]. The model consists in dividing the polycrystalline material in high (the crystal grain) and low (the boundaries) conductivity regions. The size of the high conductivity domains is assumed to be much larger than that of the low conductivity regions. As grains and grain boundaries are connected in series, the effective mobility of the polycrystalline medium is given by:

$$\frac{1}{\mu} = \frac{1}{\mu_g} + \frac{1}{\mu_b} \tag{1.11}$$

where μ_g and μ_b are respectively, the mobility in the grain and the grain boundary. If $\mu_g \gg \mu_b$, the overall mobility only depends on charge transfer across boundaries. A general assumption is that a back-to-back Schottky barrier forms at the intergrain region. The polycrystalline film is described as trap-free grains separated by boundaries with high trap density. A crucial parameter for this model is the size of the grains.

Charge transport across boundaries mostly depends on how the grain size l compares to Debye's length L_D:

$$L_D = \sqrt{\frac{\varepsilon_s KT}{q^2 N}} \tag{1.12}$$

where ε_s is the permittivity of semiconductor, q is the electron charge and N is the doping level in the grain.

If that the grain size is lower then the Debye length, the film behaves as if the traps were uniformly distributed. On the contrary, if the grains are much larger than the Debye length, charge transport is determined by the mechanism of transfer through grain boundaries.

A plot of μ/μ_g as a function of grain size is shown in Fig. 1.10: mobility tends to increase linearly with grain size at low grain sizes, and then saturates to its value in the grains.

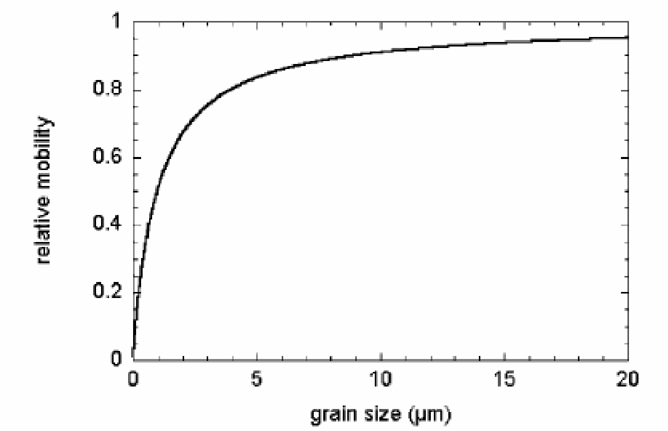

Fig. 1.10: Relative mobility as a function of grain size in a polycrystalline semiconductor film.

Until recently, the problem of contact resistance in OFETs was hardly evoked. This is because the performance of the devices was low. As the mobility of OTFT improves, limitations by contact resistance are getting more and more crucial, and finding ways to reduce them is at present a key issue.

The contact resistance [51,52] was at first calculated through modelling. Figure 1.11 shows three equivalent circuits used to model the OTFT. One is composed only of the device. In the second one, series resistances have been added at source and drain. The third circuit also includes head to toe diodes to account for nonlinearities in the contact resistance.

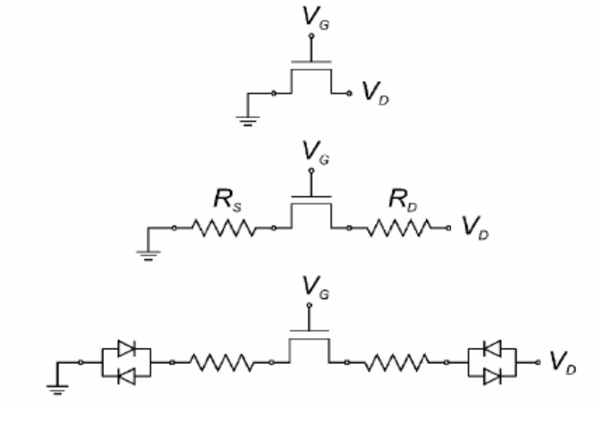

Fig. 1.11: Equivalent circuit of the OFET without (top) and with (middle and bottom) contact resistances. The bottom circuit includes diode to account for non-linearity.

The contact resistance is accounted for by introducing a voltage drop R_cI_d, where R_c is the contact resistance. That is, the drain voltage is replaced by $V_d - R_cI_d$. The resulting equation for the drain current is given by Eq. 1.13.

$$I_d = \frac{Z}{L}\mu C_i\left[(V_g - V_0)(V_d - R_cI_d)\right] \tag{1.13}$$

The channel conductance g_d is then given by Eq. 1.14

$$g_d = \frac{\partial I_d}{\partial V_d} = \left(\frac{1}{\frac{Z}{L}\mu C_i(V_g - V_0)} + R_c\right) \tag{1.14}$$

The dependence of the current/voltage characteristics on channel length can be used to extract parasitic resistances that include various components related to the contacts and other effects that are independent of channel length. In the linear regime, the overall device resistance R_{on} can be written as the sum of the intrinsic channel resistance R_{ch} and a contact resistance R_c according to Eq 1.15

$$R_{ON}(L) = R_{ch}(L) + R_c = \frac{L}{Z\mu C_i(V_g - V_0)} + R_c \tag{1.15}$$

While the contact resistance is independent of channel length, the channel resistance is proportional to the channel length.

Consequently, the relative influence of the contact resistance increases as the channel length is reduced. The contact resistance R_c can be extracted by determining R_{on} from the linear regime of the transistor characteristics and plotting the width-normalized $R_{on}W$ as a function of L for different gate voltages. This plot contains the intrinsic mobility and threshold voltage of the channel, independent of the channel length. Thus, plotting the reciprocal slope, which is equivalent to the channel conductance, versus the gate voltage should yield a straight line.

The contact resistance corresponds to the y-axis intercept of the extrapolated linear fit of R_{on} versus L. This method is known as Transfer Line Method (TLM) [53-55] and is exemplified in Fig. 1.12

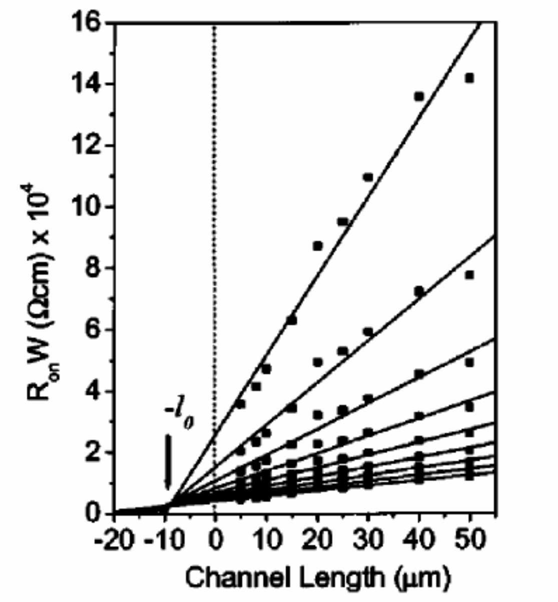

Fig. 1.12: Width normalized resistance as a function of channel length at gate voltages from −20 to −100 V.

The problem with the TLM is that it requires measurements on several devices, and it cannot be taken for granted that the contact and channel resistances do not vary from one device to another. Therefore, when plotting the total resistance as a function of channel length, scattering appears and data are not strictly aligned, as can be seen in Fig. 1.14. Moreover, the contact resistance is strongly gate-bias dependent. Furthermore, taking into account the gate bias dependence of the contact resistance in Eq. 1.15 would introduce too many independent parameters and make the fitting procedure hazardous.

References

1. Forrest, Nature 428, 911-918, (2004)
2. Reese C. et al., Materials Today (2004)
3. Dodabalapur A., Nature 434,151-152, (2005)
4. Hamers R.J., Nature 412, 489-490, (2001)
5. McCullogh, Nat. Mat. 4, 583-584, (2005)
6. Dimitrakopoulos et al., IBM J.Res. Dev. 45, 1, 11-27, (2001)
7. Dodabalapur A., Nature 434,151-152, (2005)
8. Spec. Iss. on Flex. Elect. Tech., P.1, P.2, Proc. IEEE, 93, 7, 1235, (2005)
9. Chason et al., Proc. IEEE, 93, 7, 1348, (2005)
10. Fahlman M. et al, Surface Science 500, 904–922, (2002)
11. C.K. Chiang et al., Phys. Rev. Lett. 39, 1098, (1977)
12. Torsi L. et al., Solid State Electronics 45, 1479-1485,(2001)
13. Newman et al., Chem. Mater. 16, 4436-4451, (2004)
14. Singh Th.B. etr al., Organic Electronics 6, 105–110, (2005)
15. Meijer E. J. et al., Nature Materials, 2, 678-682, (2003)
16. Singh Th. B. et al., J Appl. Phys., 97, 114508 (2005)
17. Singh Th. B. et al., Adv. Mater.17,2315-2320, (2005)
18. Ahles, M.et al., Appl. Phys. Lett. 85, 4499–4501 (2004).
19. Chua L.L. et al., Nature 434, 194-199, (2005)
20. Dimitrakopoulos et al, Adv. Mater. 14,2, 99, (2002)
21. H. Klauk et al., J. Appl. Phys. 92, 5259, (2002)
22. V. Y. Butko et al., Appl. Phys. Lett. 83, 4773, (2003)
23. Sirringhaus, Adv. Mat. 17, 2411-2425, 2005
24. Yoon et al., PNAS, 102, 13,4678 (2005)
25. Majewski et al., J. Phys. D: Appl. Phys. 37, 21-24, (2004)
26. Unni et al., J. Phys. D: Appl. Phys. 38, 1148–1151, (2005)
27. Unni et al., J. Mat. Sc. 41, 6, (2006),
28. Lavareda et al., Thin Solid Film, 427, 71, (2003)
29. Halik M. et al., Nature 431, 963-966 ,(2004)

30. Park et al., Appl. Phys. Lett., 85, 15, 3283-3285,(2004)
31. Choi Y.W. Et al., IEEE Trans. Elec.Dev., 52,12, 2819,(2005)
32. Wang A. et al., IEEE Trans. Elect. Dev., 53,1,9, (2006)
33. Veres J. et al., Chem Mat. (2004)
34. Blanchet et al., J. Imag. Sc. Tech, 47, 4, 296-303, (2003)
35. Parashkov R. et al., Proc. IEEE, 93,7,1321, (2005)
36. Chason Et al., Proc. IEEE, 93, 7, 1348, (2005)
37. Geissler M. et al., J. Am. Chem. Soc. 122, 6303-6304, (2000)
38. Delamarche E. et al., Langmuir 19, 8749-8758, (2003)
39. Louwet et al., Synt. Met.,135-136, 115-117, (2003)
40. Cosseddu et al., Appl. Phys. Lett., 88, 023406, (2006)
41. Bredas J.L. et al. PNAS 99,9, 5804–5809, (2002)
42. Salaneck et al., Phys. Rep. 319, 231, (1999)
43. Schmechel R. et al., Phys. Stat. Sol. A. 201, 6, 1215-1235, (2004)
44. Horowitz G., J. Mater. Res. 19, 7, 1946-1962, (2004)
45. Horowirz et al., Adv. Mat.,10, 12 (1998)
46. Horowitz et al., Adv.Func. Mater. 14, 11, 1069-1074, (2004,)
47. Bourguiga R. et al., Eur. Phys. J. AP 19, 117–122, (2002)
48. Horowitz et al., Adv. Mat., 12,14, 1046-1050, (2000)
49. D. Knipp, et al., J. Appl. Phys. 93, 347, (2003);
50. Bolognesi A. et al., IEEE TED, 51,12,1997-2003, (2004)
51. Necliudov et al., Solid-State Electronics 47,259–262, (2003)
52. Hamadani et al. Proc. IEEE, 93, 7, (2005)
53. Klauk H. et al., Solid-State Electronics 47, 297–301, (2003)
54. Zaumseil J. Et al., J. Appl. Phys., 93,10,6117-6124, (2003)
55. Meijer E. J. et al., Appl. Phys. Lett., 82,4576, (2003)

CHAPTER 2

An Overview on Organic Field-Effect Sensors

2.1 Introduction

For a broad range of sensing application there is a large demand for small, portable and inexpensive sensors. Specifically, chemical, biological and mechanical sensors using organic field-effect transistors are beginning to attract interest. The advantages of organic semiconductors based devices include the compatibility with plastic substrates, the low-cost and low temperature processing and the possibility of fine tuning their chemical-physical properties by precise organic synthesis. Molecular structure and morphology can be adjusted to enhance sensitivity and selectivity in chemical and biological sensors and detection limits and sensitivity also benefit from the signal amplification that is inherent in transistor devices, allowing transistor based sensors to outperform chemo-resistors as well as amperometric and potentiometric sensors. Furthermore, organic field-effect transistors are inherently flexible and very inexpensive to fabricate even for large areas, and these features make them attractive for sensing applications.... In addition, the possibility of fabrication of sensors based on thin multilayered structures, in form of sensorized flexible film, allow also to fabricate low-cost pressure and strain sensors. Under the application point of view, recognition of tactile information is very important in a variety of fields, e.g. to provide robots with an artificial sense of touch; organic field-effect transistors can be employed in fact to obtain an “electronic skin” that embeds large matrices of active, sensitive devices. At present, flexible piezoresistive materials as conductive rubber are being used to obtain sensing elements for pressure sensitive matrices, but addressing each passive sensor requires a flexible switching matrix that cannot be realized with present-day silicon based electronics.

The rapid development of organic electronics and the improvements in the compatibility of OFETs and microfluidics opens wide horizons for the use of organic semiconductor based devices in compact sensing systems or biochips.

However, several issues are still open, particularly those related to the very long term stability, the device-to-device variability, degradation mechanism and sensor lifetimes.

In this chapter we recollect the work that has been done to develop chemical, biological and mechanical sensor based on organic field-effect transistors.

2.2 Gas Sensors

The basic structure of an OFET based gas sensor is shown in Figure 2.1. The active semiconductor layer is exposed to the analyte on one side and the gate electrode is separated from the active layer by an insulator on the other side. This is simply a conventional OFET with a bottom gate, where the active layer is exposed to either gas or liquids containing the analyte of interest.

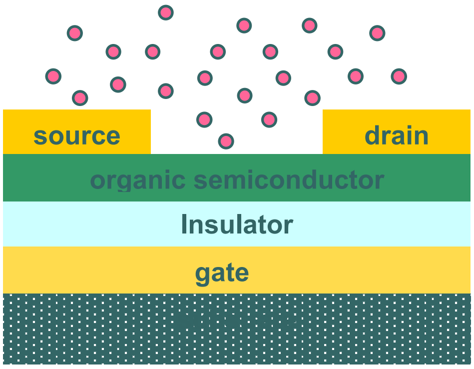

Fig 2.1: Schematic cross section of an organic field-effect transistor (OFET) used as gas sensor

OFET based gas sensors, as OFETs in general, operate in accumulation mode. Depletion mode operation can be used to lower the off-current of the device[2]. In fact, only highly pure active layers originate devices that are off already at zero gate bias [3] and no inversion mode operation can be seen in polycrystalline OFETs [4]

Detection is accomplished when the organic semiconductor is directly exposed to the analyte. The concept of using the gate bias to improve the sensor performance was first introduced when it was proposed that an OTFT could serve as a multi-parametric sensor [5].

Multi-parametric operation results from the combination of the two conductivity regimes: 3-D transport at zero gate bias and 2-D transport at $V_G > V_{t.}$. When an OTFT operates as a sensor, the response in terms of drain current can be measured in the off and on states. Given the different physical nature of these two conductivity regimes, a multi-parametric response to an analyte can be recorded. With zero gate bias, the OFET is a chemo-resistor that measures the variation of the organic film conductivity upon exposure to a chemical species. In the on state, changes in the drain current are related to variations of mobility and threshold voltage that depend, in turn, on the volume density of trapped charges and the potential barrier, respectively. The sensing mechanism can be plausibly depicted as the analyte molecules being adsorbed or trapped at the grains surface, and this changes the film mobility and V_t [6].

Reliability is one of the major issues in developing OFET based gas sensors. The transistor configuration is very helpful in this respect, particularly when they are operated in pulse mode. In fact, continuous biasing is not generally well tolerated by organic devices and current drifts are often measured. The electrical responses are evaluated on the basis of a quiescent operating point, normally fixed V_D and V_G biases in the saturated region of the I–V characteristics [7]. The transient drain current in the absence (baseline current) and presence of the analyte is measured with the device operating in pulsed mode. The reverse-gate-bias pulse applied after each forward pulse completely resets the device, restoring the original baseline. Thanks to this effect, OFET based sensors exhibit extremely good response repeatability.

Recently, the dependence of the sensor response on the surface morphology, have been investigated by Torsi et al. [8]. They used a thin film of α,ω-dihexyl-α-hexathiophene (DHα6T) deposited by vacuum sublimation. A saturated vapour of 1-pentanol in a dry air carrier gas was typically used as the analyte, the concentration of the vapour was in the thousand parts per million range and the transistors were subjected to a constant flow rate of gas, which was switched between dry air and the vapour.

In Fig. 2.2 transmission electron micrographs of samples grown at four different substrate temperatures are reported. The morphology varies from a granular morphology with very small, irregular nano-domains with diffuse grain boundaries (panels a and b) through which the vapours may penetrate the thin film and bind near the channel, to a much more regular, lamellar one exhibiting much lower surface roughness (panels c and d). These grains are large, regular, and flat, thus reducing the ability of gases to adsorb onto them. The influence of the surface morphology on the sensor response is illustrated in Fig. 2.3. The response is strong for the low temperature films, which have more grain boundaries, and weaker for the high-temperature ones with fewer grain boundaries and a more compact morphology.

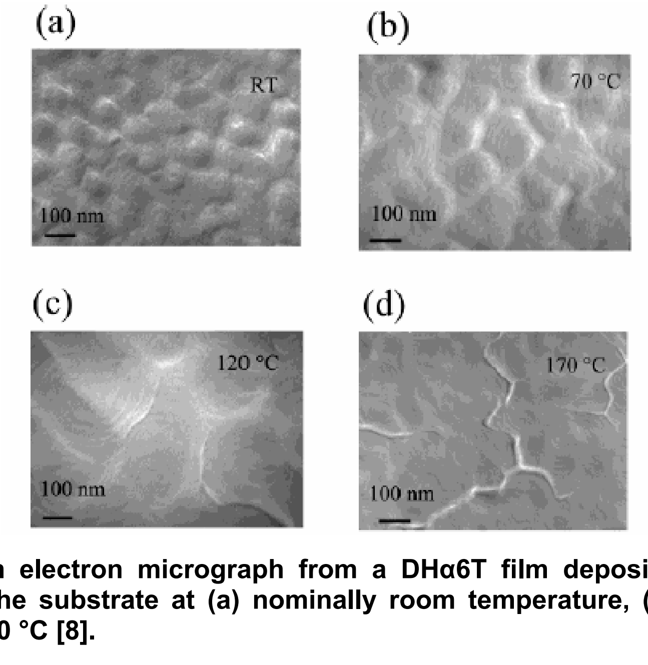

Fig. 2.2: Transmission electron micrograph from a DHα6T film deposited by thermal evaporation keeping the substrate at (a) nominally room temperature, (b) *T*=70 °C, (c) *T*=120 °C, and (d) *T*=170 °C [8].

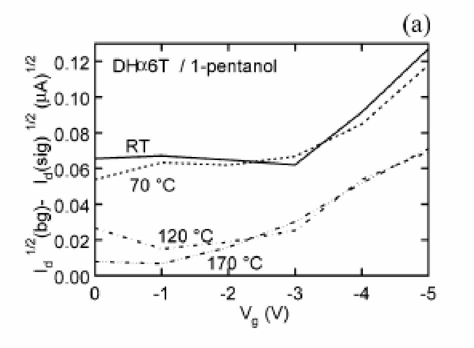

Fig. 2.3: Change in square root of drain current as a function of gate voltage, for sensors with DHα6T films deposited at different substrate temperatures exposed to 1-pentanol [8].

The morphology of DHα6T films of different thicknesses deposited at room temperature is shown in Fig. 2.4. The surface of the ultrathin film (panel a) appears flat and only few regions are covered by three-dimensional grains while the surface morphology becomes more structured as the films grow thicker (panels b-d) An increase in their height occurs as well. As a result, the number of grains in the films as well as of grain boundaries increases with DHα6T film thickness. The influence of the surface morphology on the device response is illustrated in Figure 2.5: the response increases with increasing film thickness because an increase in the thickness of the deposited film also increases the number of grains and grain boundaries, providing more sites of interaction with the vapour.

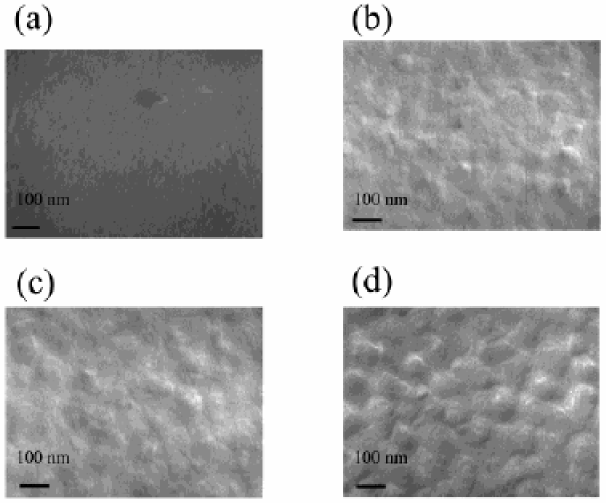

Fig. 2.4: Transmission electron micrograph from a DHα6T film of different thickness (a, 27 nm; b, 53 nm; c, 61 nm; and d, 70 nm) [8].

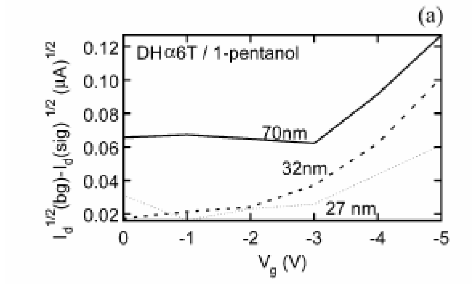

Fig. 2.5: Change in square root of drain current as a function of gate voltage, for sensors with DHR6T films of different thicknesses exposed to 1-pentanol

The authors also examined the morphology of a series of alkylsubstituted hexathiophenes (α-hexathiophene (α6T), α,ω -dibutyl- α6T (DB α6T), α,ω - didodecyl- α6T (DDD α6T), α,ω -dioctadecyl- α6T (DOD α6T), and α,ω -dihexyl- α-quaterthiophene) in order to investigate the role of chemically different linear chains, in conferring recognition properties to an OFET gas sensor.

All these molecules behave differently in terms of grain size, number of grain boundaries, morphology and molecular packing.

The larger alkyl substituents on the oligomers could enhance the device response by increasing the adsorptivity of grain surfaces, by increasing the amount and the accessiblity grain surface area. The authors demonstrate that the response is enhanced as the number of grain boundaries increases. They proposed that vapour molecules are adsorbed more readily at grain boundaries, where they are closer to the conducting channel at the interface with the dielectric and can more strongly affect the electrical response.

Tanese et al. [9] demonstrated that also the semiconductor/gate dielectric interface and the gate bias play a critical role in determining the sensing mechanism of an OFET sensor. They suggest that the strong effect of the interface properties on the OTFT sensing mechanism is due to the ability of the analyte to percolate through the active layer down to the interface with the dielectric, where the field-induced charges are located. Moreover, as the interaction between polycrystalline systems and the analyte molecules takes place at the surface of the crystalline grains in the films [8], the source-drain current decrease or increase observed upon exposure to vapour can be considered as caused by hole trapping, at the grain boundaries or at the interface of the grains with the dielectric surface, or by some kind of doping of the channel material respectively. Devices where the organic semiconductor/gate dielectric interface is composed of materials with different properties in terms of the intensity of the associate dipole moment, for instance this is the case of the interface between Pentacene (low dipole moment) and SiO_2 (highly polar), have shown to undergo both doping and trapping effects, as a current increase is observed by operating the sensors at low gate biases and a current decrease is observed operating the devices at higher gate biases. It appears that trapping is favoured at high gate voltages when materials of a different nature are interfaced, probably because the low level of matching favours the generation of trap states at the interface. Conversely, homolog interface devices exhibit an almost fully reversible current increase at all gate biases ascribed to a doping process. Conversely, devices in with the semiconductor and the gate dielectric show similar properties in terms of associate dipole moment exhibit an almost fully reversible current increase at all gate biases ascribed to a doping process.

In addition, the strategy of using properly functionalized organic semiconductors can be followed to obtain specific recognition. Tanese et al. [10] proposed an OFET gas sensor based on active polymeric layers functionalized for the detection of volatile chiral molecules. Crone et al.[7] used OFET based sensors for fabricating selective arrays. Different semiconductor as oligothiophenes, phthalocyanines, and other were exposed to a variety of gaseous analytes, including alcohols, ketones, thiols, nitriles, esters, and ring compounds. By measuring the source–drain current the authors were able to observe patterns associated with each analyte due to the variety of different response mechanisms associated with different semiconductor–analyte pairs. It is important to note that this selectivity can be further tuned by modifying both the morphology and molecular structure of the active organic materials. Crone et al. [11] have also demonstrated that OTFT sensors are superior to chemo-resistive sensors owing to the fact that they can more easily be incorporated into sensing circuits with enhanced performance over discrete sensors.

In conclusion OFET based gas sensors show superior performance compared to resistive, amperometric and potentiometric sensors. The amplification inherent to transistors enhances their sensitivity, and they offer several opportunities for achieving selectivity, including multiparameter measurements and direct integration with specific recognition elements.

Some accurate and useful reviews on organic field effect based gas sensors have been published by Torsi [12] and Mabeck [1]

2.3 Chemical and Biological Sensors

There are many applications for which the analyte of interest must be detected in an aqueous medium rather than in the vapour phase as discussed above for gas sensors. For example, biological analytes and biologically derived recognition elements are only active in aqueous media.

Therefore, it is necessary to explore the operation of OFETs in aqueous media in order to extend their applicability to a broader range of sensing needs.

OFET based chemical sensors in aqueous media in which the organic semiconductor is in direct contact with both stationary and flowing water have been demonstrated by Someya et al. [13]. They described the integration of micro-fluidic flow channels with OFETs through the definition of regions of low surface energy around the semiconductor-metal contacts. The contact regions were coated with a hydrophobic material, such as a fluorinated polymer, that repels water. With this arrangement, water flow is directed perpendicular to the electronic current flow direction with the fluid in contact with the active region of the device. They also utilized an adhesion layer to make the semiconductor film as resistant as possible to water-induced delamination from the substrate. In this way, devices that are active under standing water are also active under flowing water. The basic device structure and the integration of the device with microfluidics are shown in Fig. 2.6.

Microfluidic channels were formed by fluorochemical coating so that water guides could be realized parallel to the gold electrodes,in this way water flows across the electronic active layers perpendicular to the current flow direction.

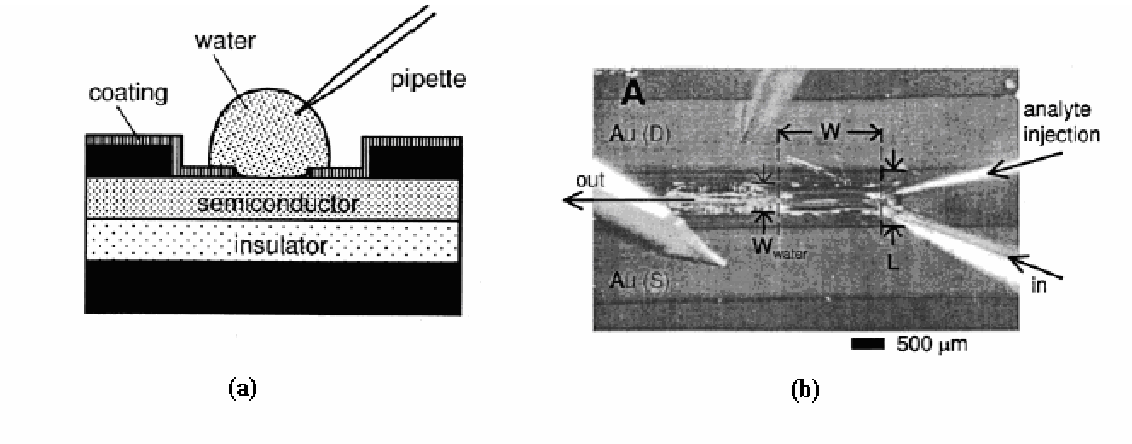

Fig. 2.6: The basic structure of the organic semiconductor device reported in [13] and the configuration of the analyte delivery system and recording electrodes during an experiment. Fluorochemical-coated layers were applied to prevent water from touching the electrodes. Surfaces of organic active layers of field-effect transistors were in direct contact with water. (b) Integration of organic transistor and microfluidics. The region between the two dashed lines in the figure is the organic active layer.

The use of the fluorinated coating near the contact provided enough contrast in the interfacial surface energy with the semiconductor surface to protect the contacts and also to define the shape of the microfluidic channel

Alternatively, in chemical sensors and biosensors in aqueous solution the gate insulator instead of the semiconductor layer can be exposed to the analyte of interest. Figure 2.7 shows the structure of an Ion-Sensitive Organic Field Effect Transistor (ISOFET).

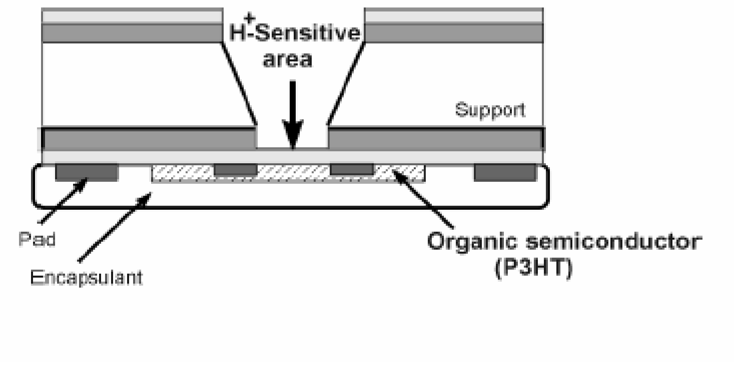

Fig 2.7: Schematic cross section of an ion-sensitive organic field effect transistor (ISOFET) [17]

In ISOFETs, instead of using a metallic gate electrode on the dielectric layer as is usually done for OFETs the dielectric layer is exposed to an aqueous solution and a Ag/AgCl electrode is used as the gate.

The electrode, that is a *nonpolarizable* interface, guarantees a constant potential drop at its interface, in other words the potential difference across is virtually fixed and consequently it acts as a “reference”. The drain current is modulated by field effect doping as in OFETs but the electric field across the insulating gate dielectric is controlled by ions at the electrolyte/insulator interface.

This setup is similar to conventional silicon-based ion-sensitive field-effect transistors (ISFETs), but the use of organic semiconductors for ISOFETs offers advantages in terms of fabrication cost and compatibility with plastic substrates. The detection mechanism in ISOFETs is similar to that of ISFETs (for an accurate description of the ISFET working principles see Chapter 4) in the sense that pH variations modifies the voltage drop across the dielectric/semiconductor interface, generating a current variation.

In p-type organic transistors for instance, the semiconductor contains positive charge carriers induced by the unintentional doping in the bulk of the polymer as well as by the field-effect that creates the accumulation layer. The bulk charge is a constant while the accumulated charge is gate voltage dependent. If a bias variation $\delta\psi$ occurs at the gate dielectric/electrolyte interface, it will be reflected in the band bending at the dielectric/semiconductor interface, leading to a charge variation

$$\delta Q = C_{ins}\delta\psi$$

where C_{ins} is the dielectric capacitance [14]. Depending on the sign of the bias, the charge in the channel will be incremented (accumulation) or decreased (depletion) by this amount. If the charge increment has a mobility μ, the variation of the current in the transistor channel is described by the equation:

$$\delta I_D = \frac{W}{L}\mu C_{ins} V_D \delta\psi \tag{2.1}$$

where W/L is the ratio between the channel width and length of the transistor. In a certain pH buffer, the potential drop at the electrolyte/dielectric interface can occur by applying an external voltage V_G on the reference electrode. When the pH buffer solution is changed while keeping V_G constant, the potential drop at the electrolyte/dielectric interface will vary with pH according to the site binding theory (see appendix Chapter 4) [15]. The proton sensitivity of FET type chemical sensors is usually described by coupling the site-binding theory with the solid state physics of the electronic device. This model is based on the fundamentals of the thermodynamic equilibrium between the H^+ concentration in the bulk of the solution and the electrical potential at the dielectric surface. The charge neutrality is postulated for the whole structure and therefore the surface charge has to be compensated by oppositely charged ions in solution. The arrangement of the ions from the dielectric surface to the bulk of the solution determines the dependence of the surface potential on the ion concentration and the surface charge. The surface of any metal oxide always contains hydroxyl groups, in the case of silicon dioxide, SiOH groups. These groups may donate or accept a proton from the solution, leaving a negatively charged or a positively charged surface group respectively, as schematically represented by Fig. 2.8.

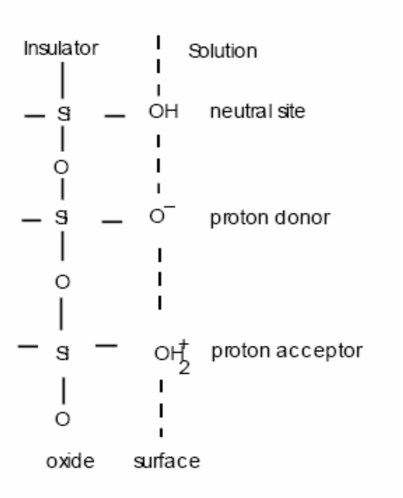

Fig. 2.8: Schematic representation of the site-binding model

The mechanism responsible for the oxide surface charge can be described by the site-binding model, which describes the equilibrium between the so-called amphoteric SiOH surface sites and the H^+ ions in the solution. The reactions are:

$$SiOH \Leftrightarrow SiO^- + H^+$$
$$SiOH + H^+ \Leftrightarrow SiOH_2^+$$

with H^+ representing the protons in the bulk of the solution. From these chemical reactions it is clear that an originally neutral surface hydroxyl site can bind a proton from the bulk solution, becoming a positive site as well as donate a proton to the solution, leaving a negative site on the oxide surface. For this reason it is called an amphoteric site [15].

For a silicon based ion-sensitive field effect transistor, the pH effect is reflected in a threshold voltage shift and the sensitivity is defined as the threshold voltage variation when the pH is changing one unit [16]. However, for the organic devices such a definition of the gate sensitivity is not easy to consider since many of assumption considered in this model are no longer valid. The charge accumulated in the channel of the organic device, the gate voltage and the voltage drop on the electrolyte/dielectric interface are related to each other via the physics of the organic transistor. The threshold voltage cannot be defined in the conventional way since the inversion layer cannot occur in these semiconductors. While the electrochemical phenomena at the dielectric/electrolyte interface are similar, the electronic conduction in organic semiconductors is different from the conduction in crystalline semiconductors. Organic materials are low-dimensional systems in which the electronic charge is transported by both band-like and hopping conduction, a large density of trapping levels is present and the charge carrier mobility is gate field-effect dependent. Despite the fact that the pH effect in the conduction mechanism is not clearly elucidated yet, its influence on the channel conductivity is obvious and it can be exploited in building-up charge detectors for low-cost applications. Bartic et al. [17] have fabricated and characterized a preliminary test device in order to investigate the ability of on organic transistor to detect charge. The device structure is shown in Fig. 2.9. A poly(3-hexilthiophene) regioregular layer acts as p-type semiconductor while a 150 nm thick layer of Silicon Nitride (Si_3N_4) is the H^+-sensitive dielectric.

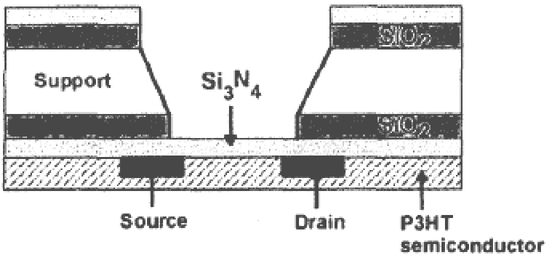

Fig. 2.9: Schematic representation of the device configuration described in [17]

Silicon nitride has two kinds of H+-specific binding sites: silanol (SiOH) and primary amine ($SiNH_2$) groups that are responsible for the surface potential generation via the following reactions taking place at the dielectric interface [18]:

$$SiOH \Leftrightarrow SiO^- + H^+$$
$$SiOH + H^+ \Leftrightarrow SiOH_2^+$$
$$SiNH_2 + H^+ \Leftrightarrow SiNH_3^+$$

When the I-V characteristics are recorded in aqueous solution, for zero bias on the reference electrode, a potential different from zero is generated at the solution/dielectric interface. This potential, which is pH-dependent, will modify the density of the accumulated charge in the organic semiconductor at the interface with the dielectric. The assumption is that the pH-dependent potential will modify the surface potential of the semiconductor and therefore the free surface charge density that determines the conductivity in the channel. The developed device has a very frail structure and is not flexible and cost efficient for a disposable platform.

As an example of pushing this technology further, Gao et al. [19] proposed a “full polymer” disposable based FET on a polymer substrate, which is integrated with a microfluidic system for pH measurement. The gate electrode is fabricated by using laser micro-machining technology and integrated on the device structure as shown in Fig. 2.10. Figure 2.11 shows the principle of polymer FET based sensor for pH detection.

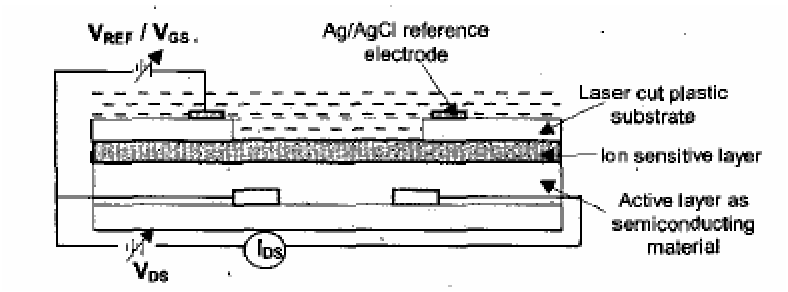

Fig. 2.10 Schematic of the device structure proposed in [18]

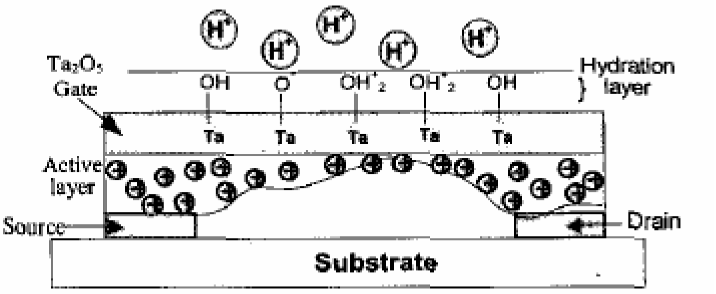

Figure 2.11: Cut view of the polymer FET sensor. The pH value determines the charge concentration on the Ta_2O_5 (gate) surface, which directly affects V_G value. By applying a fixed potential between source and drain electrodes, the I_D value is directly related to pH value.

Again P3HT is used as active semiconducting layer but in this case Tantalum Oxide has been used as the dielectric layer owing to its larger number of proton-sensitive surface sites, which improves the pH sensitivity. The polymer FET reported in this work can be integrated with disposable lab-on-a chips, which is very attractive for *in vivo* applications.

By adding specific biorecogniton layers to the gate insulator, it is also possible to construct biosensors. BioFEts can be simply obtained from an ISFET by modifying the gate or coupling it with different biological recognition elements. In such kind of devices the charge (or potential) effect is used to transduce the recognition phenomena. Since the invention of the ISFET by Bergveld various type of BioFETs have been developed using different biological recognition elements starting with enzymes and immunological species through DNA molecules to living cells and even living organisms. Some accurate and interesting review on ISFET based biosensors have been published by Shoning et al. in [20], Kasemo in [21], Hierlemann et al. in [22] and Yuqing et al in [23].

On the contrary only a few examples of ISOFET based biosensors have been presented. Bartic et al.[24] in particular have demonstrated an organic field-effect based biosensor in which an enzymatic layer of glucose oxidase was immobilized on the gate dielectric and exposed to glucose solutions with different concentrations. The effect of the biocatalytic conversion of the glucose in gluconic acid is reflected by the decrease of the drain current when the glucose is present in solution. The increase of the acid concentration (pH decrease) in the enzymatic layer is responsible for this decrease and this is in perfect agreement with the behaviour of pH sensors where the drain current increases with the pH.

We realized organic semiconductor based ion-sensitive devices that will be described in Chapter 4. The working principle is similar to ISOFET described here with the obvious differences due to the employed materials. Taking advantage of the mechanical flexibility of the insulating layer and of the whole device this type of device could be used to produce flexible smart electronic films for a broad range of application, for instance, to realize an “electronic skin” in which chemical sensors and mechanical sensors (described in Chapter 5) obtained with the same materials and processes can be integrated in a matrix.

2.4 Mechanical Sensors

Despite the wide range of gas and chemical sensors based on organic field-effect transistors reported in literature only a few examples of mechanical sensors have been published so far. Relatively little progress has been made in the field of pressure or bending recognition compared to the areas of gas and chemical sensing, mainly because mechanical sensing requires attributes of conformability and flexibility and three-dimensional large area shaping that in many cases is difficult to achieve even for organic devices. On the other hand, artificial sense of touch will be an essential feature of future generation of robot. Moreover, “wearable electronics” has become one of the hottest themes in electronics and recently organic field-effect transistors with non planar geometry have been proposed by Lee et al. [25], Bonfiglio et al. [26] and Maccioni et al. [27].

The use of "intelligent" textiles, will allow the design and production of a new generation of garments with distributed sensors and electronic functions. In this perspective, the development of flexible and low-cost processed OFET based mechanical sensors is very challenging and worthy.

The first example of a large area pressure network fabricated on a plastic sheet by means of integration of organic transistors and rubbery pressure-sensitive elements have been reported by Someya et al. [28] in 2003

The device structure is shown in Fig. 2.12.

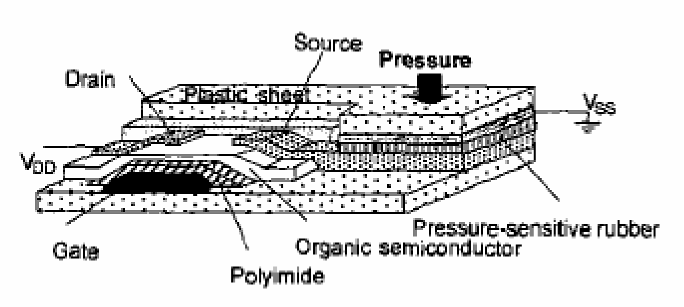

Fig. 2.12: Schematic of the device structure reported in [28]

They realized a sensor array in which organic transistors are used to address the rubber pressure-sensitive elements. The equivalent circuit diagram is shown in Fig. 2.13.

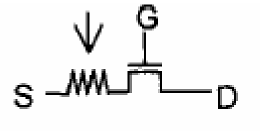

Fig. 2.13: Equivalent circuit diagram of the device.

In [29] Someya et al. have improved the fabrication technique and realized an electronic artificial "skin". Once again organic transistors are used to realize a flexible matrix which is used to read out pressure images from pressure-sensitive graphite containing rubber elements.

The obtained electronic artificial "skin" is shown in Fig. 2.14.

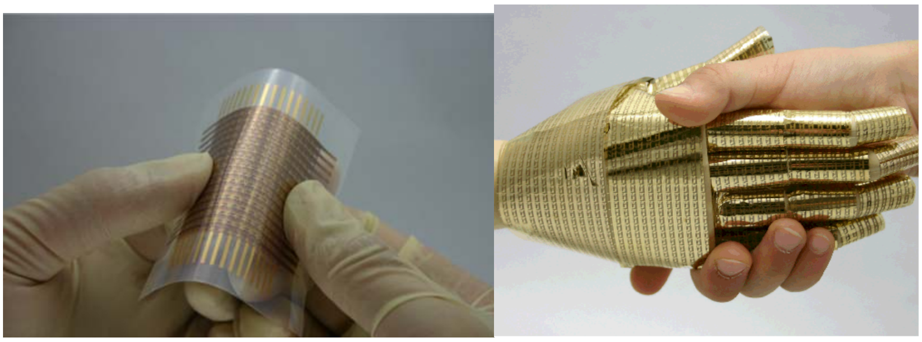

Fig. 2.14: Electronic artificial "skin" [29].

The mobility of organic transistors is comparable than that of amorphous silicon at -100V operation but this operation voltage is not realistic for artificial skin applications. At -20V the mobility is still large (0.3 cm^2/Vs) and the device still functioning. In the active driving method presented, only one transistor needs to be in the on-state for each cell where pressure is applied so this design is suitable for low-power applications where a high number of cells is required over large areas, such as electronic skin.

The device can detect a few tens of kilopascals, which is comparable to the sensitivity of discrete pressure sensors and the time response of the pressure-sensitive rubber is typically of the order of hundreds of milliseconds.

Very recently Noguchi et al. [30] have further optimized the low-cost manufacturing process realizing the flexible active matrix using ink-jet printed electrodes and gate dielectric layers.

Figure 2.15 shows the cross section of the device structure, an image of the large area pressure sensor, an image of the stand alone organic transistor and the circuit diagram. The work demonstrates the feasibility of a printed organic FET active matrix as read out circuit for sensor application.

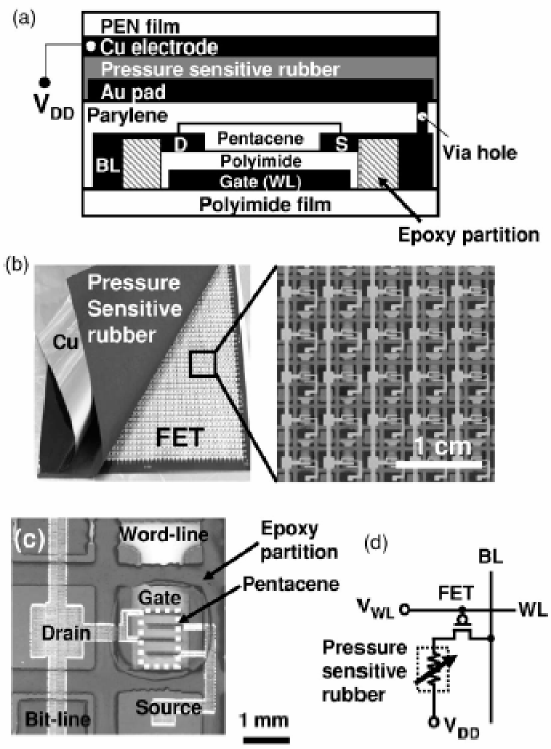

Fig. 2.15. (a) Cross section of a pressure sensor; (b) An image of a pressure sensor comprising an organic FET active matrix, a pressure-sensitive rubber, and a PEN film with a Cu electrode. A magnified image of the active matrix is also shown; (c) Micrograph of stand-alone pentacene FETs; (d) Circuit diagram of a stand-alone pressure sensor cell. [30]

A different approach has been proposed by Darlinski et al. [31]. They have studied the possibility of realizing pressure sensors based solely on organic transistors, without the need of any additional sensing element. In this way the organic device itself acts as sensor element. To study the pressure dependence of the electrical performance of these devices the authors applied mechanical force directly on the transistors using a tungsten microneedle moved by a step motor as shown in Fig. 2.16. The device substrate is placed on a balance in order to measure the applied pressure.

The authors explained the force-induced change in drain current in terms of variation on the distribution and activity of trap states at or near the semiconductor/dielectric interface. A major drawback of the reported device is that, being realized on a stiff glass substrate, it is not flexible.

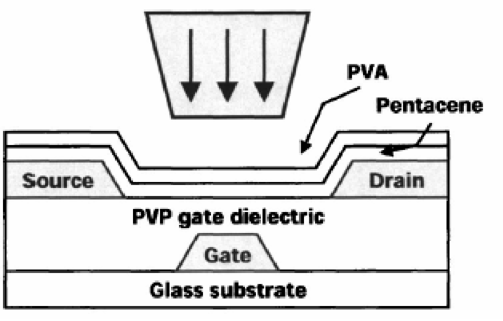

Fig. 2.16: Schematic of the device structure reported in [31]

Rang et al. [32] have investigated the hydrostatic-pressure dependence of I-V curves in organic transistors. The device was realized on a heavily doped Silicon substrate and measured in a hydrostatic pressure apparatus (an hydraulic press made by the Polish Academy of Sciences). The authors found a large and reversible dependence of the drain current of the transistor under hydrostatic pressure and suggest that the devices are suitable for sensor applications. However the device is not flexible.

On the other hand, human skin is more complex than transistor-based imitations demonstrated thus far. It also performs certain functions including thermal sensing. Someya et al. [33] have developed conformable, flexible, wide-area networks of thermal and pressure sensors in which measurements of temperature and pressure mapping were performed simultaneously. The device structure is shown in Fig. 2.17.

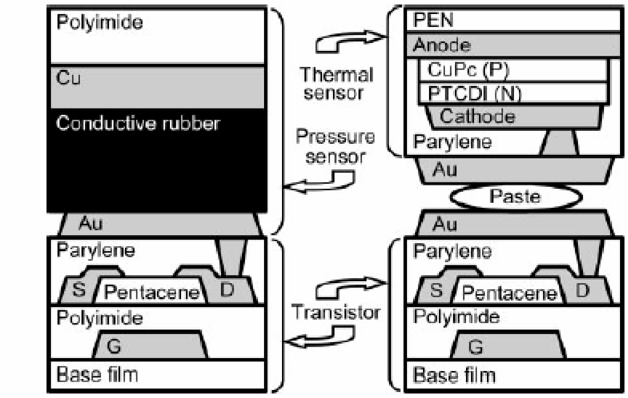

Fig. 2.17: Schematic of the device structure reported in [33] A cross-sectional illustration of the pressure (Left) and the thermal (Right) sensor cells with organic transistors is shown.

We have proposed a totally flexible structure for pressure and bend detection by using an organic field-effect transistor both as switching and sensing element (see Chapter 5). Our approach combines the flexibility of the device with a process simplification, eliminating any further process step such as rubber deposition or additional structuring.

Mechanical sensors systems can be employed also for applications other than E-skin for robots. For example, home security products ("If a pressure carpet is spread onto the floor in your house, the sensors could distinguish the family members and strangers just from footprints." [34]), life sign monitoring through wearable applications [35], and in general organic based mechanical (but also chemical, biological and so on) sensors could make many objects a little smarter.

2.5 Applications: artificial sense of touch

The skin is the largest organ of the human body. For the average adult human, the skin has a surface area of between 1.5-2.0 square meters, most of it is between 2-3 mm thick. The average square inch of skin holds 650 sweat glands, 20 blood vessels, 60,000 melanocytes, and more than a thousand nerve endings.

Skin is composed of three primary layers: the epidermis, which provides waterproofing and serves as a barrier to infection; the dermis, which serves as a location for the appendages of skin; and the hypodermis, which is called the basement membrane (see Fig. 2.18). The dermis is tightly connected to the epidermis by a basement membrane. It also contains many nerve endings that provide the sense of touch and heat

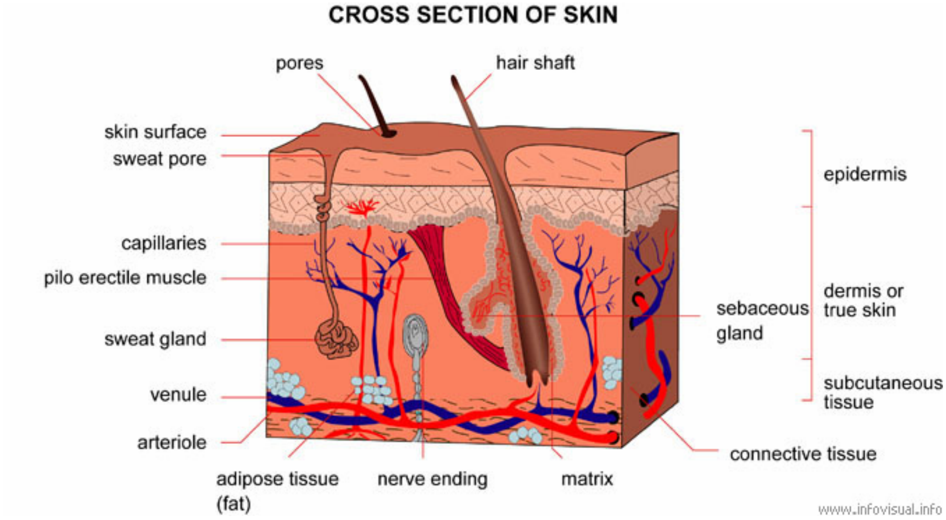

Fig.2.18: Cross section of human skin

Somatic sensation consists of the various sensory receptors that trigger the experiences labelled as touch or pressure, temperature (warm or cold), pain (including itch and tickle), and the sensations of muscle movement and joint position including posture, movement, and facial expression.

A more complex concept comes into play when the term is used in reference to human beings. Touch may simply be considered one of five human senses; however, when a person touches something or somebody this gives rise to various feelings: the perception of pressure (hence shape, softness, texture, vibration, etc.), relative temperature and sometimes pain.

Thus the term "touch" is actually the combined term for several senses. Research and development on tactile sensing has experienced an impressive growth in the last three decades, and several kinds of materials and techniques have been proposed.

The tentative specification for tactile sensors are [36]:

1. The sensor surface or its covering should combine compliance with robustness and durability.
2. The sensor should provide stable and repeatable output signals. Loading and unloading hysteresis should be minimal.

3. Linearity is important, although only monotonic response is absolutely necessary. Some degree of non-linearity can be corrected through signal processing.
4. The sensor transduction bandwidth should not be less then 100 Hz, intended as tactile image frame frequency. Individual sensing units should accordingly possess a faster response, related to their number, when multiplexing is performed.
5. Spatial resolution should be at least of the order of 1-2 mm, as a reasonable compromise between gross grasping and fine manipulation tasks.

As described in the previous paragraph, the most promising examples of “electronic skin-like” large area organic semiconductor based sensing system have been reported by Takao Someya’s group at University of Tokio [37, 33].

The development of tactile sensors is one of the most difficult aspects of robotics. Many technologies have been explored, including a carbon-loaded elastomer, piezoelectric materials, and micro-electromechanical systems. Artificial skin already exists that can detect pressure, but it is difficult to manufacture in large enough quantities to cover a robot body, and it does not stretch.

Someya have developed a skin that is stretchable, and that remains as sensitive to pressure and temperature when it is at full stretch as when it is relaxed. The arrays are less sensitive than human skin, but already mark an improvement on previous efforts, sensing temperatures in the range of 30-80 °C. Moreover the structure is flexible enough to be rolled or bent around a 2-mm bending cylinder. Someya estimates that his E-skin will be commercially available within four years and in the near future it will be possible to make an electronic skin that has function that human skin lacks by integrating various sensors not only for pressure and temperature, but also for light, humidity, strain, sound or ultrasonic.

References

1. Mabeck J.T. et al., Anal. Bioanal. Chem. 384, 343-353, (2006)
2. Torsi L., Microel. Rel. 40, 779, (2000)
3. Kats H.E. et al., Chem. Mat. 7, 2235, (1995)
4. Horowitz G. et al., Appl, Phys. Lett. 67, 258, (1990)
5. Torsi L. et al, Sens. Act. B, 67, 312–316, (2000)
6. Dimitrakopoulos C.D. et al., Adv. Mat. 14, 99, (2002)
7. Crone B. et al., Appl. Phys. Lett. 78, 2229, (2001)
8. Torsi L. et al., J. Phys. Chem. B 106, 12563-12568, (2002)
9. Tanese M. C. et al., Bios. and Bioelec. 21, 782, (2005)
10. Tanese M.C. et al., Sens. Act. B 100, 17, (2004)
11. Crone B. et al., Appl. Phys. Lett. 91, 10140, (2002)
12. Torsi L. et al., Anal. Chem. , 382, (2005)
13. Someya T. et al., Langmuir 18, 13, 5299, (2002)
14. Bartic C. et al., Sens. Act. B 83, 115, (2002)
15. Yates D.E. et al., J. Chem. Soc. Faraday I 70, 1807, (1974)
16. Bergveld P. IEEE Trans. Biom. Eng 17, 70, 1970
17. Bartic C. et al., IEDM, Technical Digest, 411 (2000)
18. Fung C.D. et al., IEEE Trans. El. Dev. 33, 3, 1986
19. Gao C. et al., IEEE Transducers ’03, (2003)
20. Schoning M.J. et al., Analyst, 127, 1137, (2002)
21. Kasemo B. et al., Surf. Sci. 500, 656, (2002)
22. Hierlemann A. et al., Proceedings of the IEEE, 91,6, (2003)
23. Yuqing M. et el., IBiotechnology Advances 21, 527-534, (2003)
24. C.Bartic et al., Appl. Phys. Lett. 82,3,475-477, (2003)
25. Lee J. B. et al., IEEE Trans. El. Dev. So52, 269, (2005)
26. Bonfiglio A. et al., IEEE Trans. Inf. Tech. Biom. 9, 319, (2005)
27. Maccioni M. et al., Appl. Phys. Lett. 89, 143515, (2006)
28. Someya T. et al. El. Dev. Meeting, IEEE, 8.4.1, (2003)
29. Someya T. et al., PNAS,101, 27, (2004)
30. Noguchi Y. et al., Appl. Phys. Lett. 89, 253507, (2006)

31. Darlinski G. et el., Appl. Phys. Lett. 97, 093708, (2005)
32. Rang Z. et al., Appl. Phys. Lett. 85, 23, 5760, (2004)
33.
34. Someya et al., PNAS 102, 35, (2005)
35. http://news.nationalgeographic.com/news/2005/08/0817_050817_robotskin.html/
36. http://www.proetex.org/
37. De Rossi D., Meas. Sci. Tech. 2, 1003, 1991
38. Kawaguchi et al., IEEE Jou. Sol.State Cir. 40, 1, 2005

CHAPTER 3

Device structures and Materials

3.1 Introduction

This chapter focuses on the device structure and employed materials: we will describe mechanical and chemical sensor structures and the employed materials.

3.2 The device structures

The basic structure consists of a pentacene-based substrate-free device, with gold bottom-contact source and drain electrodes as shown in Fig. 3.1.

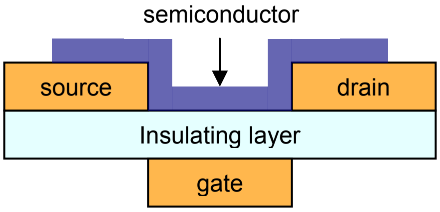

Fig. 3.1: Basic structure of the device.

The main peculiarity of this structure is that it is assembled starting from a flexible insulating film, but without any substrate. Thanks to this hallmark, both sides of the insulating layer are processable so it is possible to expose the gate side to an external medium (i.e. an electrolytic solution) or to apply the final flexible device to whatever kind of substrate (for instance a 3-D surface).

This is usually impossible for structures assembled on a rigid substrate as, typically, OFETs realized on Silicon/Silicon dioxide, in which the presence of the substrate drastically limit the flexibility of the device.

The flexible insulating layer is a thin polyethylene terephthalate sheet Mylar^{TM}, Dupont. The effective thickness varies from 900 nm to 1.6 μm depending on sample. Mylar has dielectric constant 3.3 that is close to that of silicon dioxide and a dielectric rigidity of 10^5 V/cm that allows to apply a gate bias sufficiently high to induce a field-effect in the organic semiconductor.

Thanks to its electrical and chemical characteristics, Mylar can be used as received without any further surface treatment while thanks to its mechanical properties it acts not only as gate insulator but also as mechanical support for the whole structure. This is usually impossible with conventional organic dielectric that are solution-processed, in this case as a matter of fact a flattening support is essential. In our case, on the contrary, being a flexible film, Mylar itself can act as mechanical support for the device assembly.

To form a transistor structure, gold bottom-contact source and drain electrodes are patterned on the upper side of the flexible dielectric foil, using a standard photolithographic technique, while the gold gate electrode lies on the opposite side.

Since the Mylar is transparent to UV light, in the photolithographic process for the device assembly source and drain may be used as mask for the gate patterning. This point is a distinctive feature of our structures and it is a consequence of the absence of the substrate. As a consequence of the auto-alignment between source-drain and gate electrodes (that will be described in section 3.4) all the parasitic capacitance effects due to metal overlapping are drastically limited.

Pentacene (Sigma-Aldrich) has been used as received as active layer.

By exploiting the properties of this structure, we realized a free-standing device and performed an investigation on the sensitivity of this device to mechanical stimulus. We observed a marked sensitivity of the drain current to the elastic deformation induced by a mechanical stimulus on the device channel that can be used for evaluating the strain of the substrate or for detecting a pressure applied by means of an air flow on the gate side of the free-standing device.

Figure 3.2 shows the structure of the ion-sensitive field effect transistor. The device structure is similar to the typical OFET structure shown in Fig. 3.1 except for the metallic gate, which is omitted to achieve charge sensitivity.

The gate dielectric has to be directly exposed to the ionic species from the aqueous solution. By exposing the gate side of the insulating layer to an electrolytic solution where an Ag/AgCl reference electrode is immersed it is possible to realize with a fully flexible structure a function similar to that of a silicon based Ion Sensitive Field Effect Transistor (ISFET) (see Chapter 4)

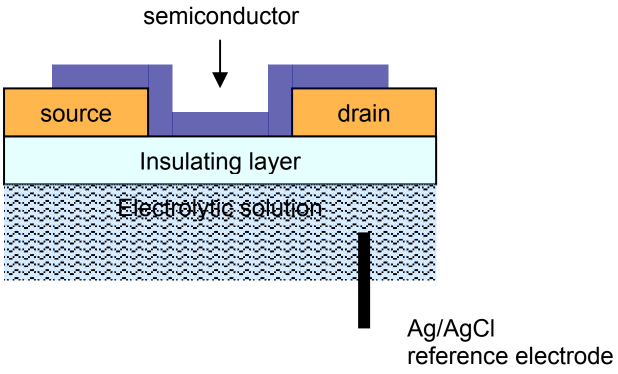

Fig. 3.2: Structure of the ion- sensitive organic field effect device.

Ion Sensitive Organic FETs (ISOFETs) fabricated on plastic substrates open the way to the fabrication of flexible devices for solution monitoring and for a number of innovative applications (as, for example, smart food packages) that are not possible at present for silicon based devices

3.3 Materials

3.3.1 Pentacene as active layer

The current benchmark material for high-performance OFETs is vacuum-sublimed pentacene [1].

Pentacene ($C_{22}H_{14}$) is a planar molecule composed of five benzene rings linked as shown in Figure 3.3. In its bulk phase, pentacene has molecules arranged in a herringbone configuration. Pentacene is reported to have two polymorphs in its bulk phase [2]. Vacuum-deposited thin films, however, differ from the bulk, forming a structure that has been referred to as the “thin film phase”. The bulk polymorph shown in Fig. 3.3 has been found to coexist with the “thin film phase” on evaporated thin films beyond a certain critical thickness.

Since charge transport properties in pentacene depend on an efficient π-orbital overlap between the molecules, the structure and molecular packing in pentacene thin films as well as the growth mechanisms that produce such structures plays a key role in determining the transport characteristics of OFETs

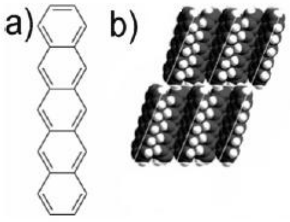

Fig. 3.3: (a) Chemical structure and (b) bulk crystalline structure of pentacene

In general, the orientation of the pentacene molecules with respect to the substrate (especially for the first monolayer) is determined by the balance between the pentacene-substrate and pentacene-pentacene interactions [3]. When pentacene is deposited onto flat, inert substrates such as some of the oxide or polymeric dielectrics (among the inert substrates, perhaps the most common is SiO_2) pentacene molecules stand nearly vertical on the substrate. On the other hand, if the substrate is a more reactive one, like clean Silicon or a clean metal, the interactions with the substrate become more important and may involve charge transfer at the interface. These induce pentacene molecules to lie flat on the surface.

On metals, the interactions between pentacene and substrate are stronger than the pentacene-pentacene interactions and the first layer grows with the long molecular axis parallel to the surface (Figure 3.4 (d)). These strong interactions lead to the formation of a large interface dipole that may increase hole injection barriers.

Substrate temperature and deposition rate as well as the base pressure of the deposition system are the most important deposition parameters that can dramatically influence thin film morphology and thus the transport characteristics.

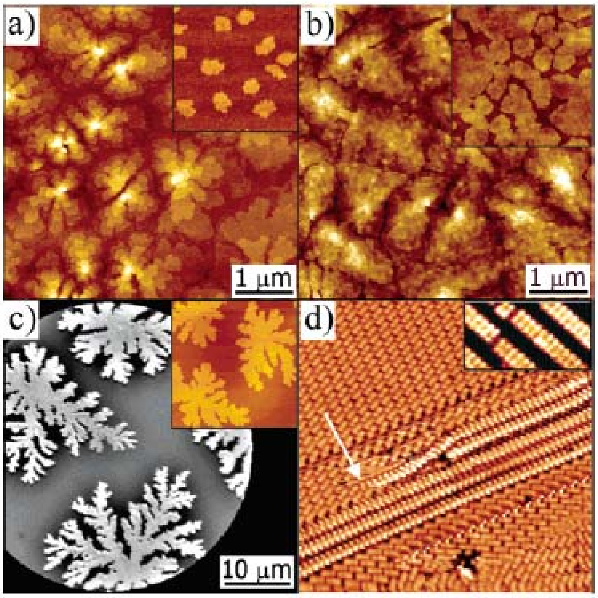

Fig. 3.4: Morphologies of pentacene films on various substrates. (a) deposition on SiO_2. Inset: sub-monolayer islands; (b) Pentacene on PEDOT:PSS. Inset: sub-monolayer islands on PMMA. (c) Sub-monolayer islands of pentacene on Si (after a layer of pentacene lying flat on the substrate). Inset: pentacene on H-terminated Si; (d) STM images of Pentacene on Ag. The arrow indicates the next pair of molecules tilting up from the planar position. Inset: STM image of pentacene on Cu showing the molecules lying flat on the substrate in an ordered manner [3]

Grain boundaries are high-volume and low-order regions that contain many morphological defects. These defects can be considered responsible for the reduced performance of bottom-contact devices compared with that of top-contact devices [4]. The morphology of the pentacene film in the transistor channel region close to the electrode edge is supposed to cause the performance limitation to the bottom-contact device.

High-quality FET devices made from thin films of pentacene typically show mobilities greater than 1.5 $cm^2/(V\ s)$ [5], values as high as 5 $cm^2/(V\ s)$ have been reported [6] and ambipolar charge transport has been observed in pentacene thin films [7].

Due to the insolubility of pentacene, solution delivery routes have been very limited, although several approaches to solubilized pentacene through conversion from solvent-based precursors have been developed [8].

These approaches typically use thermal conversion of soluble precursors, and the resultant TFT mobility is typically less than 0.1 cm^2/Vs, much lower than through vapour deposition routes.

3.3.2 Mylar as gate insulator

Among the gate insulators, perhaps the most widely used in OFETs is the Silicon dioxide. Alternatively, organic gate insulators as PVP; PVA, etc are solution-processed on planar and stiff gate supports as heavily doped Silicon or metal coated glass or plastic. This means that often the flexibility of OFETs structures are deeply reduced because of the substrate.

Mylar [9] is a biaxially oriented, thermoplastic film made from ethylene glycol and dimethyl-terephthalate (DMT). The combination of its physical, chemical and electrical properties makes Mylar a good candidate for OFETs technology. It can be used as received without any further chemical treatment and thanks to its mechanical structure it acts not only as gate insulator but also as support for the device assembly. Mylar retains good physical properties over a wide temperature range (from -70 to 150°C); some of these physical properties are summarized in Table 3.1

This polyester film exhibits also good resistance to the action of many chemical reagents, solvents, and varnishes. In addition it can be easily coated with metals and with several organic polymers.

<table>
<tr><th colspan="4">Physical properties</th></tr>
<tr><td>Surface Roughness</td><td colspan="3">38 nm</td></tr>
<tr><td>Density</td><td colspan="3">1.390 g/cm^3</td></tr>
<tr><td>Young’s modulus</td><td colspan="3">5 GPa</td></tr>
<tr><td>Poisson’s ratio</td><td colspan="3">0.38 before yield / 0.58 after yield</td></tr>
<tr><td rowspan="3">Light transmission (percent)</td><td colspan="3">Wavelenght (µm)</td></tr>
<tr><td>0.6 (visible)</td><td>0.4 (UV)</td><td>0.32 (UV)</td></tr>
<tr><td>86</td><td>82</td><td>68</td></tr>
</table>

Table 3.1: Physical properties

Table 3.2 is a summary of some electrical properties. As it can be seen the dielectric constant is close to that of Silicon dioxide while the dielectric strength allows to apply a gate bias sufficiently high for field-effect applications (tens, hundreds of Volts).

<table>
<tr><th colspan="4">Electrical properties</th></tr>
<tr><td>Dielectric Strenght (25 °C)</td><td colspan="3">10^5 V/cm</td></tr>
<tr><td rowspan="2">Dielectric Constant
(25°C)</td><td>50 Hz</td><td>1 KHz</td><td>1MHz</td></tr>
<tr><td>3.30</td><td>3,25</td><td>3.00</td></tr>
<tr><td>Volume Resistivity (25°C)</td><td colspan="3">10^{18} Ωcm</td></tr>
<tr><td>Surface Resistivity
(23°C)</td><td colspan="2">10^{16} Ω/sq
30% RH</td><td>10^{12} Ω/sq
80% RH</td></tr>
</table>

Table 3.2: Electrical properties

Mylar is available in a broad variety of widths. The drain current of a OFET is proportional to the gate insulator capacitance C_i (see Eq.1.4 and 1.9) while the capacitance is inversely proportional to the thickness of the insulating layer d_i according to Eq. 3.1.

$$C_i = \frac{\varepsilon_r \varepsilon_0}{d_i} \tag{3.1}$$

Consequently, to grant satisfactory device performance, the insulating layer must have a proper dielectric constant (ε_r) and should be as thin as possible.

3.3.3 Gold and PEDOT:PSS as conductive coating for electrodes

The contact between the electrodes and the organic layer is one of the most important factors in determining the device performance. Good contacts are expected to occur when the work function of the electrode is close to the HOMO or LUMO level of the semiconductor, depending respectively on the carrier type (electrons or holes).

Among metals, Gold is one of the most commonly used for source/drain electrodes to date because of its many advantages such as thin-film processability, chemical inertness, a work function (~5.1 eV) close to the HOMO level of p-type organic semiconductors, and possibility of surface modification by self-assembled monolayers (SAMs) to improve contacts.

The energy levels at the Gold/Pentacene interface is shown in Fig. 3.5

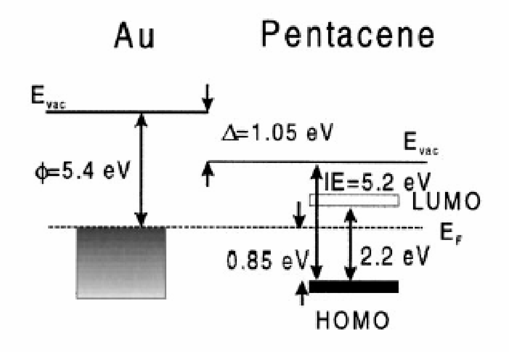

Fig. 3.5: Energy-level diagram of the Au/Pentacene interface.

The simple Schottky–Mott model, where the barrier height is given by the difference between the metal work function and the pentacene HOMO level, is not followed here. The interface exhibits an additional dipole barrier Δ that tends to lower the metal work function, and hence to increase the interface barrier height. The large interface dipole was explained by the change of the surface dipole of the metal upon adsorption of the molecule. A metal surface is characterized by an electron density tailing from the free surface into vacuum. Adsorbed molecules tend to push back these electrons, thus reducing the surface dipole and decreasing the work function of the metal [10].

It is usually observed that top-contacts, where the contact is deposited on the organic film, give rise to a reduced contact resistance. The asymmetry of the organic–metal contact, depending on whether the organic film is deposited on the metal or the metal on the organic film, has been studied on both the theoretical [11] and experimental [12] point of view.

However, the top-contact architecture presents a major drawback: patterning the device through conventional microlithography is not possible because Pentacene thin films are intolerant to exposure to the various chemicals used in typical lithographic processes; therefore top contacts are usually deposited through shadow masks. This means that the achievable minimum distance between contacts (i.e. the channel length, L) under highly controlled conditions is in the order of few microns (usually tens of microns), and this is a major drawback for the device performance because drain current is inversely proportional to L.

An alternative method for electrode patterning is soft lithography. By means of soft-lithography it is possible to obtain both bottom- and top-contact devices with sub-micrometric channel length by means of conductive polymers. The improved performance of the conductive polymer PEDOT-PSS (Poly(3,4-ethylenedioxythiophene): poly(styrene sulfonic acid)) together with patterning and printing techniques have been successively used in the design of field-effect transistors.

PEDOT:PSS is a water-soluble polymer with properties of high conductivity (~ 300 S/cm), low oxidation potential, moderate band-gap (1.6 eV), high visible light transmission, good film formation, and high stability. Films of PEDOT:PSS can be deposited by spin-coating or printing techniques at low-temperature, which is naturally compatible with plastic or paper substrates for lightweight and foldable products [13]

Fig. 3.6 Shows the energy-level diagram of the PEDOT:PSS/Pentacene interface.

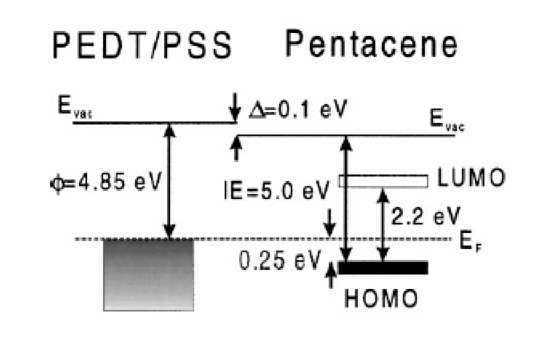

Fig. 3.6: Energy-level diagram of the PEDOT:PSS/Pentacene interface

Koch et al. [14] showed that the hole carrier injection barrier is drastically smaller at PEDOT/PSS and pentacene interfaces (0.1 eV) than at gold and pentacene interfaces (1.05 eV), although the two electrode materials have a similar work function. This smaller barrier leads to more efficient carrier injection. The difference is linked to one of the basic mechanisms of molecular level alignment on metal surfaces, i.e., the reduction by adsorbed molecules of the surface electronic tail contribution to the work function of a metal. Upon adsorption, the metal work function is lowered, leading to a large hole injection barrier. The smaller surface electronic contribution to the work function on a material like PEDOT/PSS leads to the much more favourable energy level alignment for hole injection.

References

1. Anthony J.E., Chem. Rev. 106, 5028-5048 (2006)
2. Haddon R.C. et al., J. Phys. Chem. B 106, 8288-8292, (2002)
3. Ruiz R. et al., Chem. Mater. 16, 4497-4508, (2004)
4. Dimitrakopoulos C.D. et al., Adv. Mat. 14, 2, 100-117 (2002)
5. Lin, et al., IEEE Trans. Electron Devices 44, 1325, (1997).
6. Kelley T. W. et al., Mater. Res. Soc. Symp. Proc. 771, L6.5.1., (2003)
7. Meijer E. J. et al., Nat. Mater. 2, 678, (2003)
8. Kelley T.W. et al., Chem. Mater. 16, 4413-4422, (2004)
9. www.dupontteijinfilms.com
10. Koch N. et al., Appl. Phys. Lett, 82, 14, 2281- 2283(2003)
11. N. Tessler et al. Appl. Phys. Lett. 79, 2987 (2001).
12. N.J. Watkins et al Appl. Phys. Lett.80, 4384 (2002).
13. Chen M., IEEE Proc. 93, 7, 1339-1347, (2005)
14. Koch N. et al., Appl. Phys. Lett, 82, 1, 70- 72 (2003)

CHAPTER 4

Chemical Sensors based on Organic Field- Effect Transistors

4.1 Introduction

In this chapter we report on organic semiconductor based chemical sensors. Although the organic semiconductor based FET is advantageous in terms of structural flexibility, optical transparency and adjustable component, its application is still limited due to the low carrier mobility and I_{on}/I_{off} ratio.

Recent developments have been focused on increasing conductivity, improving filed effect mobility, and amplifying current, etc. Bartic et al. [1-3] have presented an organic FET structure, which was fabricated on a Silicon substrate, but the device was not flexible, has a very frail structure and is not cost efficient for a disposable platform.

However, our motivation for the development of the organic semiconductor based chemical sensor is to build a cheap and disposable device rather than to attain a high speed and better performance comparable to the Silicon based semiconductor devices. Our device [4] uses an external Ag/AgCl reference electrode to apply gate-source voltage. Such approach limits the miniaturization of the sensor and increases the difficulties of the interface between electronic circuits and sensors. For biomedical and health applications, due to the safety requirements, single-use devices are highly desirable. Moreover the relatively high voltages usually required for OFET operation are a problem for sensing applications. This implies the need of a efficient choice of very cheap materials and fabrication technologies. Furthermore by employing single-use sensors, the drift in the sensor response that usually affect organic devices id circumvented. In this chapter at first we will present the ISFET theory that is the basis of the device working mechanism.

Then the device processing and the set-up for the electrical characterizations will be illustrated in detail. Finally the results of our experiment will be commented.

4.2 The ISFET theory

4.2.1 The Gouy-Chapman model: interfacial double layer phenomena

The double layer model is used to visualize the ionic environment in the vicinity of a charged surface [5] One of the first principles which we must recognize is that matter at the boundary of two phases possesses properties which differentiates it from matter freely extended in either of the continuous phases separated by the interface. When talking about a solid-solution interface, it is perhaps easier to visualize a difference between the interface and the solid than it is to visualize a difference between the interface and the extended liquid phase. Where we have a charged surface, however, there must be a balancing counter charge, and this counter charge will occur in the liquid. The charges will not be uniformly distributed throughout the liquid phase, but will be concentrated near the charged surface. Thus, we have a small but finite volume of the liquid phase which is different from the extended liquid. This concept is central to electrochemistry, and reactions within this interfacial boundary that govern external observations of electrochemical reactions. We consider the metal now in contact with aqueous media containing a high concentration of ions. When the metal interface carries an excess of charge, this is counter-balanced by the accumulation of ionic charge, of opposite sign, on the solution side of the interface. Helmholtz treated the double layer mathematically as a simple capacitor, based on a physical model in which a single layer of ions is adsorbed at the surface. This can be described using:

$$\sigma = \frac{\varepsilon\varepsilon_0}{d}E \text{ and } C = \frac{\partial\sigma}{\partial E} = \frac{\varepsilon\varepsilon_0}{d} \qquad (4.1)$$

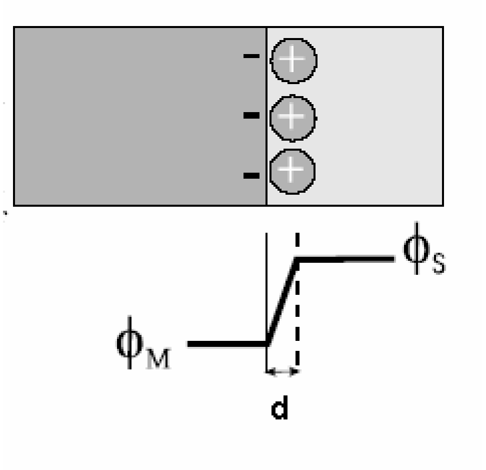

Fig. 4.1 The Helmotz model

This model neglects the fact that the conductivities of the two sides of the capacitor are distinctly different, requiring a thicker layer of charge on the solution side of this double layer, so-called *diffuse layer of charge.*

Starting with the Helmholtz model, one can imagine that the diffuse layer of charge could be divided into particular regions. The largest concentration of charge would exist near the electrode surface since electrostatic forces are believed to overcome thermal fluctuations, suggesting two regions, an inner layer and diffuse layer.

The inner layer contains anions and cations that are close to the metal surface. Electrostatics play a dominant role in determining the composition of this inner layer. In many cases, a large concentration of anions will still exist near the metal even for positive charge densities on the metal surface. The anions can chemically interact with the metal atoms, called *specific adsorption*. Charge contained in this layer is generally denoted as σ_i The inner layer can be further divided into two layers, the inner and outer Helmholtz planes. The *Inner Helmholtz Plane* (IHP) is defined as the distance from the electrode surface of the centre of an ion after loss of its solvation shell. The potential is $\phi(x_1)$ at a distance x_1 from the metal surface. The *Outer Helmholtz Plane* (OHP) is the centre of solvated ions at the closest approach to the metal the potential is $\phi(x_2)$ at a distance x_2 from the metal surface.

The diffuse layer extends from the OHP to the bulk of solution and contains the non-specifically adsorbed ions that behave as an ionic cloud.

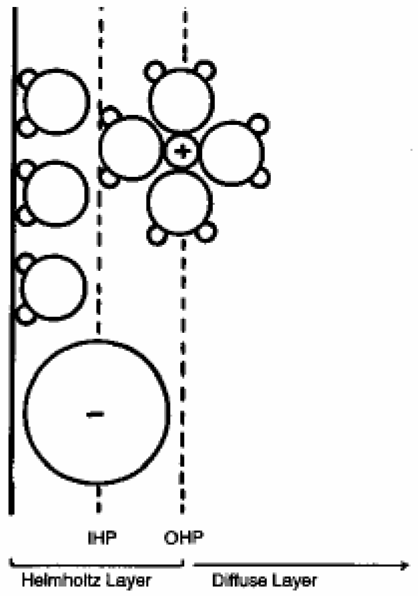

Fig. 4.2 The Helmhotz double layer

With this model, the electrical double layer behaves as two capacitors in series. This is demonstrated mathematically with the Gouy-Chapman-Stern theory.

The Gouy-Chapman model only treats the diffuse part of the double layer. We will use this model to describe the interface starting at the OHP ($x=x_2$), then we will put the Helmholtz model and the Gouy-Chapman model together as proposed by Stern yielding the GCS model of the electrode/electrolyte interface. The diffuse layer is assumed to be in equilibrium with the bulk of solution. The solution is divided into “laminae” of equal thickness starting at the OHP near the electrode surface, extending into the bulk of the electrolyte. The ions present in each of the “laminae” are not all of equal energy since potential decays away from the electrode surface. The “laminae” can be considered as energy states so the concentration in two “laminae” have a ratio determined by the Boltzmann factor. The reference “laminae” exists in the bulk, far from the electrode with a concentration of c_i^0 and $\phi_S=0$ with a population in any other “laminae” determined by:

$$c_i(x) = c_i^0 \, exp\left(-z_i e\phi / kT\right) \tag{4.2}$$

where ϕ and z are the potential and the signed charge on ion i.

The total charge in any “laminae” is the sum over all ions:

$$\rho(x) = \sum_i n_i z_i e = \sum_i z_i e c_i^0 \, exp\left(-z_i e\phi / kT\right) \tag{4.3}$$

The Poisson equation is used to calculate the electric potential that results from a given charge distribution in a medium of dielectric constant ε:

$$\nabla^2 \phi = -\rho(x,y,z)/\varepsilon \tag{4.4}$$

The dielectric constant is invariant with distance from the electrode and the ionic charges are interacting with the electric field as point charges in this model. For this one dimensional model, the total charge per volume (ρ) is related to the potential at any distance x by:

$$\frac{d^2\phi}{dx^2} = -\frac{\rho(x)}{\varepsilon} \tag{4.5}$$

Combining the Poisson and Boltzmann expression yields:

$$\left(\frac{d^2\phi}{dx^2}\right) = \frac{-e}{\varepsilon} \sum_i z_i c_i^0 \, exp\left(-z_i e\phi / kT\right) \tag{4.6}$$

Realizing that $\frac{d^2\phi}{dx^2} = \frac{1}{2}\frac{d}{d\phi}\left(\frac{d\phi}{dx}\right)^2$ simplifies the Poisson-Boltzmann and gives:

$$d\left(\frac{d\phi}{dx}\right)^2 = \frac{-2e}{\varepsilon} \sum_i z_i c_i^0 \, exp\left(-z_i e\phi / kT\right) d\phi \tag{4.7}$$

Thus integrating yelds:

$$\left(\frac{d\phi}{dx}\right)^2 = \frac{2kT}{\varepsilon} \sum_i c_i^0 \, exp\left(-z_i e\phi / kT\right) + const \tag{4.8}$$

Far from the electrode surface, x→∞, ϕ=0 and (dϕ/dx)=0, which allows determination of the constant of integration:

$$\left(\frac{d\phi}{dx}\right)^2 = \frac{2kT}{\varepsilon} \sum_i c_i^0 \left[exp\left(-z_i e\phi / kT\right) - 1 \right] \tag{4.9}$$

The strength of the electric field (dϕ/dx) at any point in the diffuse layer is given by:

$$\left(\frac{d\phi}{dx}\right)=\pm\left(\frac{2kT}{\varepsilon}\right)^{\frac{1}{2}}\left\{\sum_i c_i^0\left[exp\left(-z_i e\phi/_{kT}\right)-1\right]\right\}^{\frac{1}{2}} \tag{4.10}$$

For an electrolyte where the salt has only one cation and anion of the same charge, ie KCl, (called also a z-z electrolyte), equation 4.10 can be written as:

$$\left(\frac{d\phi}{dx}\right)=-\left(\frac{8RTc_{bulk}}{\varepsilon}\right)^{\frac{1}{2}} sinh\left(\frac{zF\phi}{2RT}\right) \tag{4.11}$$

An expression for the potential profile in the diffuse region can be determined by integrating equation 4.11 with boundary conditions of $\phi=\phi_2$ and $x=x_2$ at the OHP and defining for a z-z electrolyte:

$$\int_{\phi_2}^{\phi}\frac{d\phi}{sinh\left(\frac{zF\phi}{2RT}\right)}=-\left(\frac{8RTc_{bulk}}{\varepsilon}\right)^{\frac{1}{2}}\int_{x_2}^{x}dx \tag{4.12}$$

where ϕ_2 is the potential at the OHP and is the potential drop across the double layer which extends from the OHP (x_2) to the bulk of solution. Integration results in:

$$tanh\left(\frac{zF\varphi}{4RT}\right)=exp(-k(x-x_2))tanh\left(\frac{zF\varphi_2}{4RT}\right) \tag{4.13}$$

where $k=\sqrt{\frac{2F^2z^2c_{bulk}}{\varepsilon RT}}$ is the inverse of the Debye lenght that characterizes the decay of potential from the OHP plane near the electrode surface to the bulk of solution.

The charge contained within the diffuse part of the double layer is calculated using the Gauss law:

$$q=\varepsilon\oint EdS \tag{4.14}$$

where E is given by Eq. 4.10.

Integrating we obtain:

$$\sigma_s=-(8\varepsilon RTc_{bulk})^{\frac{1}{2}} sinh\left(\frac{ze\phi_2}{2RT}\right) \tag{4.15}$$

The charge on the metal surface is the same but opposite in sign to the charge in solution.

4.2.2 An electrolyte-semiconductor-insulator structure

The electrolyte-insulator-semiconductor (EIS) structure for an ISFET is analogous to the metal-oxide-semiconductor (MOS) capacitor for a MOSFET.[5]

In order to polarize the EIS structure, a reference electrode must be inserted to close the circuit. The reference electrode is characterized by the fact that the potential difference across it is virtually fixed

In an EIS structure the presence of an insulator (e.g. SiO_2 or Si_3N_4) induces a specific charge distribution, which is caused by the formation of surface groups. When a Silicon dioxide insulator exposed to an aqueous solution interacts with H^+ ions in the following way:

$$\left[SiOH_2^+\right] \underset{k_1^-}{\overset{k_1^+}{\rightleftarrows}} \left[SiOH\right] + \left[H^+\right]_s \tag{4.16}$$

$$\left[SiOH\right] \underset{k_2^-}{\overset{k_2^+}{\rightleftarrows}} \left[SiO^-\right] + \left[H^+\right]_s \tag{4.17}$$

The subscript s in $\left[H^+\right]_s$ means that the concentration of protons is *near* the surface of the insulator, and $\left[SiOH_2^+\right]$, $\left[SiOH\right]\left[SiO^-\right]$ are the concentrations of the proton *binding sites* present on the oxide surface. Under equilibrium conditions, the kinetic reactions (4.16), (4.17) result in equilibrium constants:

$$K_+ = \frac{\left[SiOH\right]\left[H^+\right]_s}{\left[SiOH_2^+\right]} \tag{4.18}$$

$$K_- = \frac{\left[SiO^-\right]\left[H^+\right]_s}{\left[SiOH\right]} \tag{4.19}$$

By multiplying together the two equilibrium constants, we obtain:

$$K_+K_- = \frac{\left[SiO^-\right]\left[H^+\right]_s^2}{\left[SiOH_2^+\right]} \tag{4.20}$$

Concentrations of binding sites can be transformed into fractions of sites θ_+, θ_0, θ_-, giving:

$$\frac{[SiO^-]}{[SiOH_2^+]} = \frac{\theta_-}{\theta_+} \tag{4.21}$$

where θ_+, θ_0 and θ_- satisfy the constraint:

$$\theta_- + \theta_+ + \theta_0 = 1 \tag{4.22}$$

Moreover, under equilibrium conditions, the concentration of protons at the surface of the insulator can be related to the one in the bulk via the Boltzmann equation

$$[H^+]_S = [H^+]_b \, exp\left(\frac{q(\phi_b - \phi_0)}{kT}\right) \tag{4.23}$$

where (ϕ_b- ϕ_0) is the potential drop between electrolyte bulk and insulator surface. By assuming ϕ_b=0 and by substitution of Eq. 4.23 and 4.21 into 4.20 we finally obtain

$$K_+K_- = \frac{\theta_-}{\theta_+}[H^+]_b^2 \, exp\left(-2q\phi_0 / kT\right) \tag{4.24}$$

By taking logarithms of both sides and dividing by 2 we obtain:

$$\frac{1}{2}ln(K_+K_-) = \frac{1}{2}ln\frac{\theta_-}{\theta_+} + ln[H^+]_b - \frac{q\phi_0}{kT} \tag{4.25}$$

Being:

$$ln[H^+]_b \approx 2.303 log[H^+]_b = -2.303 pH_b \tag{4.26}$$

the Eq. 4.25 can be written in pH terms as follow (we drop the subscript b from now on):

$$\frac{1}{2}ln(K_+K_-) = \frac{1}{2}ln\frac{\theta_-}{\theta_+} - 2.303pH - \frac{q\phi_0}{kT} \tag{4.27}$$

Equation (4.27) holds true for any pH value and, for a given insulator, the ratio θ_-/θ_+ is a given function of pH. In other words, for a given insulator, there is a specific pH value for which

$$\theta_- = \theta_+ \tag{4.28}$$

This specific value is known as the point of zero charge of the material and is indicated as pH_{pzc}.

By setting $\phi_0=0$ for pH= pH_{pzc} (since only differences in potential are ever physical meaningful), we obtain:

$$\frac{1}{2} ln(K_+K_-) = -2.303(pH - pH_{pzc}) \tag{4.29}$$

Thus, we can finally write Eq. 4.29 as:

$$2.303(pH - pH_{pzc}) = \frac{1}{2} ln \frac{\theta_-}{\theta_+} - \frac{q\phi_0}{kT} \tag{4.30}$$

or:

$$\phi_0 = -2.303 \frac{KT}{q} \Delta pH + \frac{1}{2} \frac{KT}{q} ln \frac{\theta_-}{\theta_+} \tag{4.31}$$

where
$$\Delta pH = pH - pH_{pzc} \tag{4.32}$$

At room temperature we have:

$$2.303 \frac{kT}{q} \approx 59mV \tag{4.33}$$

Equation 4.31 relates the potential ϕ_0 and pH and is the basis for utilizing an EIS ad a pH sensor. The value of ϕ_0 can be deduced by knowing the profile of the potential in the electrolyte.

The charge density σ_0 of the surface sites in the insulator is given by:

$$\sigma_0 = qN_s(\theta_+ - \theta_-) \tag{4.34}$$

where N_s is the total number of available binding sites per unit area.

The condition of charge neutrality for the EIS system is

$$\sigma_d + \sigma_0 + \sigma_s = 0 \tag{4.35}$$

where σ_d is the charge density diffuse in the electrolyte, σ_0 is the charge density on the insulator surface and σ_s is the charge density inside the semiconductor.

The same procedure followed for SiO_2 can be followed for other insulators, such as Si_3N_4. Unfortunately for Si_3N_4 the reactions are more complicated. On the other hand Si_3N_4 is more appropriate than SiO_2 for designing a silicon based pH meter.

4.2.3 ISFET operation

The Ion-Sensitive Field Effect Device transistor was reported first by Bergveld [6]. The structure of an ISFET, shown in Fig. 4.3, is fundamentally a MOSFET which can be rendered H^+ sensitive by eliminating its metal gate electrode in order to expose the gate insulator to the solution.

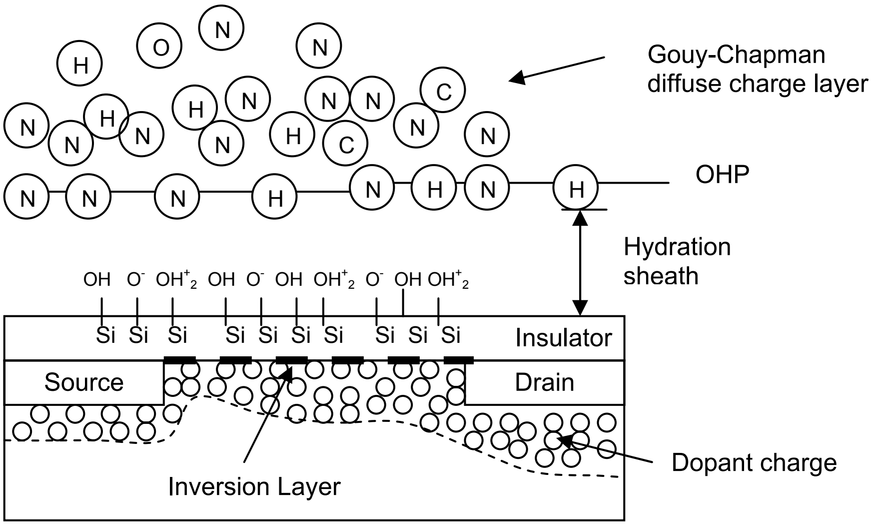

Fig. 4.3: Schematic representation of an ISFET with an expanded view of semiconductor-insulator-electrolyte interface (SiO2)

The ISFET is in fact nothing else than a MOSFET with the gate connection separated from the chip in the form of a reference electrode inserted in an aqueous solution which is in contact with the gate oxide. Therefore, most of the papers dealing with the ISFET operational mechanism start with the theoretical description of a MOSFET. The general expression for the drain current of the MOSFET and thus also of the ISFET in the non-saturated mode is:

$$I_D = \frac{Z}{L}\mu C_i\left[(V_G - V_{th})V_D - \frac{V_D^2}{2}\right]$$

The gate insulator of an ISFET senses the H^+ ion concentration, generating an interface potential on the gate; the corresponding change on drain-source current is observed. As already stated, the operation mechanism of the ISFET originates from the pH sensitivity of the inorganic gate oxide, that can be explained by the site dissociation model previously described. The measurable property of an ISFET can be identified in terms of flat-band potential. V_{FB} that is directly related to the threshold voltage V_{th}. Let us consider a system consisting of: a reference electrode, which contains a stable solid-liquid interface, an electrolyte, an insulating layer, a silicon substrate and a metal back contact. In the usual electrochemical representation, this system is written as:

M | Si | Insulator | Electrolyte | Reference electrode |M’

The most important measurable parameter of this system is the V_{FB} defined as the voltage applied to M’ which makes the silicon surface potential zero:

$$V_{FB} = \left(E_{ref} - \varphi_{lj}\right) - \left(\varphi_{eo} - \chi_{e}\right) - \frac{\Phi_{Si}}{q} - \frac{Q_0}{C_{ox}} \tag{4.36}$$

where the E_{ref} is the reference electrode potential relative to vacuum, φ_{lj} is the liquid-junction potential difference between the reference solution and the electrolyte, φ_{eo} is the potential drop in the electrolyte at the insulator-electrolyte interface; X_e is the surface dipole potential of the solution, Φ_si is the work function of Silicon, C_{ox} and Q_0 are the insulator capacitance and effective charge per unit area.

Thus, the flat band voltage and therefore the threshold voltage is the quantity measured in chemically sensitive electronic devices based on the field-effect principle. We can write:

$$V_{th}(ISFET) = V_{th}(MOSFET) + E_{ref} + \varphi_{lj} + \chi_{e} - \varphi_{eo} - \frac{\Phi_{M}}{q} \tag{4.37}$$

where Φ_M is the work function of the metal back contact of the semiconductor relative to vacuum. Equation 4.37 replaces the MOSFET threshold voltage in the expressions of the drain current. The main source of the pH sensitivity among the terms in Eq. 4.37 is the potential drop in the electrolyte at the insulator electrolyte interface.

The origin of the potential φ_{eo} is the interaction of the insulator surface with ions present in the electrolyte. The main feature of theory for this interaction is that the presence of discrete surface sites is assumed. We can reconsider the dimensionless equilibrium constants K_a and K_b reported in Eq.A.3 and A.4

$$K_a = \frac{[SiO^-][H^+]_s}{[SiOH]} \tag{4.38}$$

$$K_b = \frac{[SiOH_2^+]}{[SiOH][H^+]_s} \tag{4.39}$$

On the oxide surface, there is a fixed number of surface sites per unit area, N_s:

$$N_s = [SiO^-] + [SiOH_2^+] + [SiOH] \tag{4.40}$$

Depending on the chemical equilibrium of the surface sites, a surface charge density σ_0 [C/m^2] exists:

$$\sigma_0 = q([SiOH_2^+] - [SiO^-]) = -qB \tag{4.41}$$

where B is the number of negatively charged groups minus the number of positively charged groups in moles per unit area. The combination of Eqs. 4.38, A.39 and A.41 yields:

$$\sigma_0 = qN_s\left(\frac{[H^+]_s^2 - K_aK_b}{K_aK_b + K_b[H^+]_s + [H^+]_s^2}\right) \tag{4.42}$$

Equation 4.42 shows the relation between the activity of the protons at the oxide surface $[H^+]_s$ and the surface charge density σ_0 in terms of the total number of available sites N_s and the intrinsic dissociation constants K_a and K_b. The effect of a small change in the surface proton activity $[H^+]_s$ on the surface charge density, σ_0, can be found from Eq.4.41:

$$\frac{\partial \sigma_0}{\partial pH_s} = -q\frac{\partial B}{\partial pH_s} = -q\beta_{int} \tag{4.43}$$

where the change in $[H^+]_s$ is expressed in its corresponding pH_s, and the resulting change in σ_0 in the change in the net number B of basic groups. By definition, $\frac{\partial B}{\partial pH_s}$ represents the buffer capacity β_{int} of the oxide surface. It is called intrinsic in this case, because it is only capable of buffering small changes in the surface pH (pH_s) and not in the bulk pH (pH_b), under normal conditions.

The ability of the electrolyte to store charge in response to a change in the electrostatic potential is the differential capacitance

$$C_S = \frac{d\sigma_S}{d\varphi_{eo}} \tag{4.44}$$

A change with the bulk pH_b induces a change in pHs, which in turn results in a change in the surface potential φ_{eo}

$$\frac{d\varphi_{eo}}{dpH_S} = \frac{d\sigma_S}{dpH_S}\frac{d\varphi_{eo}}{d\sigma_S} = -\frac{q\beta_S}{C_S} \tag{4.45}$$

under the condition that C_s is independent of φ_{eo} which in most cases is a reasonable assumption. Equation 4.45 indicates that for a small value of dpH_s, a large value of $d\varphi_{eo}$ will take place when the surface has a large intrinsic buffer capacitance β_s, especially in combination with a small electrical surface capacitance C_s.

According to the Boltzmann distribution :

$$\left[H^+\right]_S = \left[H^+\right]_b \exp\left(-q\varphi_{eo}/kT\right) \tag{4.46}$$

we can write,

$$\varphi_{eo} = 2.3\frac{KT}{q}\left(pH_S - pH_b\right) \tag{4.47}$$

Since an ISFET measures the gate insulator-electrolyte interface potential φ_{eo} as a function of the pH on the bulk pH_b Eq.4.47 must be differentiate to determine the pH sensitivity of the ISFET:

$$\frac{d\varphi_{eo}}{dpH_b} = 2.3\frac{KT}{q}\left(\frac{dpH_S}{dpH_b} - 1\right) = 2.3\frac{KT}{q}\left(\frac{dpH_S}{d\varphi_{eo}}\frac{d\varphi_{eo}}{dpH_b} - 1\right) = \frac{2.3\frac{KT}{q}}{2.3\frac{KT}{q}\frac{dpH_S}{d\varphi_{eo}} - 1} \tag{4.48}$$

Rearranging Eq. 4.48 and combining it with Eq.4.45 we obtain:

$$\frac{d\varphi_{eo}}{dpH_b} = -2.3\frac{KT}{q}\frac{1}{2.3\frac{C_s}{\beta_s}+1} = -2.3\alpha\frac{kT}{q} \tag{4.49}$$

where

$$\alpha = \frac{1}{2.3\frac{KT}{q^2}\frac{C_S}{\beta_S}+1} \tag{4.50}$$

is a dimensionless sensitivity parameter which varies between 0 and 1 depending on the intrinsic buffer capacity and the differential capacitance.

The pH sensitivity of an ISFET with an inorganic oxide as the gate material can then be described through the parameter α which approach unity for large values of β_S/C_S. This means that surfaces with a large buffer capacity and low electrolyte concentration show at best a maximum response of 59.3 mV at 25°C. [5]

Since the first papers of Bergveld in 1970, about 600 papers appeared in the literature devoted on ISFETs and another 150 on related devices, such as EnzymeFETs (ENFETs), ImmunoFETs (IMFETs), etc. These are listed and discussed in a very useful review paper by Bergveld itself [7].

4.3 Device processing and electrical characterization

As introduced in Chapter 3, the device consists of a pentacene-based substrate-free structure, with gold bottom-contact source and drain electrodes.

The insulator layer, responsible for the sensitivity of the device, is a 900 nm thick Mylar foil. Mylar is used as gate insulator and also as mechanical support of the whole device. As for ISFET and ISOFET devices, our device owes this sensitivity to the presence of amphoteric sites on the surface of the dielectric layer. In our case, it was not known a priori if the dielectric layer could present specific binding sites for protons.

First of all the Mylar foil is clamped to a cylindrical plastic frame (2.5 cm in diameter) in order to obtain a suspended membrane with both sides available for processing. The foil is then cleaned with acetone, washed with deionised water and finally dried with a nitrogen flux.

Then, bottom-contact gold electrodes (nominal thickness 100 nm) usually with W/L=100 (W=5 mm and L=50 µm are the channel width and length, respectively) are thermally evaporated and patterned on the upper side of the flexible dielectric foil, using a standard photolithographic technique.

The gate electrode is made of an electrolytic solution in which an Ag/AgCl electrode is immersed. The electrode is used to ensure a stable electrical contact with the solution when it is biased with respect to the source electrode.

Acid solutions (pH~2-3) are obtained using citric acid ($C_6H_8O_7$) with molar concentration 10^{-3}; weak basic solutions (pH~9) are obtained using sodium phosphate (Na_2HPO_4,) with molar concentration 10^{-3}, strong basic solutions (pH~12) are obtained using sodium hydroxide, (NaOH) with molar concentration 10^{-3}.

Usually before measuring, the device with the reference electrode were kept for about half a hour in a solution with a pH of 7 to allow stabilization. In order to avoid aging effects measurements are performed immediately after the Pentacene deposition. Pentacene films with a thickness of 50 nm are grown by vacuum-sublimation at a nominal deposition flux of about 1 Å/s.

The output drain current is used to indicate the pH response of the organic device when measured in different electrolytic solutions and for the same biasing conditions. Alternatively it is possible to held constant the drain bias conditions (I_D and V_{DS}) and measure the variations in the gate-source voltage induced by the pH changes in the electrolytic solution [8].

To do this a low-cost auxiliary circuit module have been realized. The circuit in Fig.4.4 is the voltage controlled floating current source. The electrical characteristics were carried out in at room temperature in air using a HP4155A.

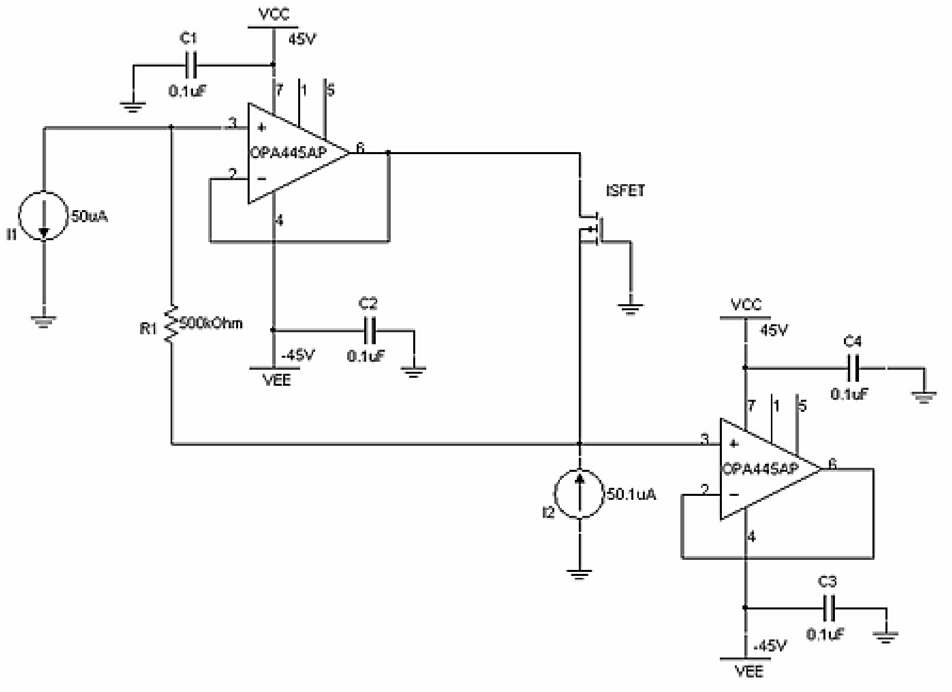

Fig. 4.4: Floating current source for biasing the ion-sensitive device

4.4 Results and discussion

Figure 4.5 and Fig. 4.6 show the output characteristic and the transfer characteristic of the device biased as a *p*-channel FET taken with a pH of 7.

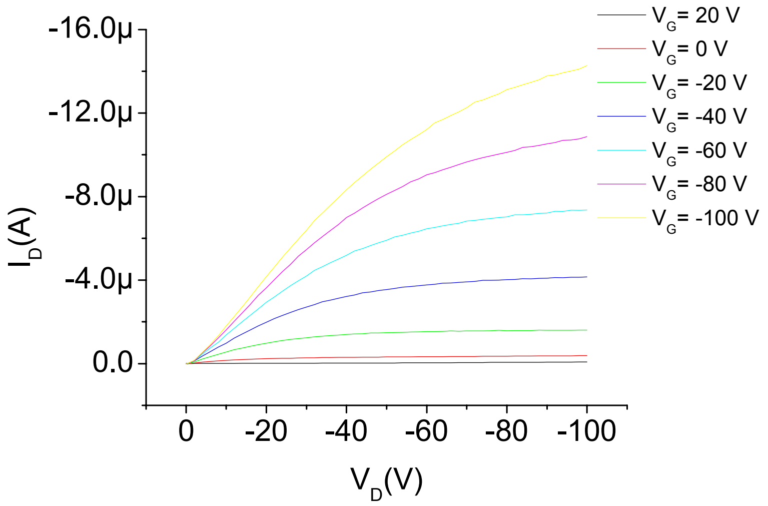

Fig. 4.5:. Output characteristics of an organic ion sensitive device on 900-nm-thick Mylar gate dielectric taken with a pH 7 solution.

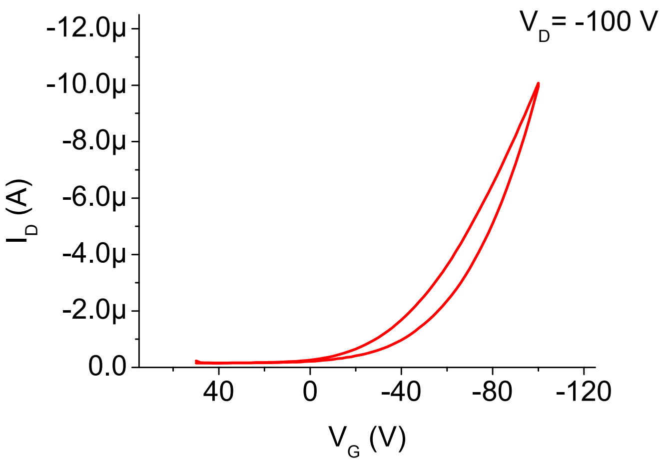

Fig. 4.6: I_D vs. V_G taken with a *p*H 7 solution.

These curves have been registered in presence of an electrolytic solution with a *p*H of 7 after the reference electrode has been left to stabilize in the same solution for about half a hour. This procedure has been done with the aim of obtaining more stable measurements. As can be seen, the device has the typical behaviour of organic *p*-type field effect transistors working in accumulation mode with increasing negative values of I_D with increasing negative V_D values and with a clear field-effect induced by the gate voltage similarly to OFETs with a metallic gate.

It can be observed that the transfer characteristic has a small hysteresis effect, that is normally observed also in devices with the metallic gate contact [9]. This indicates that there is a parasitic capacitance effect due, in this case, to the charged layer at the interface between the insulating layer and the solution and probably also to charge trapping effects in the organic semiconductor (possibly affected also by barrier injection effects at the metal–semiconductor interface and by bias stress of the device). It is interesting to notice that this hysteresis effect is of the same order in all ion-sensitive devices, while in organic transistors this effect is extremely variable and it is dependent on metal electrodes overlapping.

Figure 4.7 shows the output characteristic and the transfer characteristic curves taken on the same sample exposed to 3 different pH values. As can be seen there is a decrease of the current with acid solutions and an increase with basic solutions that clearly indicate that there is an accumulation of ions at the interface between the insulating layer and the solution.

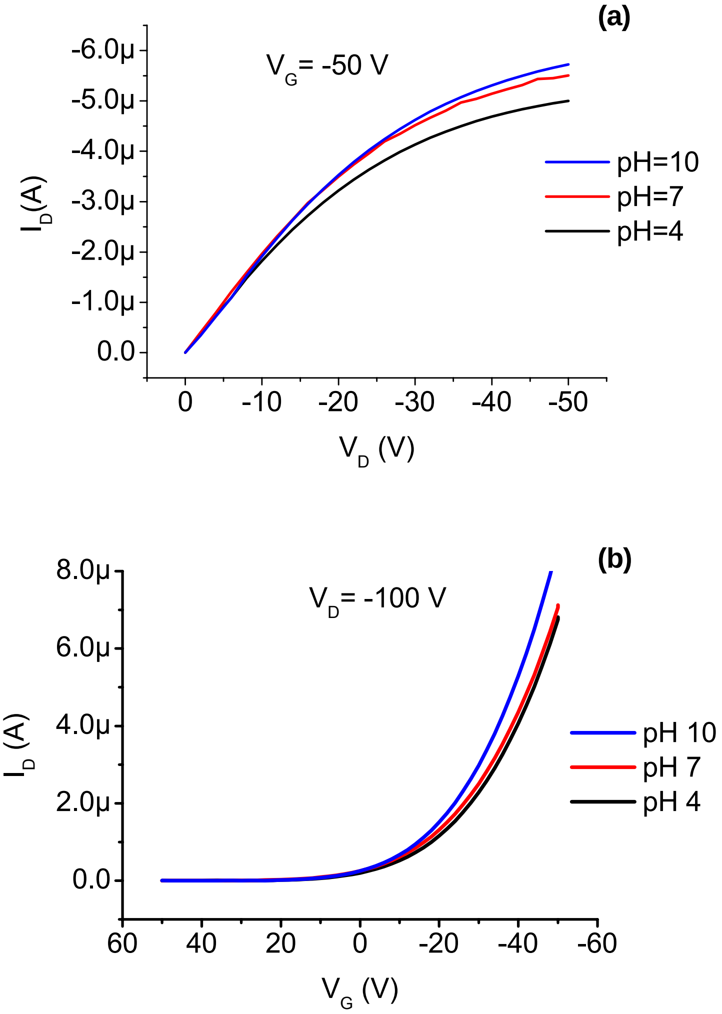

Fig. 4.7: Output characteristics (a) and (b) I_D vs. V_G taken with a 3 different *p*H values

Ion sensitivity results from the presence on the surface of the insulating layer of specific sites for H^+ ions in the electrolytic solution [10]. Depending on the pH values in the solution, the processes over the surface of the insulating layer generate a local charge accumulation, which is limited in a very thin hydration layer on the surface as described in the previous sections.

When negative charge density is increased, as for basic solutions, holes accumulate in the channel in higher density than in the case of neutral or acid solutions. As a consequence, the negative current recorded with fixed values of V_D and V_G is higher. Conversely, in the case of acid solutions, the positive charge accumulated at the insulator/solution interface causes a decrease of the hole density in the channel and a (negative) lower value of I_D.

The curves reported in Fig. 4.7, taken with different pH values, show a non-linear response with respect to the pH value. This aspect can be related to the fact that is not possible to know a priori the time required to achieve the true stabilization of the current.

We have investigated also the stability of the response by recording the current variation in time. Figure 4.8 shows I_D versus time while the pH value is kept constant at 7.

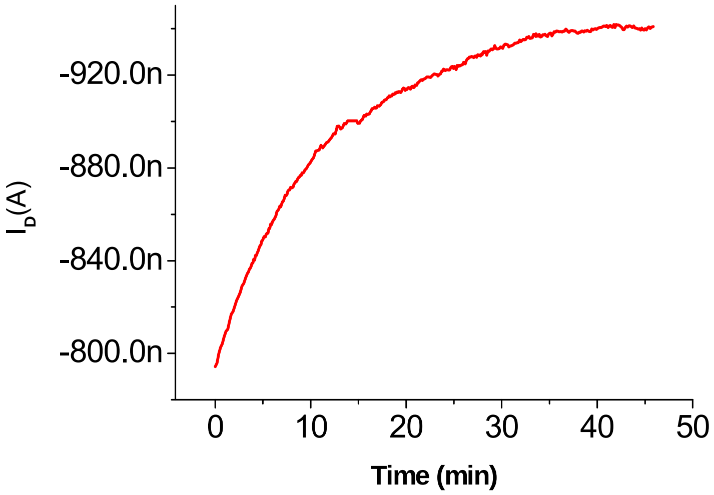

Fig. 4.8: I_D vs. Time curve taken with a pH value of 7 showing the time required to stabilize the current after the application of the voltages.

The current flowing in the channel shows a capacitive behaviour: after a time interval of more than 30 min, the current stabilizes to a saturation value that depends on the pH value of the solution. Therefore, before recording the characteristics, the device and the reference electrode were kept for at least 30 min in the pH solution to achieve stabilization.

As can be seen from Fig. 4.9 (taken in the saturation regime by leaving a 30 min hold time after every *p*H variation), there is once more a decrease of the current with acid solutions and an increase with basic solutions. In this case the current variation is linear and reversible. These features are highly desirable for practical application involving chemical sensors.

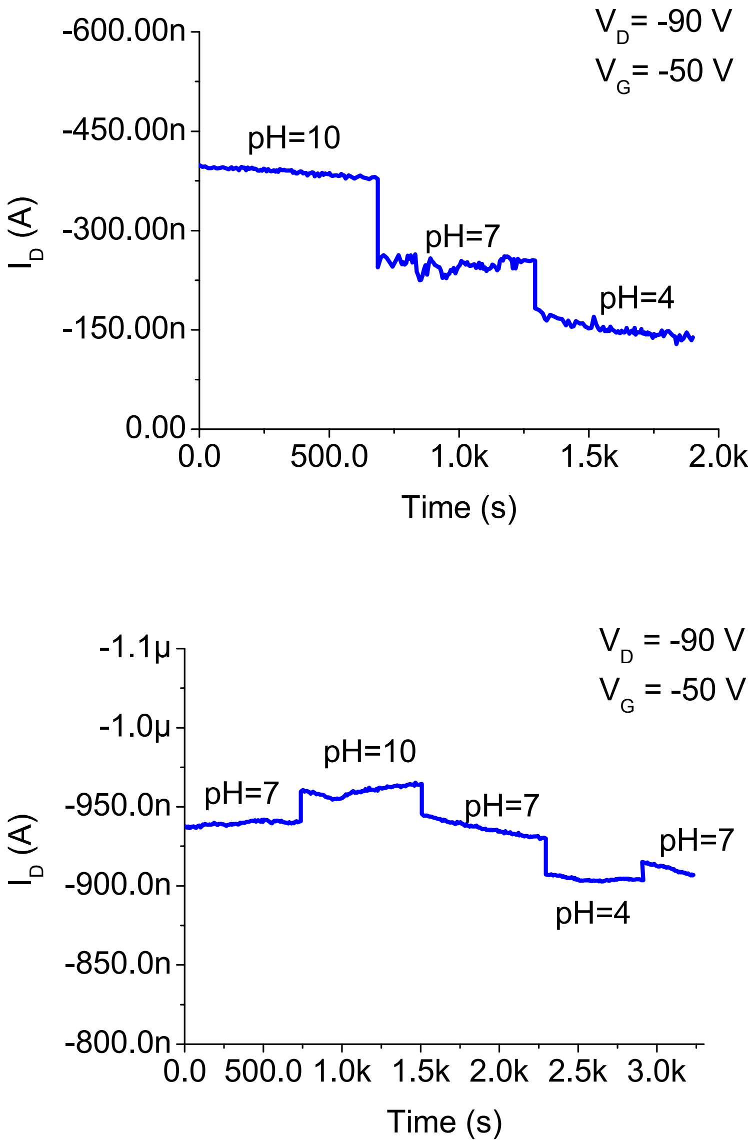

Fig. 4.9: I_D vs. Time curve taken with different pH values of the electrolytic solution (saturation regime)

The observed sensitivity concerns both the saturation region and the triode region how can be seen in Fig. 4.10 taken in the linear region. The curve is recorded without living a hold time after every pH variation.

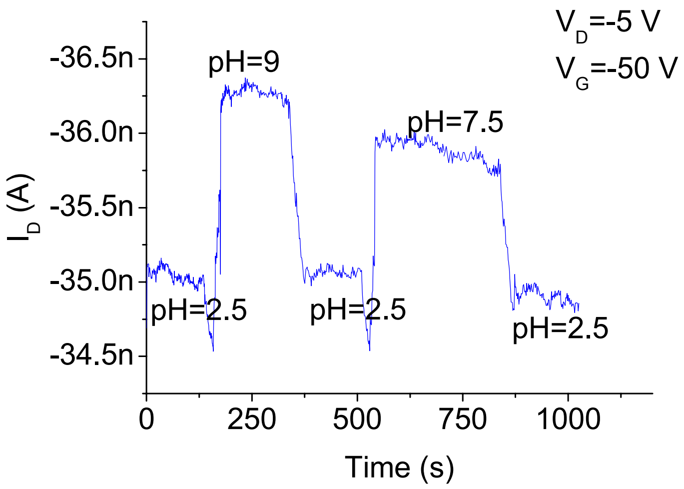

Fig. 4.10: I_D vs. Time curve taken with different pH values of the electrolytic solution (linear regime)

The dependence of the transistor current on the pH value of the solution must be related to a variation of the threshold voltage of the device. This working principle is valid both for ISFETs and ISOFETs, as already demonstrated by C. Bartic et al., with the obvious differences due to the specific features of organic semiconductor based devices (as low current and high operating voltages).

The macroscopic electronic behaviour of organic ion sensitive transistors may be reasonably described by the same equations as for inorganic ion-sensitive transistors. At low gate bias values, the charge carrier mobility can be assumed constant and the current flowing between source and drain is well described by the equation 4.1:

$$I_D = \frac{Z}{L}\mu C_i\left[(V_G - V_t)V_D - \frac{V_D^2}{2}\right] \tag{4.51}$$

The threshold voltage V_t is given by:

$$V_t = V_{FB} - \frac{Q_B}{C_i} + 2\phi_F \tag{4.52}$$

where V_{FB} is the flat-band voltage, Q_B is the depletion charge in the silicon and φ_F the Fermi-potential.

The variations of the threshold voltage can be attributed to a charge variation at the solution-insulator interface that can be explained in the frame of the Gouy–Chapman–Stern theory. According to this theory, an insulator exposed to an aqueous solution interacts with H^+ ions and causes a redistribution of the charge in the solution. When the structure formed by the insulator and the electrolytic solution is completed by a semiconductor layer located at the opposite side of the insulator, as in the case of MOSFET and OFET structures, the charge variation at the insulator/solution interface capacitively induces a redistribution of charge in the semiconductor. In field effect devices, this variation is directly detectable through the variation of the threshold voltage of the device.

The resulting equation for the flat-band voltage is thus given by:

$$V_{FB} = E_{ref} - \Psi_0 + \chi_{sol} - \frac{\Phi_s}{q} - \frac{\Phi_{ss} + \Phi_{ins}}{C_i} \tag{4.53}$$

in which E_{ref} is the reference electrode potential relative to vacuum, ψ_0 is the surface potential, which results from a chemical reaction, usually governed by the dissociation of insulator surface groups, χ_{sol} is the surface dipole potential of the solution, which is a constant, Φ_S Φ_{ins} are the semiconductor and insulator workfunction respectively and Q_{ss} is the surface state density at the semiconductor surface.

Because all terms are constant with pH except ψ_0, it is this term which makes the device sensitive to the electrolyte pH, which is controlling the dissociation of the insulator surface groups.

Then the sensitivity of the devices can be evaluated by extracting the threshold voltage from the $\sqrt{I_D}$-V_G curves in the saturation regime. Figure 4.11 shows an example of V_{th} vs. pH plot. As can be seen the variation of the threshold voltage is linear with respect to pH.

Alternatively it is possible to measure the sensitivity keeping constant the drain bias conditions (I_D and V_D in the linear regime) and measuring the variations of the gate-source voltage induced by the pH changes in the electrolytic solution.

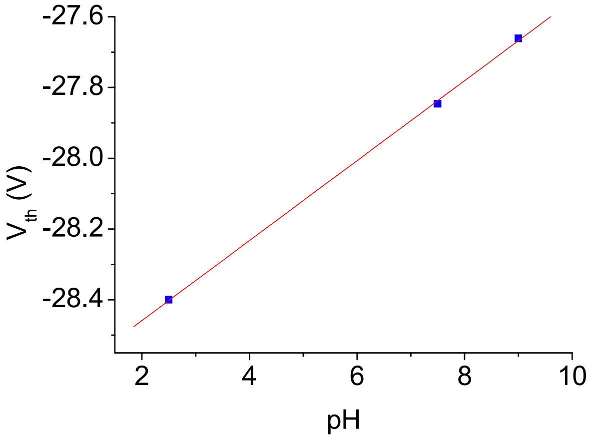

Fig. 4.11: V_{th} vs. pH

As can be derived from Eq. 4.51 in the linear region when I_D and V_D are keeping constant the variation of the threshold voltage induced by the variation of the pH in the solution causes an identical variation in the gate voltage V_G.

In this way the sensitivity can be expressed by the Eq.4.54

$$S = \frac{\Delta V_G}{\Delta pH} = \frac{\Delta V_{th}}{\Delta pH} \tag{4.54}$$

An example of V_G vs. Time is shown in Fig. 4.12.

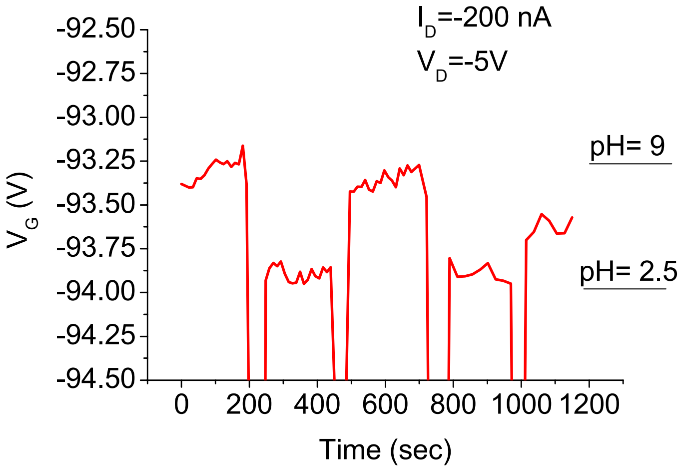

Fig. 4.12: V_G vs. Time curve taken with different pH values of the electrolytic solution.

The estimated sensitivity is in the range of 50-100 mV/pH with a variability from sample to sample. As demonstrated in section 4.2.3 the maximum sensitivity achievable is 59.3 mV. A sensitivity value higher than 59.3 mV is not physically meaningful. This means that the estimated sensitivity can not be attributed only to the phenomena occurring at the insulator/electrolyte interface, but also to other contribution due to the conduction mechanism on the organic semiconductor (for instance drift effects, degradation, ecc.). These features are not clearly elucidated yet and need further investigations.

The chemical structure of Mylar is reported in Fig. 4.13 while the components proportion in standard PET samples derived from XPS analysis is shown in Fig. 4.14 [11]

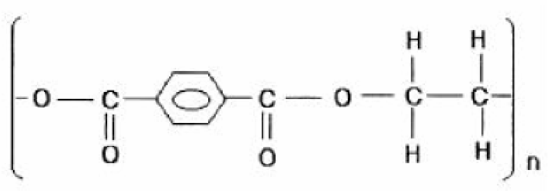

Fig. 4.13: Chemical structure of Mylar

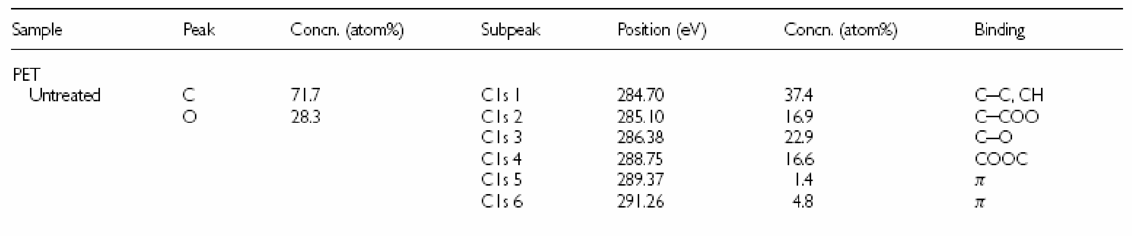

Sample	Peak	Concn. (atom%)	Subpeak	Position (eV)	Concn. (atom%)	Binding
PET						
Untreated	C	71.7	C1s 1	284.70	37.4	C—C, CH
	O	28.3	C1s 2	285.10	16.9	C—COO
			C1s 3	286.38	22.9	C—O
			C1s 4	288.75	16.6	COOC
			C1s 5	289.37	1.4	π
			C1s 6	291.26	4.8	π

Fig. 4.14: Detailed Evaluation of XPS spectra for a PET film

We used Mylar film for the first-time as dielectric insulator in a ion-sensitive device, so unfortunately a site-binding model that explains in detail the mechanism at the surface for this material has not been developed yet. On the other hand Mylar (and PET in general) is a widely used biocompatible material. For this reason many approaches to the modification and functionalization of the polymer surface by wet chemistry, plasma processes or UV treatment have been reported in the literature [11-14].

These surface modification approaches demonstrate that it is possible to improve the reactivity of the PET surface in order to generate specific groups on the surface or to immobilize biomolecules. In our case we believe that these groups are responsible for the observed sensitivity of the devices when exposed to variable pH solution.

For future applicative perspectives, it would be desirable to use these sensors not only to detect pH but also other kinds of analytes. Therefore the possibility of funtionalizing the insulating layer with specific groups capable of selectively couple to the analyte to detect would be very useful.

However chemical functionalization of metal is a much easier task than grafting molecules on polymeric surfaces. Well know processes as thiol self assembly could be a very easy to apply to this kind of device structure.

One of the possible development of the ion-sensitive strategy concerns the realization of floating gate devices in a similar way to that reported for inorganic devices in [15,16]

References

1. C. Bartic et al. , IEEE Transducers '01 (2001)
2. C.Bartic et al., Appl. Phys. Lett. 82,3,475-477, (2003)
3. C.Bartic et al., Sensors and Actuators B 83, 115-122, (2002)
4. A. Loi et al., Appl. Phys. Lett. 86, 103512, (2005)
5. Grattarola et al., Bioelectronics handbook, Mc Graw Hill, 1999
6. Bergveld P., IEEE Trans. Biomed. Eng., BME 19, 342-351, (1972)
7. Bergveld P, Sens. Act. B, 88, 1-20, (2003)
8. Casans S. et al., EDN, May 1, 92 (www.edn.com)
9. A.R. Brown, et al., Synth. Met., 88, 37 (1997)
10. Bergveld P. , IEEE Sensor Conference (2003)
11. Heitz et al., Biotechn. Appl. Biochem. 39, 59, (2004)
12. Mougenot P. et al., Jou. Coll. Interf. Sc. 177,162-170 (1996)
13. Hu J. et al., Adv. Funct. Mater. 13, 9, 692, (2003)
14. Jain R. et al., Wiley Periodicals, (2003)
15. Barbaro M. et al., IEEE Trans.Elec. Dev. 53, 1, 158, (2006)
16. Barbaro M. et al., IEEE Elect. Dev. Letters, 27, 7, 595, (2006)

CHAPTER 5

Mechanical Sensors based on Organic Field-Effect Transistors

5.1 Introduction

In this chapter we report on organic semiconductor based mechanical sensors. Papers regarding this kind of sensors have already been published [1-3] or are due to be submitted soon for publication. The proposed device is completely flexible, it is entirely processed at room temperature and combines in itself both switching and sensing functions. These are very interesting hallmarks since only a few examples of organic mechanical sensors have been reported in literature and none of them exploits all the potential advantages of organic devices. Taking advantage of the full mechanical flexibility of the insulating sheet, attractive developments can be foreseen for this "electronic film", for instance, a matrix combining different sensing devices (chemical, temperature, etc.) for robotic skin applications.

5.2 Device processing and electrical characterization

As illustrated in Chapter 3 the basic device structure is shown in Fig. 5.1

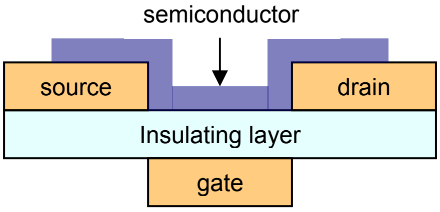

Fig. 5.1 Mechanical sensor structure

The device consist of a Pentacene substrate-free structure with gold-bottom-contact source and drain electrodes.

For mechanical sensors a 1.6 μm thick Mylar foil is used as gate insulator and also as mechanical support of the whole device. First of all the Mylar foil is clamped to a cylindrical plastic frame (2.5 cm in diameter) in order to obtain a suspended membrane with both sides available for processing. The foil is then cleaned with acetone, washed with deionised water and finally dried with a nitrogen flux.

Then, bottom-contact gold electrodes (nominal thickness 100 nm) usually with W/L=100 (W=5 mm and L=50 μm are the channel width and length, respectively) are thermally evaporated and patterned on the upper side of the flexible dielectric foil, using a standard photolithographic technique.

The gold gate electrode is patterned on the opposite side of Mylar film. Since the Mylar is transparent to UV light, source and drain may be used as shadow mask for the gate patterning. Therefore, a thin photoresist layer is spin-coated on the lower side of the Mylar layer and then it is exposed to UV light projected through the Mylar itself. In this way, source and drain electrodes act as a mask for the UV light and a perfect alignment between source and drain and the impressed photoresist is obtained. After the development process, a gold layer (nominal thickness 100 nm) is vacuum-sublimed and patterned by means of lift-off etching with acetone.

In this way, the channel area of the device included between source and drain contacts, is precisely gate-covered on the opposite part of the insulator (see Fig. 5.1), thus limiting all the parasitic capacitance effects due to source-drain and gate metal overlapping [4]. Residual hysteresis can be interpreted both in terms of border effects and with trapping charge effects in the semiconductor [5-7].

This one-mask photolithographic process is shown in Fig. 5.2.

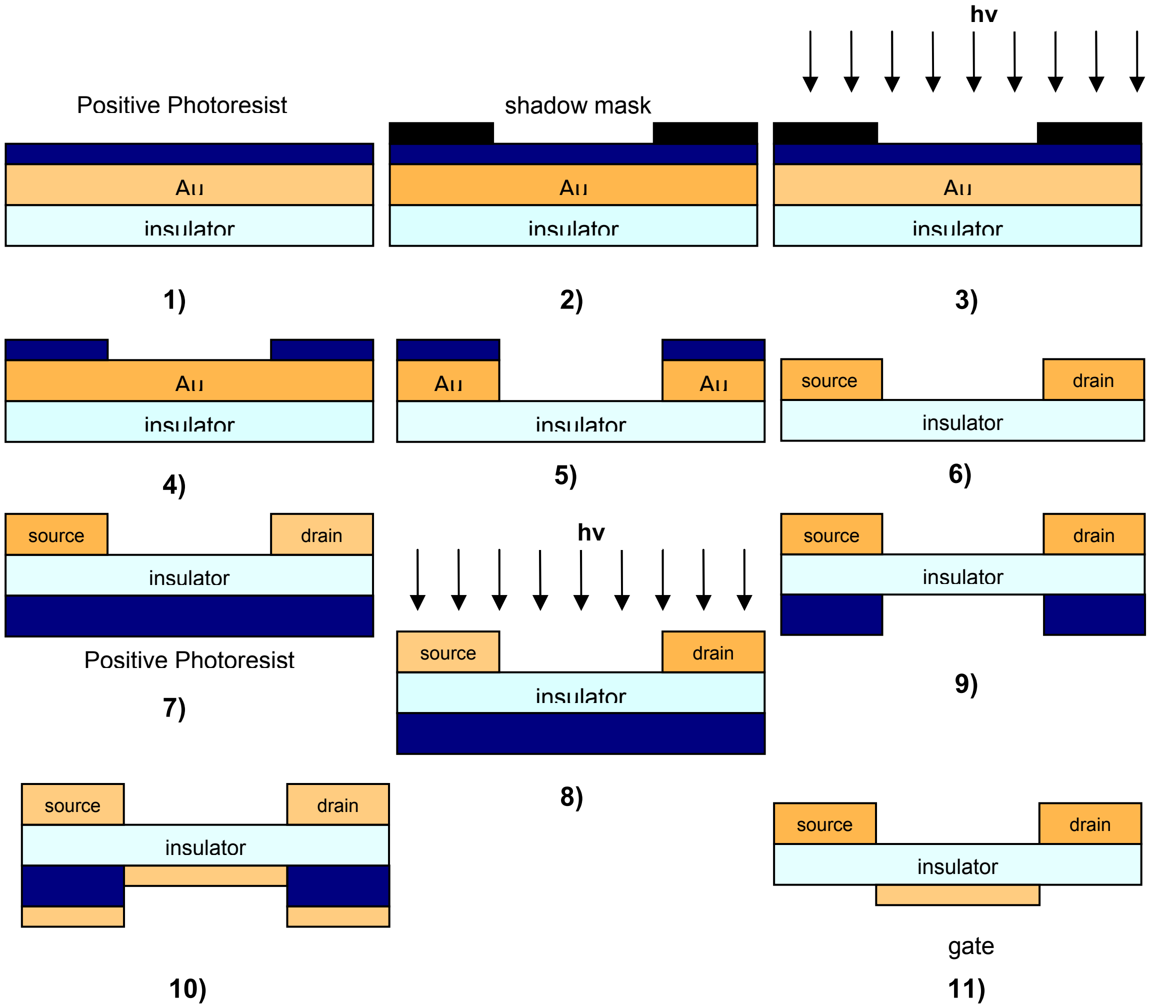

Fig. 5.2: One-mask photolithographic process for electrodes patterning:1) positive photoresist layer deposition on gold surface; 2) and 3) photoresist layer exposure to UV light using a shadow mask for the source and drain definition; 4) photoresist layer after developing; 5) gold layer after chemical etch using KI/I mixture; 6) device after photoresist removal; 7) photoresist deposition on the bottom side of insulator; 8) photoresist exposure through source and drain electrodes; 9) photoresist after developing; 10) gold deposition by means of thermal evaporation; 11) final device structure after lift-off with acetone.

In order to study the influence of structural effects (in particular of the contact/semiconductor interface) on the pressure sensitivity, we have also realized, on the same insulating layer, couples of bottom-contact and top-contact devices with the same active layer.

In this case, source and drain contacts are patterned by means of soft lithography using the conductive polymer PEDOT:PSS [8]. The procedure for realizing both kinds of processes on the same dielectric is shown in Fig 5.3.

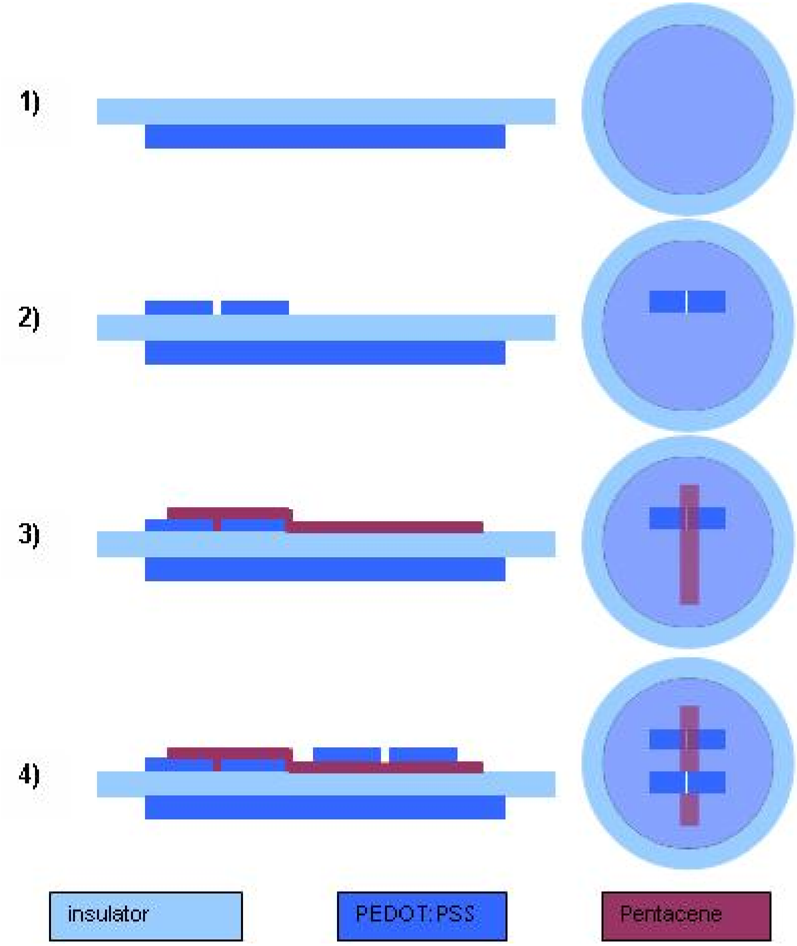

Fig. 5.3: Realization procedure of bottom- and top-contact device on the same insulating layer and with the same active layer: 1) gate deposition by means of spin coating of PEDOT:PSS in the bottom-side of Mylar film; 2) source and drain patterning of the bottom-contact device by means of microcontact-printing; 3) vacuum sublimation of the pentacene layer on top of the whole insulator film; 4) source and drain patterning of the top-contact device by means of microcontact-printing

For making a bottom-contact device, source and drain contacts of the bottom-contact device are first patterned on a portion of the Mylar foil. Then, the semiconductor layer is grown by vacuum-sublimation on top of the whole insulating foil. In the case of top-contact devices, the semiconductor film is deposited first and then source and drain electrodes are patterned directly on the semiconductor film. aside the bottom-contact device by means of microcontact-printing (µCP) as well.

The same organic semiconductor is deposited at once on both devices, in order to have the same thickness and quality of the semiconductor in the channel of each transistor. Contacts are obtained by means of microcontact-printing by using a PDMS (polydimethylsiloxane) stamp, in this way, the geometry of the contacts is also exactly the same; and in conclusion the only difference between the two devices is the interface between semiconductor and contacts. Pentacene film with a thickness of 50 nm is grown by vacuum-sublimation at a nominal deposition flux of about 1 Å/s.

To study the correlation between the pressure applied on the device and its electrical performance, we have used the experimental set-up shown in Fig. 5.4: a pressurization chamber provided with a manometer and an air valve. The chamber has a circular aperture on the top and the free-standing device is clamped at the edge (2.5 cm in diameter) of a cylindrical frame fixed at the aperture. When the pressurized air flows into the chamber it deforms the freestanding device.

Fig. 5.4: Pressurization chamber for mechanical sensors testing

The marked sensitivity of the drain current to an elastic deformation induced by a mechanical stimulus and the fact that the device is so thin and flexible that it can be applied to whatever surface can be exploited also to detect through the variation of the current on the device channel any mechanical deformation of the surface itself. In this case the device is applied on a flexible substrate, usually a strip of paper or a thin plastic sheet, in order to easily handle the device and then it is wrapped around cylinders of different radii of curvature.

In a further experiment the device has been glued with the gate side internally exposed to a suspended stainless steel cantilever. On the opposite extreme of the cantilever different weights are suspended in order to produce a measurable deformation to the cantilever and on the device glued on it

Electrical characteristics with and without applied mechanical stimulus are carried out at room temperature in air, by using a HP 4155 Semiconductor Parameter Analyzer without any extra ad-hoc read-out circuit or equipment.

5.3 Results and discussion

The device has the typical behaviour of an organic p-type field effect transistor. The conductance of the organic semiconductor in the channel region is switched on and off by the gate electrode, which is capacitively coupled to it through the dielectric layer. The gate bias (V_G) controls the current (I_D) flowing between the source and drain electrodes under an imposed bias (V_D). Applying a negative gate voltage causes an accumulation of carriers and increases the conductance. Typical recorded values of hole mobilities are in the range of 10^{-3}-10^{-2} cm^2/Vs, while threshold voltages are in the order of some tens of Volts.

To verify the possible dependence of the transistor current on a mechanical stimulus applied to the device, we performed several kinds of experiments. For instance, we measured output curves while applying a constant pressure.

Figure 5.5 shows the drain current I_D versus the drain voltage V_D at different values of V_G and the transfer characteristics in the linear and in the saturation regime the with different pressures applied.

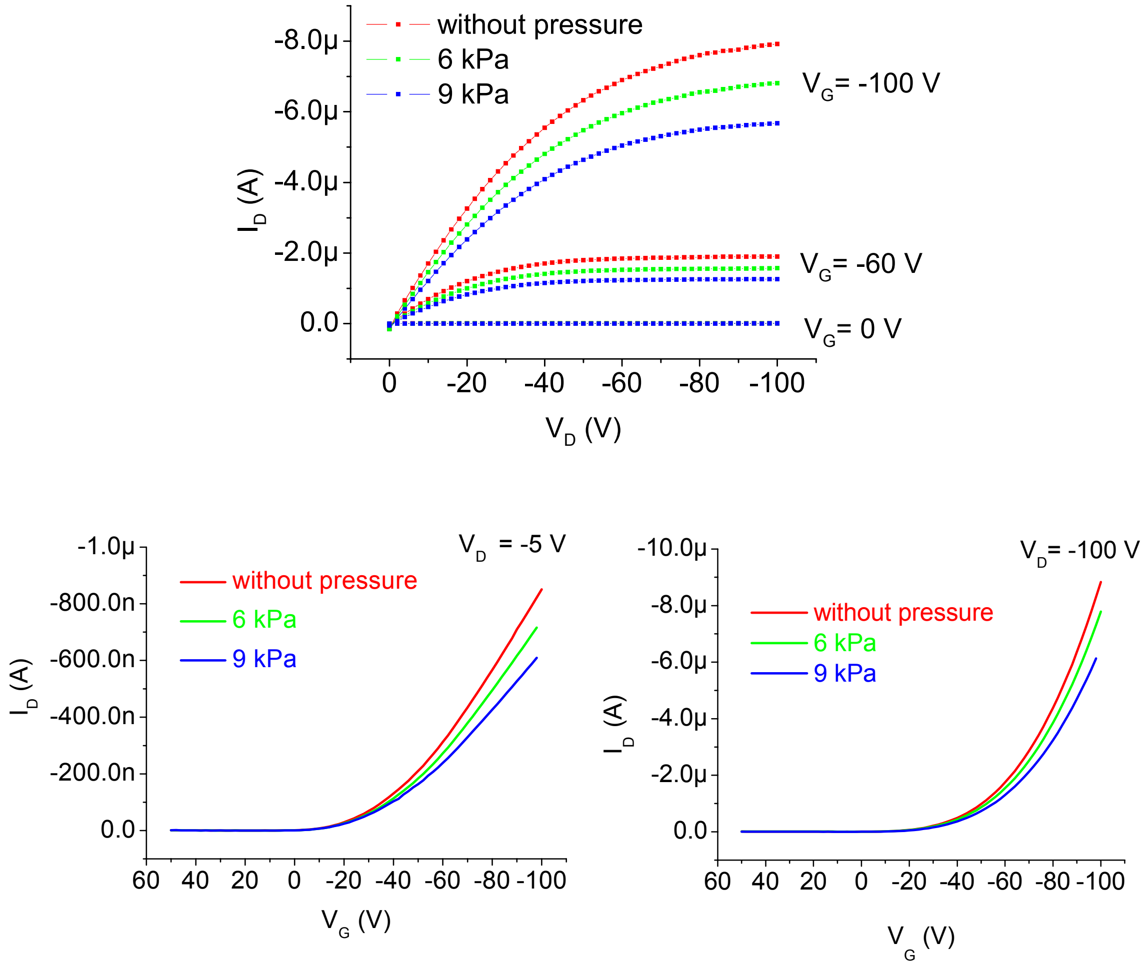

Fig. 5.5: Comparison between output curves and transfer characteristics with different pressure states

It can be noticed that while the global shape of each curve is unvaried with respect to the curve taken without applying a pressure, there is a decrease of the current when a pressure is applied. The observed sensitivity concerns both the triode region and the saturation region.

On the other hand, we performed time-measurements with constant bias and varying pressures. Figures 5.6, 5.7, 5.8 show the time variation of I_D (in the linear region) while pressure is applied to the device.

In Fig. 5.6 the current variation in response to different increasing values of applied pressure is displayed. From this figure, it can be noticed that the drain current variation is linear with respect to the applied pressure.

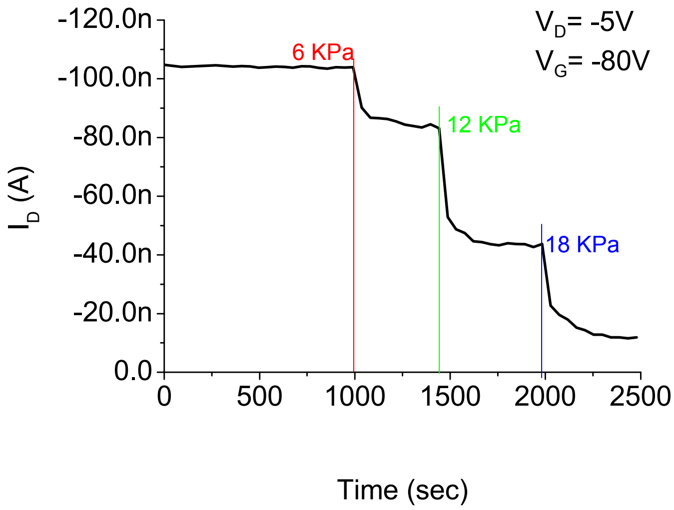

Fig. 5.6: I_D vs. Time curve with different applied pressures

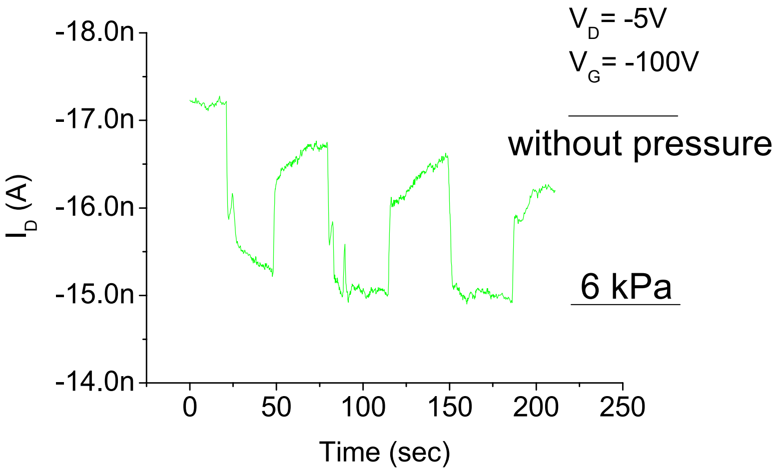

Fig. 5.7: Reversibility of I_D vs. Time

Figure 5.7 shows what happens when a constant value of pressure is repeatedly applied and removed according to a time sequence. As it can be observed, the drain current variation is reproducible, and reversible despite the presence of a hysteresis. The sensor responds very fast to the mechanical stimulus (i.e. within tens-hundreds of milliseconds) but the time required to reach the steady state is much higher (tens-hundreds of seconds) with a significant variability from sample to sample.

Figure 5.8 shows the sensor response to a "breathing-like" signal. The pressurised air flow is applied and removed according to a natural human breathing-in and –out rhythm. As it can be seen the sensor response is once more fast and reversible and reproducible despite the hysteresis.

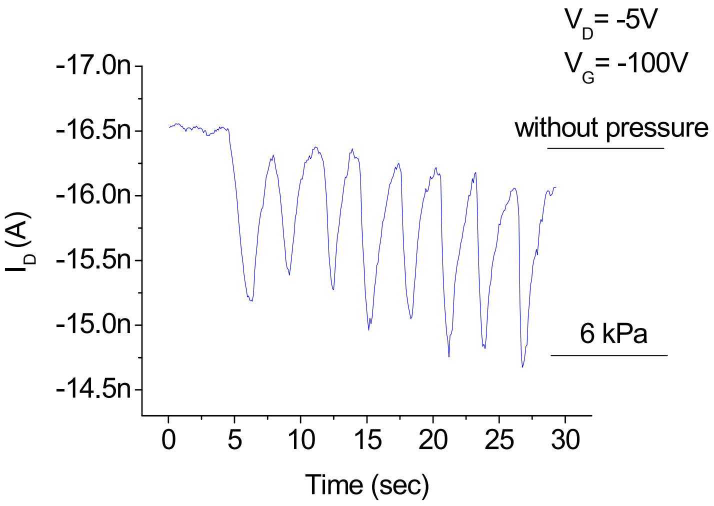

Fig. 5.8: I_D vs. Time

This kind of time instability and hysteresis can be due to several factors. Often also structural effects of devices contribute to these problems: for instance, parasitic capacitance effects due to metal electrodes overlapping negatively affect the time response of field effect devices. In order to prevent this problem, during device assembly, we have realized an auto-alignment of contacts and therefore this effect should be minimized, or, at least negligible. On the other hand, it is worth noting that the device has been measured in air and it is not encapsulated; as both these factors are known to cause drift and in general to negatively affect the device performances, we cannot exclude degradation effects in the semiconducting layer due to humidity, oxygen, etc. Indeed these issues deserve more investigation, since faster dynamics, reproducibility and reversibility are obviously desirable for practical applications.

To characterize the performances as a sensor, a sensitivity parameter must be defined. Starting from I_D-V_D curves it is obvious to define sensitivity as ΔI/Δp. The sensitivity has been evaluated with 5 different values of pressure. The sensitivity is gate voltage dependent and is higher in the saturation region than in the linear one. Therefore, from these data, it seems that the best bias working point for employing this device as a pressure detector is with a bias corresponding to the maximum value of current. Figure 5.9 shows the sensitivity vs. gate voltage derived from one significant sample.

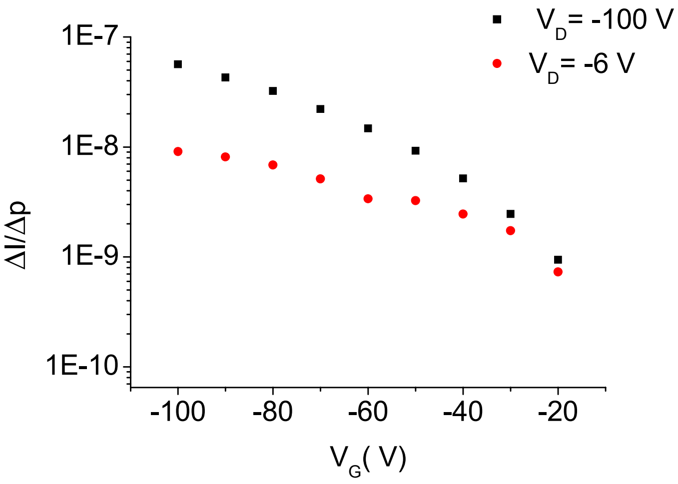

Fig. 5.9: ΔI/Δp vs. V_G

To explain the possible cause of the observed sensitivity of the current to the pressure, it is necessary to take into consideration all parameters affecting the drain current of a field effect transistor. According to the ideal model, this current is satisfactorily described in the linear regime by the Eq. 5.1

$$I_D = -\frac{W}{L}\mu C_i\left[\left(V_G - V_{th}\right)V_D - \frac{V_D^{\ 2}}{2}\right] \tag{5.1}$$

Variations of W/L ratio, mobility μ, insulating layer capacitance C_i, threshold voltage V_{th} can in principle be related to the pressure-induced variation of the drain current. Firstly, W and L may undergo some modifications when the device is deformed, but it should be noticed that both the mechanical stimulus applied by means of an air flow and the insulating layer are mechanically isotropic. Therefore, the width W and the length L of the transistor channel change at the same extent, thus keeping constant their ratio. Secondly, a possible thinning of the insulating film thickness d_i should induce an increase in the insulating layer capacitance C_i being $C_i=\varepsilon_i/d_i$. We have performed capacitance vs. frequency measurements for on simple capacitors where the Mylar foil is the dielectric layer between gold plates, for different pressures applied on the it obtaining the results shown in Fig. 5.10

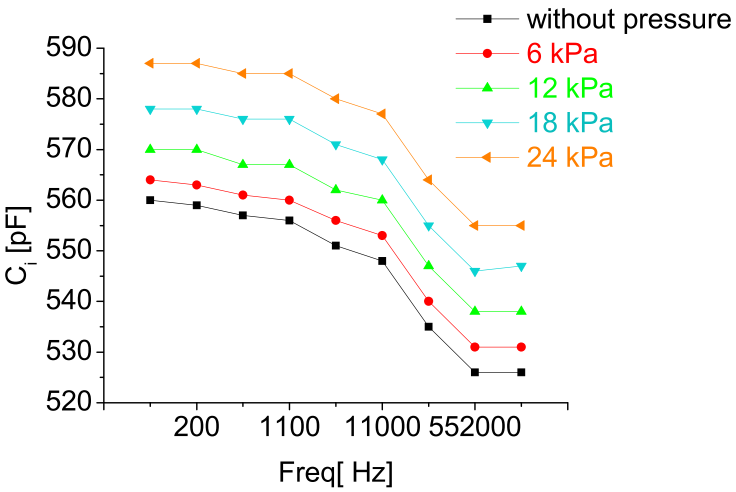

Fig. 5.10 Capacitance vs. Frequency with different applied pressure for a Mylar capacitor.

As expected, the applied pressure causes an increase in the insulating layer capacitance. Considering the expression of the drain current in Eq. 5.1, this increase in the dielectric capacitance, should result in an increase in the drain current. On the contrary, we always observe a decrease in the drain current, meaning that this effect is always negligible. Therefore, the observed sensitivity must be attributed to a different, non-geometrical effect.

In order to verify this hypothesis, mobility and threshold voltage have been extracted by fitting our data with Eq. 5.2:

$$I_D = -\frac{W}{L}\mu C_i\left[(V_G - V_{th})(V_D - R_s I_D) - \frac{(V_D - R_s I_D)^2}{2}\right] \tag{5.2}$$

where also the contact resistance Rs is taken into account.

Maximum current varies from sample to sample (this is absolutely normal in organic semiconductor based devices not encapsulated and measured in air), therefore it would not make any sense to make a statistic on different devices, by using this parameter. Much more meaningful is the investigation of the behaviour of the relative variation of the maximum current vs. pressure. In Fig. 5.11 the relative variation of the maximum current recorded on a set of three samples (V_D= -100V, V_G= -100 V) has been plotted against pressure. It can be noticed that there is an uncontroversial linear dependence of this parameter on the pressure.

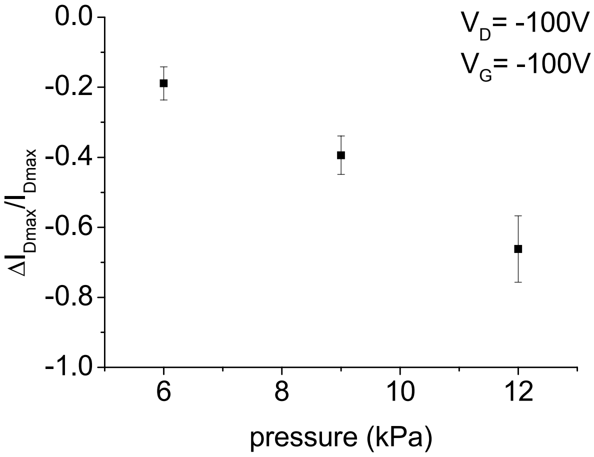

Fig. 5.11: $\Delta I_{Dmax}/I_{Dmax}$ vs. pressure (three samples)

Figure 5.12 shows mobility (a) and threshold voltage (b) plotted against pressure. The extracted values of mobility and threshold voltage show a similar linear dependence but the standard deviation is higher. This can be partially attributed to the fact that mobility and threshold voltage result from an extrapolation that is affected by possible failures of the fitting model.

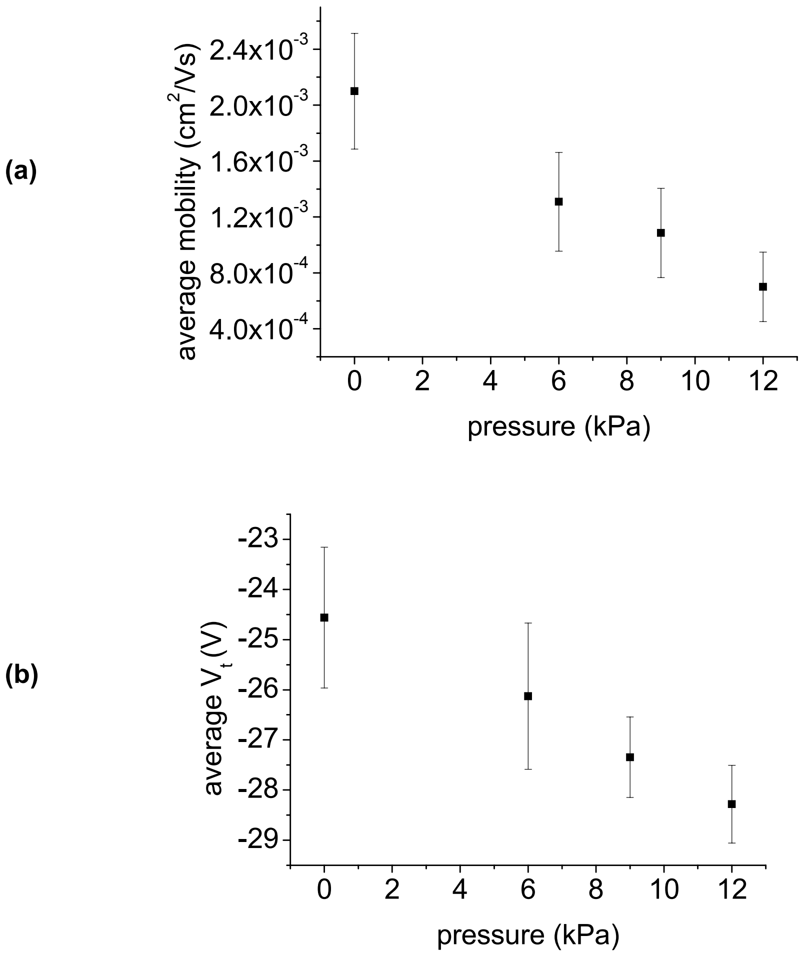

Fig. 5.12: (a) average mobility vs. pressure (three samples) ; (b) average threshold voltage vs. pressure (three samples)

We also extract the contact resistance by fitting our data with Eq. 5.2. However this parameter shows a different behaviour from sample to sample and sometimes also in the same sample for different measurements as shown in Fig. 5.13. Furthermore, occasionally the fitting model aborts and returns a contact resistance value that is not physically meaningful (i.e. negative). These feature suggest that a better model for the contact resistance should be used.

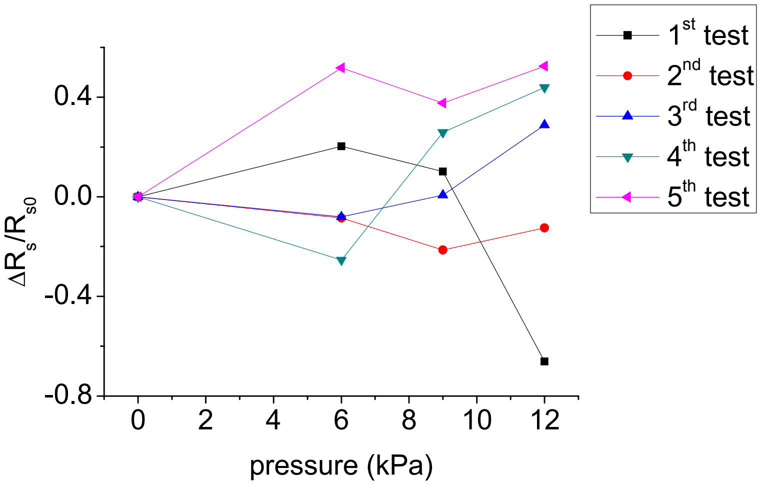

Fig. 5.13 Contact resistance vs. pressure (1 sample, 5 tests)

In Fig. 5.14 we show the relative variation of I_{Dmax} in the same sample for five different measurements (periodically repeated in time during several hours).

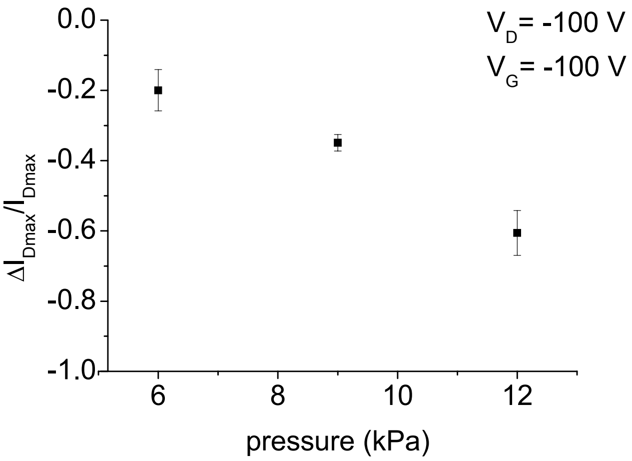

Fig. 5.14: $\Delta I_{Dmax}/I_{Dmax}$ vs. pressure (1 sample, 5 consecutive tests)

Again we can observe that there is a linear and reproducible behaviour, despite the fact that the data is extracted from curves taken during prolonged measurement sessions (6-7 hours), thus causing mechanical and electrical stress to the device.

Another interesting observation can be done on I_D-V_G curves, shown in Fig. 5.15: here the sweeping of the gate voltage from positive to negative values and vice versa causes in the drain current a hysteresis phenomenon, that enlarges when pressure is increased.

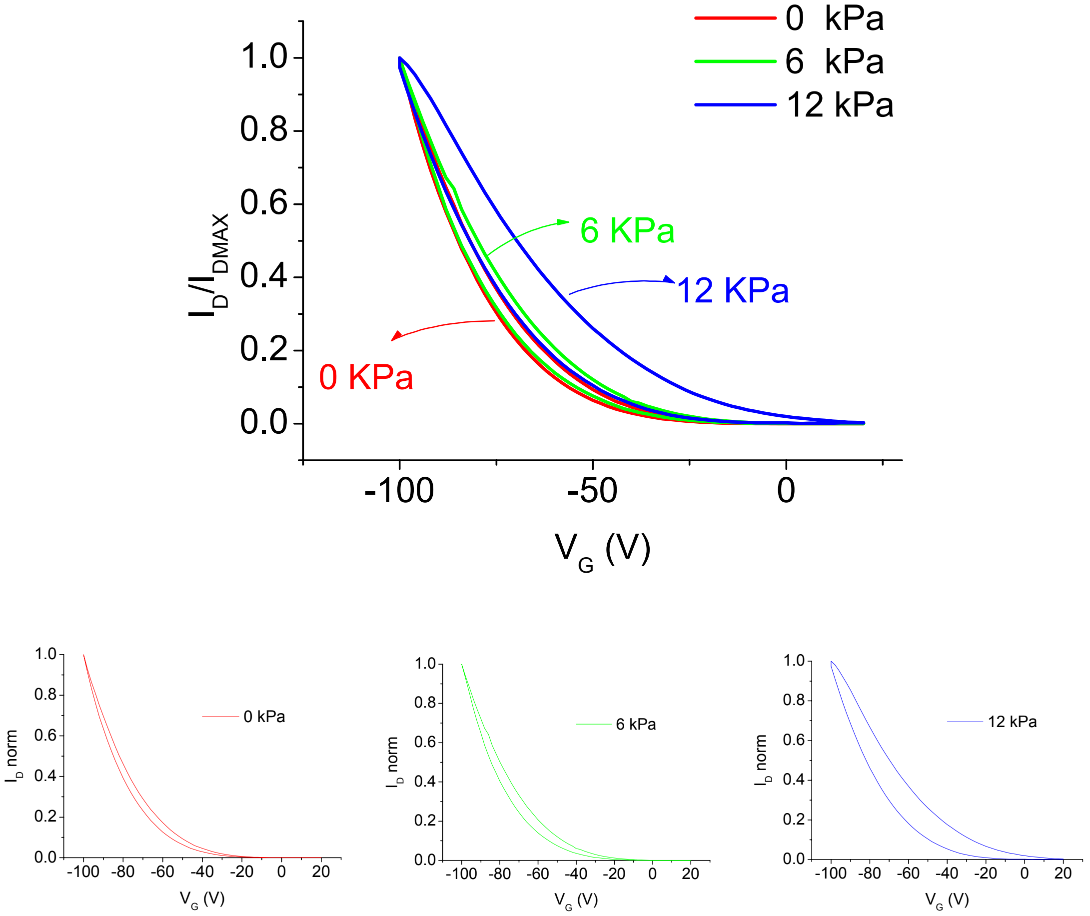

Fig. 5.15: Hysteresis in I_D vs. V_G curves with different applied pressures.

This fact suggests that the pressure-induced changes in drain current can be related not only to a direct dependence of the semiconductor conductivity on the pressure applied to the device but also to the distribution and activity of trap states that typically affect contact resistances, threshold voltages [4,10,11] and hysteresis [12].

To further clarify these observations, we decided to perform experiments on devices with different structures. In particular, we assembled couples of bottom-contact and top-contact devices using PEDOT:PSS as conductive material for electrodes ad described in section 5.2.

The goal of the experiment was to check if these different structures behave differently when a pressure is applied and to see which parameter is mostly affected. As a matter of fact, the different metal-semiconductor interface is expected to affect the behaviour of the electrical characteristics of the transistors even if no pressure is applied. In fact, the morphology of the pentacene film in the device channel region close to the electrode edges is different in top-contact and bottom-contact device. In the bottom-contact structure near to the edge of the electrodes there is an area with a large number of grain boundaries that are linked to the creation of charge carrier traps that are responsible of the reduced performance in bottom-contact device than in top-contact devices. [13]

The results of measurements in top-contact and bottom-contact devices are shown in Fig. 5.16, 5.17, 5,18. In the bottom-contact device we can observe a sharp dependence of the threshold voltage (Fig. 5.16 (a)) and hysteresis (Fig. 5.17) on the applied pressure, whereas for the top-contact device no correlation has been found between threshold voltage and pressure (Fig. 5.16 (b)) and also the hysteresis phenomenon is negligible in this case (Fig. 5.18).

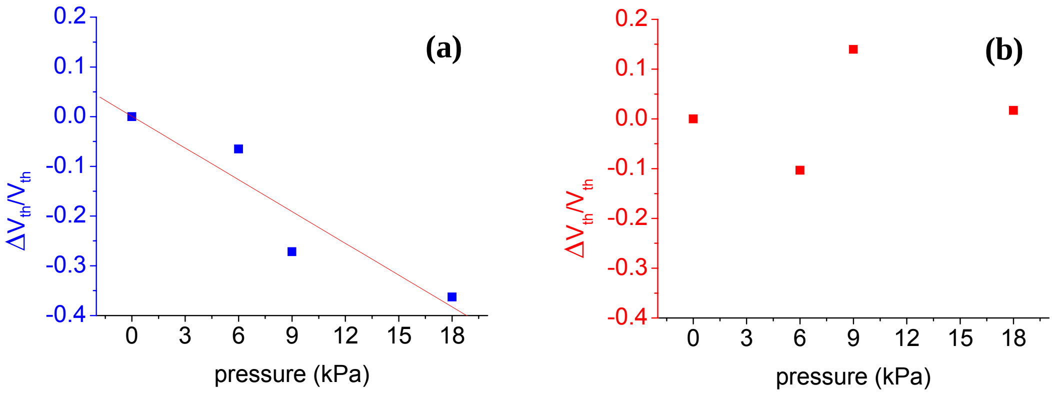

Fig. 5.16: Threshold voltage vs. pressure comparison between bottom-contact (a) and top-contact devices (b)

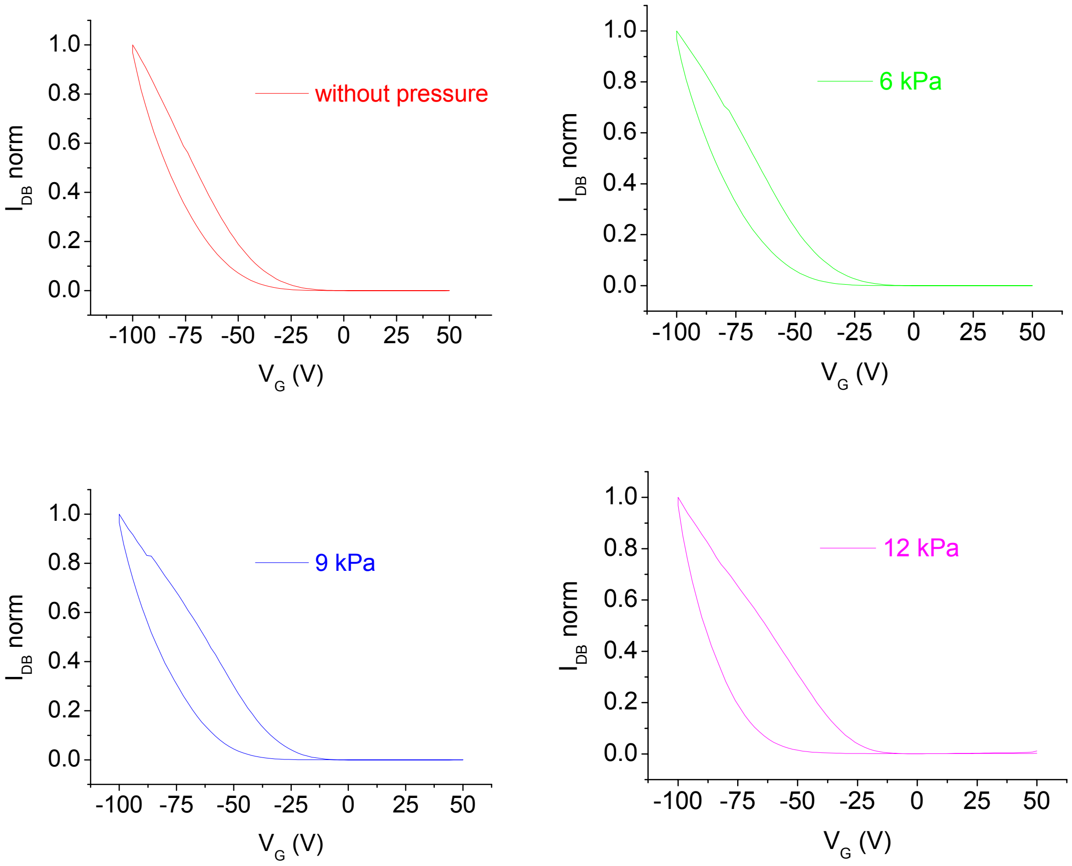

Fig. 5.17: **Hysteresis in I_D vs. V_G curves with different applied pressures in bottom-contact devices (V_D= -100 V)**

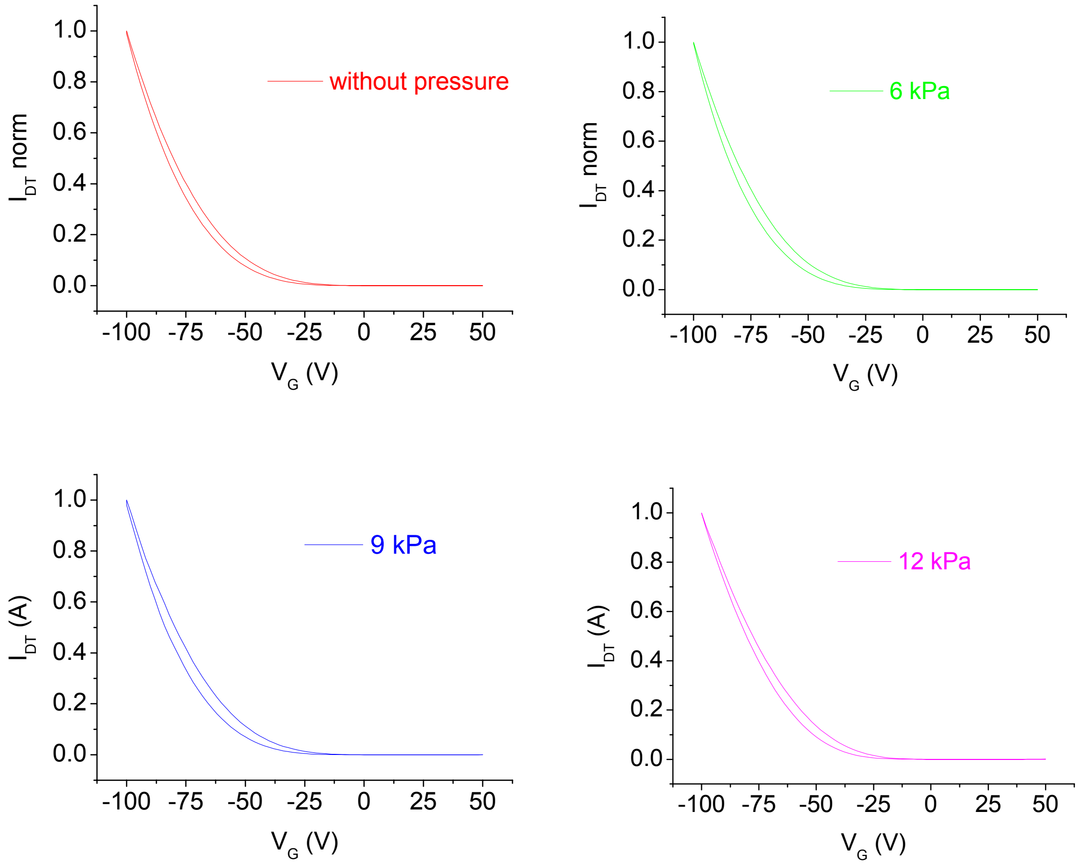

Fig. 5.18: **Hysteresis in I_D vs. V_G curves with different applied pressures in top-contact devices (V_D= -100 V)**

Contact resistance effects cannot be evaluated with the same model in top and bottom-contact devices: in the bottom-contact structure the semiconductor layer is grown on top of source and drain electrodes, so there is a direct carrier injection from the electrode to the device channel and the contribution to R_S may be attributed to the contact between electrodes and semiconductor, while in the top-contact structure in addition to the contribution to R_S due to source and drain contacts, there is a further voltage drop due to the fact that the current injected from the electrodes must vertically travel through the semiconductor layer before reaching the channel. For these reasons a direct comparison of the pressure-dependence of the contact resistance is not possible and needs further investigations.

The different dependence of threshold voltage and hysteresis on pressure in bottom-contact and top-contact devices confirms the role of insulator/semiconductor and metal/semiconductor interfaces in determining the pressure sensitivity of the device.

On the other hand, mobility has a very similar behaviour in the two devices, (see Fig. 5.19) indicating also a direct contribution of the semiconductor in the channel to the observed sensitivity.

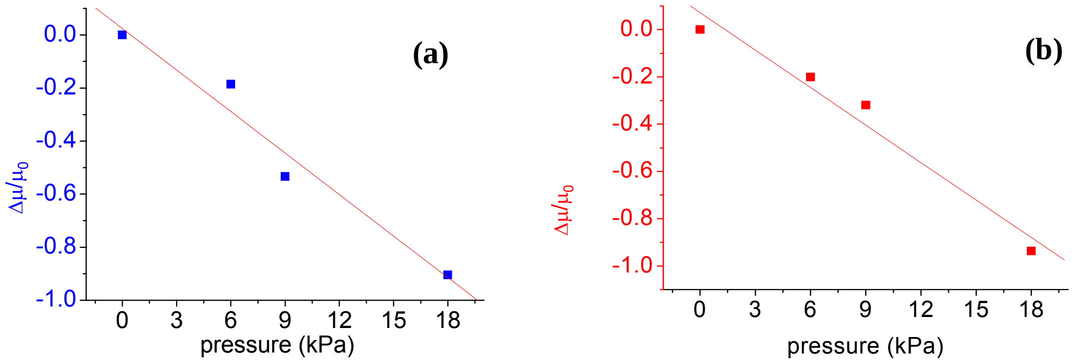

Fig. 5.19: Mobility vs. pressure comparison between bottom-contact (a) and top-contact devices (b)

Despite the fact that the underlying mechanism of the observed pressure sensitivity is not completely clear yet from our experiment we can derive that besides a decrease of pentacene mobility in the channel that is observed in both bottom- and top-contact device and that can be probably attributed to morphological modification of the pentacene layer under stress, we suppose that interface effects in the source/drain surrounding areas, due once again to the morphological modification of pentacene layer under stress, may be also responsible for drain-source current variations in bottom contact devices.

In order to investigate the sensitivity of the device to different mechanical stimuli, we also performed experiment in order to detect the strain induced in a suspended stainless steel cantilever. To do this the gate side of the device is glued to an extremity of the cantilever and on the opposite extremity different weights are suspended in order to obtain a measurable deformation to the cantilever and on the device glued on top of it.

The experimental set-up is shown in Fig. 5.20

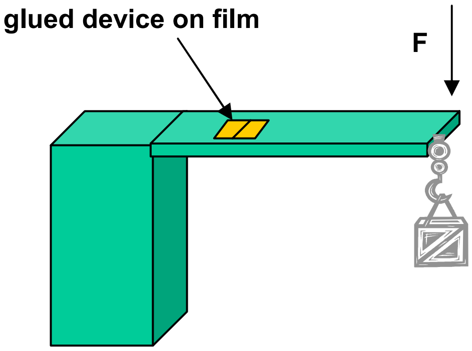

Fig. 5.20: Experimental set-up for the cantilever bending detection

The strain induced in the cantilever has been calculated using Eq. 5.3:

$$\varepsilon = \frac{M_f}{EW}. \tag{5.3}$$

where M_f is the bending moment $M_f = F * x$ (F is the applied Force and x is the distance of the device channel), E is the Young modulus of the stainless steel ($E = 2.1*10^7 \,{}^{Kg}\!/_{cm^2}$) and W is the modulus of resistance ($W = \frac{1}{6}bh^2$, where b and h are the width and the thickness of the cantilever). Figure 5.21 shows the maximum drain current as a function of the strain. As it can be seen the variation has not a monotonic behaviour. Furthermore we can not observe any dependence of mobility, threshold voltage and contact resistance on the induced strain. Moreover the device response shows a strong dependence on the pasting material (i.e. liquid graphite or copper tape). At present, this set-up is not very useful for understanding the correlation between the mechanical deformation and the device dynamics.

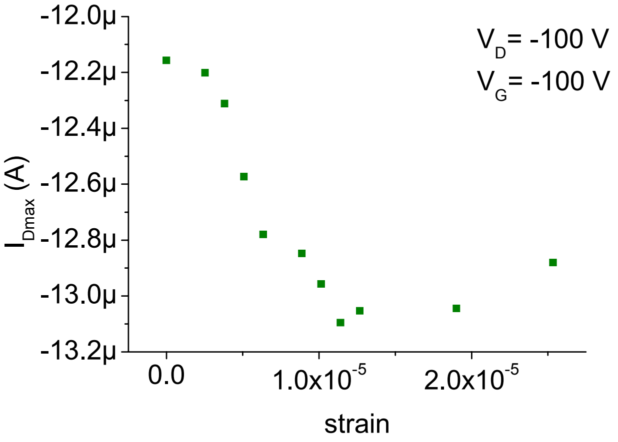

Fig. 5.21: I_{Dmax} vs. strain of a cantilever

However, the marked sensitivity of the drain current to an elastic deformation can be used not only to detect a pressure but also to map the bend of a substrate. To do this the free-standing device is fixed on a substrate, usually a thin strip of paper, and this it is wrapped around cylinders of different radii of curvature.

The variations of the maximum drain current (V_D= -100V, V_G= -100 V) as a function of the radius of the cylinders are shown in Fig. 5.22.

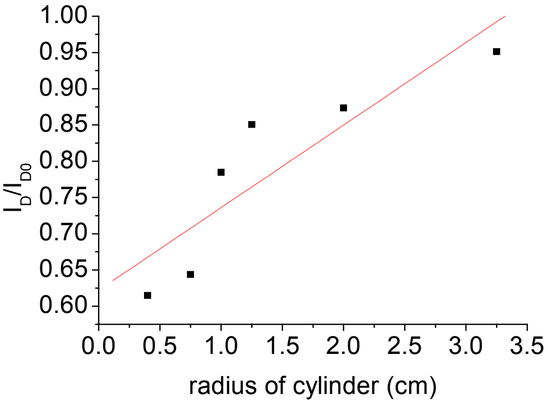

Fig. 5.22: I_D/I_{D0} vs. radium of cylinder

As it can be seen, also in this case (as for pressure sensors), the drain current variation is more or less linear. The maximum drain current at different pressure values is normalized with respect to the maximum value obtained for the unbent device. As it can be observed for a radius of 3.5 cm the I_D/I_{D0} ratio is close to unity and the variation of the current is hardly detectable.

Again, the sensitivity has been defined as ΔI/Δr and estimated from I_D-V_D curves. Figure 5.23 shows the sensitivity derived from one significant sample.

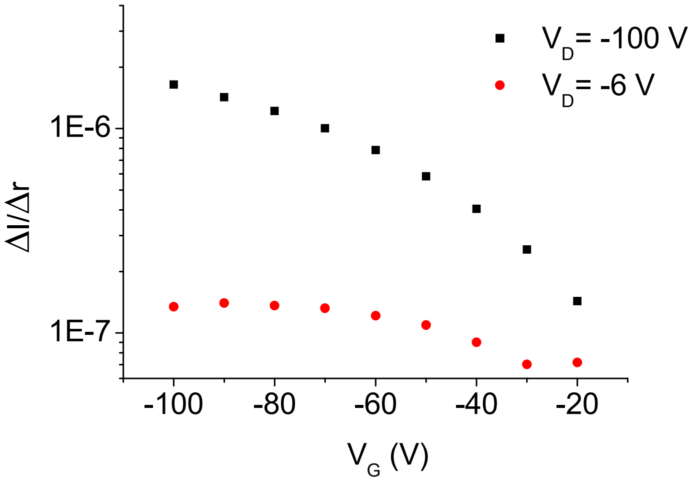

Fig. 5.23: ΔI/Δr vs. V_G

As for pressure sensors, the sensitivity is gate voltage dependent and is higher in the saturation region than in the linear one.

Figure 5.24 shows the time variations of the drain current: the device is bent and unbent according to a time sequence. In particular, as it can be seen in Fig. 5.24 (b) the radius of curvature has been kept constant while the bending frequency has been changed. Also in this case the current variations are reproducible and reversible with a small hysteresis effect.

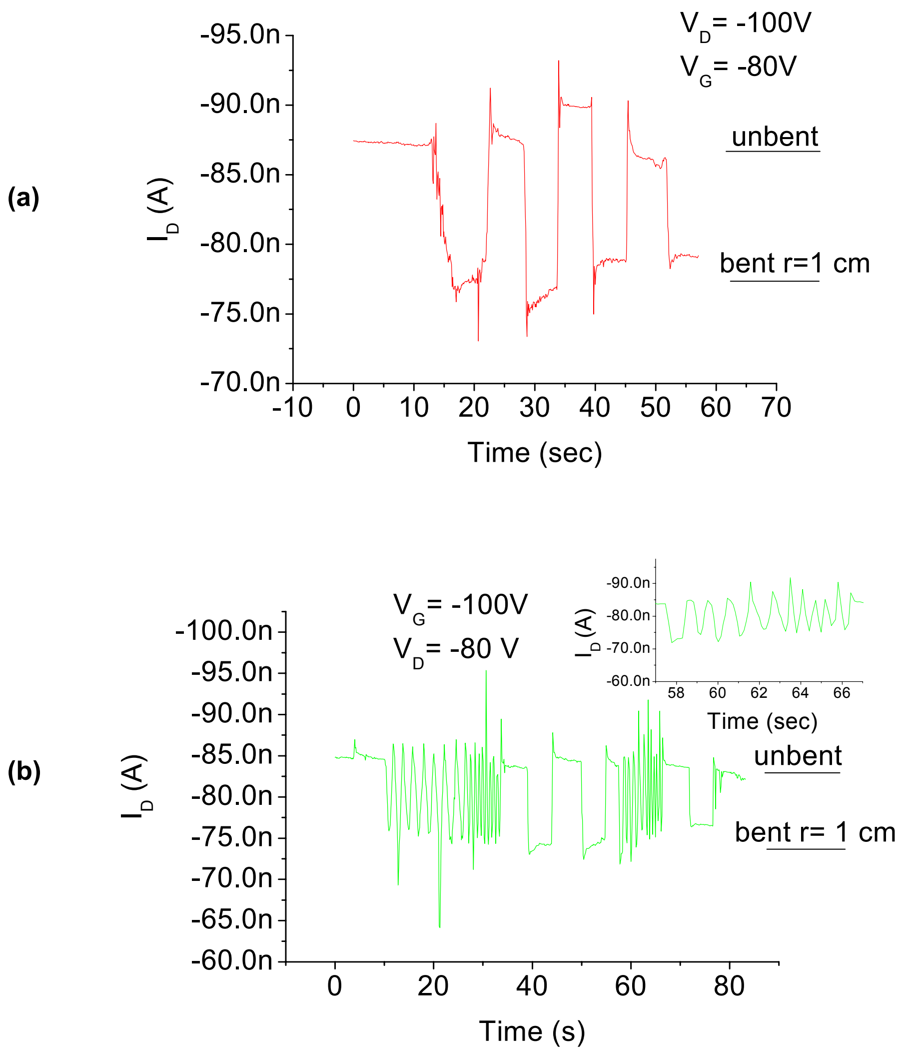

Fig. 5.24: (a) I_D vs. Time; (b) I_D vs. Time at different bending frequencies. Inset: detail for 57sec<t< 67 sec

Figure 5.25 shows what happens when the device is bent and unbent with different radii of curvature. The variation are quasi-linear and the device responds very fast to the mechanical stimulus but the time required to reach the steady state is much higher as in pressure experiment.

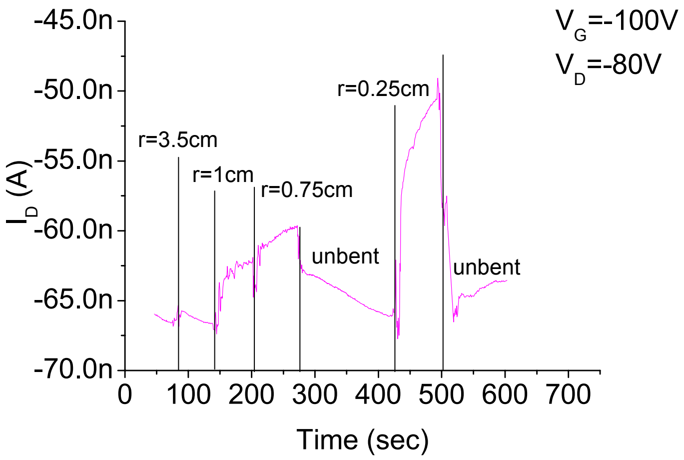

Fig. 5.25: I_D vs. Time curve with different applied pressures

We extracted mobility, threshold voltage and contact resistance by fitting our data with Eq. 5.2. The results are shown in Fig. 5.26, 5.27, 5.28. As for pressure sensors we observe detectable variations of these parameters. The values are normalized with respect to the values obtained for the unbent device. Once more, as in the case of the maximum current, it can be observed that for a bending radius of 3.5 cm the variations of the parameters are barely detectable. It can be assumed that the maximum radius of curvature perceptible is around 3.5 cm.

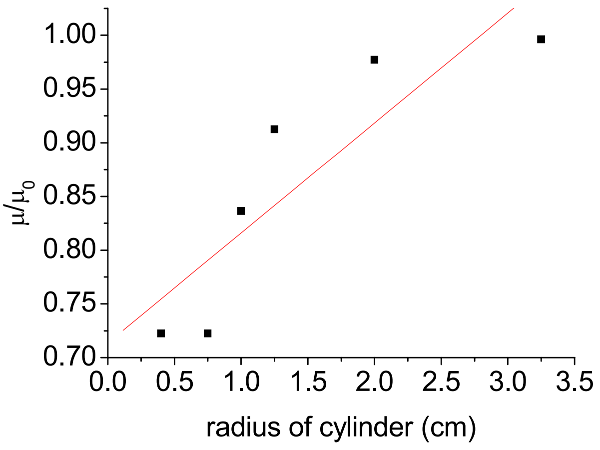

Fig. 5.26: Mobility vs. radius of curvature for a significant sample

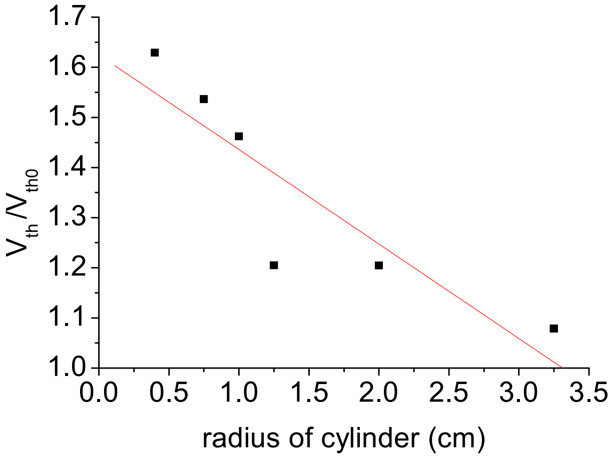

Fig. 5.27: Threshold voltage vs. radius of curvature for a significant sample

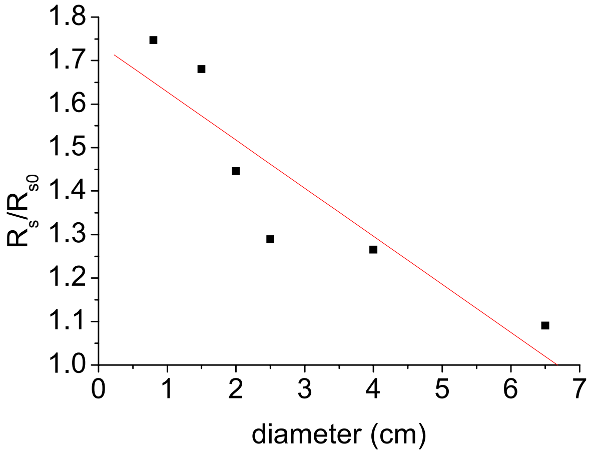

Fig. 5.28: Contact resistance vs. radius of curvature for a significant sample

As for the pressure experiment the data shows that the variations in the drain current can be related to mobility and threshold voltage and in this case also contact resistance variations. These variations can be probably attributed to the morphology modification of the semiconductor layer under stress, that can be related to mobility variations, and also to the variations of the activity and probably to the distribution of charge carrier trap states near the semiconductor/electrodes interfaces, that can be related to threshold voltage and contact resistance variations. [4,10,11]

5.4 Conclusions

We realized a flexible OTFT structure where the organic semiconductor device performs both sensing and switching functions. By exploiting the properties of this structure, the sensor can be combined with any kind of substrate or it can be used as a free-standing device. Measurements recorded on different devices with the same structure and on devices with different structures suggest that the underlying mechanism responsible for the observed sensitivity could be related not only to a pressure-induced decrease of pentacene mobility in the channel, but also to interface effects at the contacts/semiconductor boundary. However the correlation between the device sensitivity mechanism and the mechanical stimulus applied is not well understood and needs more investigations. To this aim work is in progress to realize real-time AFM measurements during the electrical characterization under stress.

Moreover, for practical application time stability and low operating voltages are highly desirable. At the device level a better time stability can be obtained using a proper encapsulation layer to protect the semiconductor layer from exposure to external agent (i.e. humidity, light, etc), Obviously the encapsulation layer must be flexible in order to allow a proper device deformation under stress. Thanks to the properties of the structure, in particular to the absence of the substrate it is also possible to use both sides of the insulating layer to modify the structure in order to improve the sensitivity of the sensor: In this way double gate structures can be developed and flexible sensing elements can be added, allowing to integrate on the same structure also possible other elements as flexible variable capacitors or resistors. For a broad range of innovative applications as sensors networks for life signs monitoring, sensorized clothes, smart textiles and robotics (i.e "electronic skin") there is an increasing demand of low-cost and flexible mechanical sensor. Work is in progress to realize sensor arrays and sensor matrices in order to achieve large area mechanical sensitivity.

References

1. I. Manunza et al., Appl. Phys. Lett. 89, 143502, (2006)
2. I. Manunza et al., Mater. Res. Soc. Symp. Proc. 965,(2007)
3. I. Manunza et al., Bios.Bioelec, in press
4. Horowitz G.,. J. Mater. Res. 19, 1946-1962, (2004)
5. Bonfiglio A. et al, Appl. Phys. Lett. 82,20, 3550-3552, (2003)
6. F. Garnier et al., Science (Washington, DC, U.S.) 265, 1684 (1994).
7. M. Halik, et al., , Appl. Phys. Lett. 81, 289 (2002).
8. A. R. Brown, et al., Synth. Met. 88, 37 ~1997!
9. Cosseddu et al., Appl. Phys. Lett., 88, 023406, (2006)
10. Pernistich K.P. et al., J. Appl. Phys. 96, 6431-6438, (2004)
11. Schroeder R. et al., Appl. Phys. Lett. 83, 3201-3203 (2003)
12. Lindner Th et al., J. Appl. Phys. 98, 114505, (2005)
13. Dimitrakopoulos C.D. et al., Adv. Mat. 14,2, (2002)

Conclusions

We have realized organic field-effect device for detecting chemical and physical parameters. The devices are completely flexible and have been shown performance similar to analogous organic devices reported in the literature.

Ion-sensitive organic field effect transistors have been shown to be responsive to changes in the pH of an electrolytic solution. The device is assembled starting from a flexible insulating foil that is responsible of the device sensitivity through chemical reactions at the electrolytic/insulator interface. At present, the device is a low-cost pH detector but in the future it would be possible to obtain properties of chemical selectivity by means of a proper funtionalization of the insulating layer or by modifying the device structure in order to realize bio-sensors or DNA detectors.

Also physical sensors have been realized. In particular the marked sensitivity of the drain current to an elastic deformation induced by a mechanical stimulus and the fact that the device is so thin and flexible that it can be applied to whatever surface can be exploited to detect through the variation of the current on the device channel any mechanical deformation of the surface itself or to detect a pressure applied by means of a pressurized air flow to the gate side of the free-standing device. Many attractive application can be found for this kind of devices in particular: electronic-skin for robotic applications, smart textiles and sensorized clothes.

At present for both chemical and physical sensors several aspects need further clarifications. In particular the physics of the working mechanisms deserve more investigations. At the device level several problems due to hysteresis effect and long term stability can be sorted out by adding a proper encapsulation layer in order to prevent contamination of the semiconductor layer from external agents as humidity, light, etc. Furthermore for practical application in sensorics low operating voltages are required. In this perspective an accurate choice of materials and the integration of a low voltage bias circuit can help to achieve this target.

Acknowledgments – Ringraziamenti

A conclusione di questi tre anni di lavoro ci sarebbero tante persone da ringraziare e tanti momenti da ricordare. Ci vorrebbe un capitolo a parte in cui riportare come dal quaderno degli esperimenti tutto ciò che ha contribuito dal punto di vista umano al completamento di questo cammino. Purtroppo non è possibile ma a tutte le persone che non saranno citate qui assicuro che conservo nel mio cuore e nei miei ricordi il loro prezioso contributo.

Ringrazio innanzitutto la Prof. Annalisa Bonfiglio per avermi dato la possibilità di intraprendere questa carriera di studio e per aver supportato e guidato il mio lavoro.

Ringrazio Luisa per tutte le volte che ha corretto gli articoli con me e perché ho sempre potuto contare su di lei per tutto. Ringrazio Simo perché ha fatto più di quanto pensa. Ringrazio tutte le amiche e gli amici che mi hanno supportato e sopportato soprattutto negli ultimi tempi. Ringrazio Emi per avermi dato amore e serenità e per un sacco di altri motivi che non dirò qui.

E sempre alla fine ringrazio mamma e papà, per aver voluto sempre il meglio per me e per tutto ciò che sempre hanno fatto e faranno per me.

Table of contents

Chapter 1 – Organic Electronics

1.4 Organic Field-Effect Transistors

Chapter 2 – An overview on Organic Field-Effect Sensors

Chapter 3 – Device structures and Materials

Chapter 4 – Chemical Sensors based on Organic Field-Effect Transistors

Chapter 5 – Mechanical Sensors based on Organic Field-Effect Transistors